Title: ^{230}Th normalization: New insights on an essential tool for quantifying sedimentary fluxes in the modern and Quaternary ocean

Authors: Costa, Kassandra M.[1]; Hayes, Christopher T.[2]; Anderson, Robert F.[3,4]; Pavia, Frank J.[3,4,5]; Bausch, Alexandra[3,4,6]; Deng, Feifei[7]; Dutay, Jean-Claude[8]; Geibert, Walter[9]; Heinze, Christoph[10]; Henderson, Gideon[7]; Hillaire-Marcel, Claude[11]; Hoffmann, Sharon[12]; Jaccard, Samuel L.[13]; Jacobel, Allison W.[14,15]; Kienast, Stephanie S.[16]; Kipp, Lauren[3,16]; Lerner, Paul[17]; Lippold, Jörg[18]; Lund, David[19]; Marcantonio, Franco[20]; McGee, David[21]; McManus, Jerry F.[3,4]; Mekik, Figen[22]; Middleton, Jennifer L.[3]; Missiaen, Lise[23]; Not, Christelle[24]; Pichat, Sylvain[25,26]; Robinson, Laura F.[27]; Rowland, George H.[27]; Roy-Barman, Matthieu[8]; Tagliabue, Alessandro[28]; Torfstein, Adi[29,30]; Winckler, Gisela[3,4]; Zhou, Yuxin[3,4]

Affiliations:

1. Dept. of Geology and Geophysics, Woods Hole Oceanographic Institution, Woods Hole, MA, USA
2. School of Ocean Science and Engineering, University of Southern Mississippi, Stennis Space Center, MS, USA
3. Lamont-Doherty Earth Observatory of Columbia University, Palisades, NY, 10964 USA
4. Department of Earth and Environmental Sciences, Columbia University, New York, NY, USA
5. Present Address: Division of Geological and Planetary Science, California Institute of Technology, Pasadena, 91125 CA, USA
6. Present Address: Department of Earth System Science, Stanford University, Stanford, California 94305, USA
7. Department of Earth Sciences, University of Oxford, South Parks Road, Oxford, OX13AN, UK
8. Université Paris-Saclay, CNRS, CEA, UVSQ, Laboratoire des sciences du climat et de l'environnement, 91191, Gif-sur-Yvette, France.LSCE, IPSL, Laboratoire CEA, UVSQ, CNRS, F-91191 Gif sur Yvette, France
9. Alfred Wegener Institute for Polar and Marine Research, Bremerhaven, Germany
10. Geophysical Institute and Bjerknes Centre for Climate Research, University of Bergen, Bergen, Norway.
11. GEOTOP, Université du Québec à Montréal, C.P. 8888 Succ. Centre-Ville, Montréal, Quebec H3C 3P8, Canada
12. Department of Earth and Ocean Sciences, University of North Carolina Wilmington, Wilmington, NC, USA
13. Institute of Geological Sciences and Oeschger Center for Climate Change Research, University of Bern, Bern, Switzerland
14. Dept. of Earth, Environmental, and Planetary Sciences, Brown University, Providence, RI, USA
15. Institute at Brown for Environment and Society, Brown University, Providence, RI, USA
16. Department of Oceanography, Dalhousie University, Halifax, Nova Scotia, Canada
17. NASA Goddard Institute for Space Studies and Center for Climate Systems Research, Columbia University, New York, New York, USA
18. Institute of Earth Sciences, Heidelberg University, Heidelberg, Germany
19. Department of Marine Sciences, University of Connecticut, Groton, CT, USA
20. Department of Geology and Geophysics, Texas A&M University, College Station, Texas 77843, USA
21. Department of Earth, Atmospheric and Planetary Sciences, Massachusetts Institute of Technology, Cambridge, MA, USA.
22. Grand Valley State University, Department of Geology Allendale, MI 49401, USA
23. Climate Change Research Centre, University of New South Wales, Sydney, Australia

24. Department of Earth Sciences, The University of Hong Kong, Hong Kong, China
25. Université de Lyon, Laboratoire de Géologie de Lyon (LGL-TPE), Ecole Normale Supérieure de Lyon, CNRS UMR5276, 46 allée d'Italie, 69007 Lyon, France
26. Max Planck Institute for Chemistry, Climate Geochemistry, Hahn Meitner Weg 1, 55128 Mainz, Germany
27. School of Earth Sciences, Wills Memorial Building, University of Bristol, Bristol BS8 1RJ, UK
28. School of Environmental Sciences, University of Liverpool, Liverpool L69 3GP, UK
29. The Fredy and Nadine Herrmann Institute of Earth Sciences, The Hebrew University, Jerusalem 91904, Israel
30. Interuniversity Institute for Marine Sciences, Eilat 88103, Israel

Abstract

^{230}Th-normalization is a valuable paleoceanographic tool for reconstructing high-resolution sediment fluxes during the late Pleistocene (last ~500,000 years). As its application has expanded to ever more diverse marine environments, the nuances of ^{230}Th systematics, with regards to particle type, particle size, lateral advective/diffusive redistribution, and other processes, have emerged. We synthesized over 1000 sedimentary records of ^{230}Th from across the global ocean at two time slices, the Late Holocene (0-5000 years ago, or 0-5 ka) and the Last Glacial Maximum (18.5-23.5 ka), and investigated the spatial structure of ^{230}Th-normalized mass fluxes. On a global scale, sedimentary mass fluxes were significantly higher during the Last Glacial Maximum (1.79-2.17 g/cm^{2}kyr, 95% confidence) relative to the Holocene (1.48-1.68 g/cm^{2}kyr, 95% confidence). We then examined the potential confounding influences of boundary scavenging, nepheloid layers, hydrothermal scavenging, size dependent sediment fractionation, and carbonate dissolution on the efficacy of ^{230}Th as a constant flux proxy. Anomalous ^{230}Th behavior is sometimes observed proximal to hydrothermal ridges and in continental margins where high particle fluxes and steep continental slopes can lead to the combined effects of boundary scavenging and nepheloid interference. Notwithstanding these limitations, we found that ^{230}Th-normalization is a robust tool for determining sediment mass accumulation rates in the majority of pelagic marine settings (> 1000 m water depth).

1. Introduction

Burial fluxes of different components of marine sediment provide insight into a wide variety of surface processes that are central to the Earth system, including marine export productivity, windblown dust deposition on the sea surface, carbon storage as organic matter and calcium carbonate, and hydrothermal activity on the seafloor. The traditional approach to calculating marine burial fluxes relies on determining the average mass accumulation rates based on age model tie points, intervening sediment thickness, and average sediment dry bulk density (e.g., Broecker, 1971). The temporal resolution of this approach is limited by the robustness of the age model, including the number of chronological tie points and their associated errors (e.g., Francois et al., 2004). Furthermore, this approach can easily be biased by sediment redistribution on the seafloor (e.g., Johnson & Johnson, 1970), where lateral sediment transport can exceed the vertical rain of particles from the water column. As a result, constant flux proxies such as ^{230}Th have been developed to provide more robust estimates of mass accumulation on the seafloor.

Constant flux proxies are geochemical parameters with well-constrained and stable source functions, such as ^{230}Th (Bacon, 1984; François et al., 2004) and ^{3}He (Marcantonio et al., 1996; Schlosser & Winckler, 2002; Winckler et al, 2004; McGee & Mukhopadhyay, 2013). ^{230}Th is produced by the steady decay of uranium dissolved in seawater, after which it is rapidly removed by sinking particles and buried on the seafloor (see Section 2) (Bacon, 1984; François et al., 1990, 2004; Suman & Bacon, 1989). Because the ^{230}Th production rate is relatively uniform in space and time, variability in ^{230}Th concentrations in the sediment can theoretically be attributed to variable dilution by changes in sediment mass flux. Thus, sedimentary ^{230}Th concentrations can be used to reconstruct changes in sediment mass fluxes over time. This technique, ^{230}Th normalization, allows both high resolution sediment mass flux reconstructions independent of age model tiepoints and isolation of only the vertical component of sedimentation, regardless of the amount of lateral sediment transport.

^{230}Th has been used to assess burial fluxes for more than 35 years (Bacon, 1984), with the first comprehensive review of its use, advantages, and limitations published more than a decade ago (François et al., 2004). In the intervening 15 years, analysis of ^{230}Th has become more commonplace, with advances in methodology (e.g., evolving from alpha counting to inductively-coupled-plasma mass spectrometry) resulting in an order of magnitude increase in the amount of data available. At the same time, the GEOTRACES program and associated modelling studies have improved our understanding of ^{230}Th cycling in the modern ocean. With these changes in mind, and the increasing utilization of sedimentary ^{230}Th across the global ocean, we have produced an updated compilation that provides an overview of the methodology and current understanding of the ^{230}Th normalization technique on a global scale.

2. Background: The Marine Geochemistry of ^{230}Th

In this section, we review the current understanding of ^{230}Th systematics in the ocean, provide an updated ^{230}Th production rate, provide revised lithogenic and authigenic correction equations, and present recommendations for best practices in future studies.

2.1 *Production of ^{230}Th in the water column*

^{230}Th is produced in seawater by radioactive decay of long-lived ^{234}U. Because the marine residence time of uranium (~400,000 years, Henderson, 2002) is orders of magnitude longer than the ocean mixing time (~1000s years), ^{230}Th production is ubiquitous in the water column and occurs at a relatively uniform rate. This production rate (β_{230}, in units of decays per cubic centimeter per thousand years, dpm/cm^{3}kyr) can be calculated using the activity of uranium in seawater (A_{234U}, which is equivalent to the concentration of ^{234}U multiplied by the decay constant of ^{234}U), and the decay constant of ^{230}Th (λ_{230}), as demonstrated by François et. al (2004). As more precise values of the decay constants are determined, β_{230} is progressively refined over time. Uranium concentrations are conservative and scale with salinity (Chen et al., 1986; Owens et al., 2011), but this relationship is defined in terms of the major uranium isotope,

^{238}U. We thus rewrite Equation 1a as Equation 1b by replacing the activity of ^{234}U with the activity of ^{238}U multiplied by the $^{234}U/^{238}U$ activity ratio in seawater (1.1468, Andersen et al., 2010). We can then replace the concentration of ^{238}U with the salinity (S) relationship of Owens et al. (2011) to obtain Equation 1c. Finally, we use the latest half-life for ^{230}Th (75,584 ± 110 yrs, Cheng et al., 2013) to calculate its decay constant, and we assume a salinity of 35 to determine the mean ocean β_{230} (Equation 1d).

$$\beta_{230} = \lambda_{230}\, A_{234U} \tag{1a}$$

$$\beta_{230} = \lambda_{230}\, A_{238} \, * \left(\frac{A_{234U}}{A_{238U}}\right)_{SW} \tag{1b}$$

$$\beta_{230} = \lambda_{230}\, [0.0786 * S - 0.315\,] * \left(\frac{A_{234U}}{A_{238U}}\right)_{SW} \tag{1c}$$

$$\beta_{230} = \left(\frac{ln(2)}{75{,}584}\right) [0.0786 * 35 - 0.315\,] * 1.1468 = 2.562 \pm 0.05 * 10^{-5}\, \frac{dpm}{cm^3 kyr} \tag{1d}$$

Salinity variations affect β_{230} at a rate of $0.08266*10^{-5}$ dpm/cm^{3}kyr for each change in salinity by 1 (unitless, according to the practical salinity scale of 1978). This rate is only slightly greater than the error associated with β_{230}, and statistically significant changes to β_{230} require relatively extreme changes in salinity. For example, β_{230} is about 10% lower in water with S=32 compared to S=35, and β_{230} is 10% higher in water with S=38 compared to S=35. Salinity variations within the water column are unlikely to greatly affect the net ^{230}Th production on the timescales of sedimentation, and in general, we recommend using a single β_{230} for each record to maintain consistency.

Unlike uranium, which is highly soluble, ^{230}Th is strongly particle-reactive and is thus rapidly removed from seawater by sorption onto sinking particles (particle scavenging, Bacon and Anderson, 1982). Dissolved and particulate ^{230}Th concentrations generally increase linearly with water depth, a feature best explained by reversible scavenging, a process by which ^{230}Th adsorbed onto the surface of sinking particles continuously exchanges with the dissolved ^{230}Th pool as particles settle through the water column (Bacon & Anderson, 1982; Nozaki et al., 1987). As ^{230}Th is highly insoluble, its residence time in seawater does not exceed a few decades (20-40 years; Nozaki et al., 1981).

2.2 *Analytical methodology*

Analysis of thorium (^{230}Th, ^{232}Th) and uranium (^{238}U, ^{235}U, ^{234}U) generally proceeds by aliquoting 100-200 mg of sediment, spiking with ^{229}Th and ^{236}U, complete acid digestion, column chromatography to isolate and concentrate the nuclides, and measurement by inductively coupled plasma mass spectrometry (ICP-MS) (e.g., as described in Fleisher and Anderson, 2003). The specific details of this procedure may vary between laboratories, based on, e.g., available instrumentation, sample throughput, and required precision. For example, the digestion usually includes a “cocktail” of nitric acid, hydrofluoric acid, and perchloric acid (e.g., Jacobel et al., 2017), but some studies replace perchloric acid with hydrochloric acid and hydrogen peroxide (e.g., Skonieczny et al., 2019) and others omit any chlorinated acid altogether (e.g., Palchan and Torfstein, 2019). Some digestions are also assisted by pressurized microwave systems (e.g., Thöle et al., 2019).

Prior to the 1990s, in the early development of the proxy, Th and U nuclides were analyzed by alpha spectrometry, a slow process of counting individual nuclide decays which further required an additional electroplating step in sample preparation (e.g., Anderson and Fleer, 1982). Today, most measurements are conducted via multi-collector ICP-MS. Some studies use single-collector ICP-MS to increase throughput (e.g., Costa and McManus, 2017; Pichat et al., 2004), primarily at the expense of precision on the low-abundance ^{234}U. The majority of studies report uncertainties based on the reproducibility of sediment standards (e.g., Costa and McManus, 2017; Thöle et al., 2019; Palchan and Torfstein, 2019), although the specific standards vary from laboratory to laboratory.

2.3 *^{230}Th in marine sediments*

The total ^{230}Th measured in sediment includes not just ^{230}Th scavenged from the water column (or excess ^{230}Th, $^{230}Th_{xs}$ hereafter) but also lithogenic and authigenic non-excess components. The $^{230}Th_{xs}$ is calculated by subtracting the contributions of the lithogenic and authigenic ^{230}Th activities as follows (Henderson and Anderson, 2003):

$$A_{230Thxs} = A_{230Th}^{total} - A_{230Th}^{lith} - A_{230Th}^{auth} \quad (2)$$

Lithogenic ^{230}Th ($^{230}Th_{lith}$) is derived from the incorporation of continental material, hereafter referred to as lithogenic material, into marine sediments. Non-excess ^{230}Th is also derived from the *in situ* decay of authigenic U, which is precipitated under reducing sedimentary conditions. While this ^{230}Th is not authigenic *sensu stricto*, we refer to it as authigenic ^{230}Th ($^{230}Th_{auth}$) for simplicity. These two additional sources of ^{230}Th must be quantified and subtracted, following the procedures detailed below.

2.3.1 Lithogenic correction

Depending on its location, a core site can receive substantial lithogenic input from rivers, aeolian dust, and/or iceberg discharge. Lithogenic material contains lattice-bound ^{232}Th (10.7 ppm for upper continental crust on average, Taylor & McLennan, 1995), while biogenic material (e.g., calcium carbonate, opal) is virtually devoid of this isotope. Thus, the lithogenic ^{230}Th activity can be determined as follows:

$$A_{230Th}^{lith} = \left(\frac{A_{238U}}{A_{232Th}}\right)_{lith} * A_{232Th} \quad (3)$$

where $(A_{238U}/A_{232Th})_{lith}$ is the lithogenic ratio of ^{238}U to ^{232}Th in activity units. This correction relies on three assumptions: i) the lithogenic fraction of the sediment is at secular equilibrium for ^{238}U and ^{230}Th, ii) the $(A_{238U}/A_{232Th})_{lith}$ is known, and iii) all measured ^{232}Th is lattice-bound rather than adsorbed. Generally, studies calculating $^{230}Th_{xs}$ use prescribed $(A_{238U}/A_{232Th})_{lith}$ based on the recommendations summarized by Henderson and Anderson (2003): Atlantic (0.6 ± 0.1), Pacific (0.7 ± 0.1) and Southern Ocean (0.4 ± 0.1). However, the $(A_{238U}/A_{232Th})_{lith}$ values that have been employed within each basin vary substantially amongst publications (Supplementary Figure 1), rendering data comparison, compilation and modeling difficult.

While the bulk silicate Earth $(A_{238U}/A_{232Th})_{lith}$ is ~0.74 (Allegre et al., 1986), U and Th can be fractionated in continental materials by igneous processes, chemical weathering, transport, and sedimentation. In particular, U dissolves much more easily in oxygenated water than Th, so that, e.g., deeply weathered continental rocks are expected to be depleted in U relative to Th. This mobilization of U contributes to the highly variable $(A_{238U}/A_{232Th})_{lith}$ observed in sedimentary rocks (0.15 to 155, Adams & Weaver, 1958) compared to fresh, unweathered igneous rocks (0.4 to 1.6, Bourdon & Sims, 2003). It can thus be difficult to predict the relevant $(A_{238U}/A_{232Th})_{lith}$ for deep sea sediments, which may integrate material from multiple geological sources with highly variable $(A_{238U}/A_{232Th})_{lith}$. Several studies have highlighted that the most appropriate $(A_{238U}/A_{232Th})_{lith}$ value can diverge substantially from the recommended value for a given ocean basin (Walter et al., 1997; Pichat et al., 2004; Costa and McManus, 2017; Missiaen et al., 2018). For instance, input from young volcanic provinces and/or inland regions with high runoff may locally deviate the $(A_{238U}/A_{232Th})_{lith}$ value from that of the basin average (Pichat et al., 2004). At the same time, the observed variability in deep-sea sediments is markedly lower than the variability reported for potential parent rock material (Missiaen et al., 2018), suggesting that the integrative nature of marine deep-sea sediment mixes individual lithogenic signals towards a more homogeneous $(A_{238U}/A_{232Th})_{lith}$ range.

Early approaches to refining $(A_{238U}/A_{232Th})_{lith}$ estimates either measured bulk sediment ratios in predominantly lithogenic sediment (Veiga-Pires & Hillaire-Marcel, 1999) or applied a range of $(A_{238U}/A_{232Th})_{lith}$ based on a compilation of possible lithogenic sources (Pichat et al., 2004). Later studies argued that the minimum measured bulk sediment $(A_{238U}/A_{232Th})_{lith}$ over the studied time series would be the closest estimate to the actual $(A_{238U}/A_{232Th})_{lith}$ (Böhm et al., 2015; Costa & McManus, 2017; Lippold et al., 2009; Mulitza et al., 2017). Another approach has been to use (A_{234U}/A_{238U}) to identify sediment with no authigenic contribution, within which the bulk sediment (A_{238U}/A_{232Th}) would be a more accurate estimate for the local lithogenic value (Bourne et al., 2012). This approach assumes a seawater (A_{234U}/A_{238U}) of 1.1468 (Andersen et al., 2010) and a lithogenic (A_{234U}/A_{238U}) of 1 (i.e., secular equilibrium). However, (A_{234U}/A_{238U}) ratios below secular equilibrium are known to occur frequently, particularly in slowly accumulating deep-sea sediments (e.g., Ku et al., 1965; DePaolo et al., 2012), and so this approach should be used with caution. Finally, sequential sediment leaching has been applied to isolate the lithogenic fraction of sediment, and it has demonstrated substantial variability (0.4 to 0.7) in $(A_{238U}/A_{232Th})_{lith}$ within a single sediment core in the Atlantic (Missiaen et al., 2018). This range exceeds the uncertainty that is usually associated with $(A_{238U}/A_{232Th})_{lith}$ in the literature (+/- 0.1) and presents a challenge to the treatment of $(A_{238U}/A_{232Th})_{lith}$ as a constant through time.

Refining $(A_{238U}/A_{232Th})_{lith}$ is important because of the propagating effects on $^{230}Th_{xs}$ calculations, particularly in sediment with a high proportion of lithogenic material (Burckel et al., 2016; Guihou et al., 2010; Hoffmann et al., 2018; Lippold et al., 2012). An accurate evaluation of the $(A_{238U}/A_{232Th})_{lith}$ value can be key to properly reconstructing the amplitude and timing of $^{230}Th_{xs}$ changes, especially for shallow coastal sediment cores, which receive significant lithogenic inputs (>30% of the total sediments). Future studies should aim to i) develop a simpler method to evaluate the temporal $(A_{238U}/A_{232Th})_{lith}$ variations from routine measurements and ii) further investigate the importance of adsorbed vs. lattice-bound ^{232}Th for lithogenic corrections when using the ^{230}Th normalization technique. Given the available tools, we recommend the following treatment for future $^{230}Th_{xs}$ records: i) evaluate the detrital contribution to the sediment (% lithogenic) using the measured bulk ^{232}Th activities, ii) assess the sensitivity/robustness of the $^{230}Th_{xs}$ record to changes in the $(A_{238U}/A_{232Th})_{lith}$ value, iii) include appropriate uncertainties on $(A_{238U}/A_{232Th})_{lith}$, of, for example, at least 10 % at 2σ, and iv) propagate the uncertainties and potential temporal variability in $(A_{238U}/A_{232Th})_{lith}$ into the calculations for $^{230}Th_{xs}$.

2.3.2 Authigenic correction

After subtraction of lithogenic ^{230}Th, the residual ^{230}Th concentration must be corrected for authigenic ^{230}Th, which may have accumulated in the sediment due to the decay of non-lithogenic uranium, commonly known as authigenic uranium (U_{auth}). The precipitation of U_{auth} in marine sediments is the primary sink of U from the ocean (Klinkhammer & Palmer, 1991; McManus et al., 2005) and occurs when soluble U(VI) is reduced to U(IV) (Anderson, 1982). This transformation is thought to be microbially-mediated (Francis et al., 1994; Ganesh et al., 1997; Lovley et al., 1991; Sani et al., 2004) and occurs in reducing porewaters where oxygen is limited by a combination of low bottom water oxygen and/or a high organic carbon rain rate (Finneran et al., 2002; McManus et al., 2005). As the reduction and precipitation of U begins in porewaters, it creates a concentration gradient between high-U seawater and low-U porewater that transfers U from seawater to sediment as long as reducing conditions are maintained (Anderson et al., 1989; Barnes & Cochran, 1990). In some sedimentary environments, typically those characterized by well-oxygenated bottom water and low organic productivity, no U_{auth} is found and the magnitude of the authigenic correction will be negligible. In other environments, particularly those where porewater redox conditions are variable and the conditions for U_{auth} precipitation are periodically or continuously sustained, uncertainties arising from the U_{auth} correction can be substantial.

Assuming that the lithogenic endmember is known for a site (see Section 2.3.1), U_{auth} activity (A_{238U}^{auth}) can be quantified as follows:

$$A_{238U}^{auth} = A_{238U}^{total} - \left(\frac{A_{238U}}{A_{232Th}}\right)_{lith} * A_{232Th} \tag{4}$$

This U_{auth} then decays to $^{230}Th_{auth}$ since the time of deposition (t), as in Equation 5a and as described in François et al. (2004). However, because this process does not occur at secular equilibrium, the ingrowth rate itself will vary as a function of time. To account for this disequilibrium ingrowth, we incorporate the ^{230}Th age equation, as used for dating corals and speleothems (Edwards et al., 2003), into the $^{230}Th_{auth}$ calculation (Equation 5b, Henderson & Anderson, 2003).

$$A_{230Th}^{auth} = A_{238U}^{auth} * \left(1 - e^{-\lambda_{230}*t}\right) \quad (5a)$$

$$A_{230Th}^{auth} = A_{238U}^{auth} * \left[\left(1 - e^{-\lambda_{230}*t}\right) + \frac{\lambda_{230}}{\lambda_{230} - \lambda_{234}} * \left(e^{-\lambda_{234}*t} - e^{-\lambda_{230}*t}\right) * \left(\left(\frac{A_{234U}}{A_{238U}}\right)_{SW} - 1\right)\right] \quad (5b)$$

The divergence between equations 5a and 5b increases with higher lithogenic corrections (Section 2.3.1) and lower U_{auth} activity. For example, the $^{230}Th_{auth}$ activity would be about 0.8% lower for equation 5a than for equation 5b for a theoretical 400 ka sediment with bulk ^{238}U of 9 dpm/g, bulk ^{232}Th of 1 dpm/g, and $(A_{238U}/A_{232Th})_{lith}$ of 0.6. If instead bulk ^{238}U were 3 dpm/g, holding all other variables constant, the $^{230}Th_{auth}$ activity would increase to about 2.6% lower for equation 5a than for equation 5b. Equation 5a always underestimates $^{230}Th_{auth}$ relative to equation 5b.

The use of equation 5b involves two assumptions: first, that the age of the sediment and the age of the U_{auth} deposition are contemporaneous. This assumption is almost certainly an oversimplification as U_{auth} is deposited at the porewater redox front beneath the sediment-water interface, making the age of the U_{auth} inherently younger than the sediment in which it is measured. However, given the long halflife of U and considering average marine sedimentation rates of a few cm/kyr, the age offset between the sediment and U_{auth} is typically negligible. A second, potentially more critical assumption, is that all of the U_{auth} that contributed to the production of ^{230}Th is still present in the sediment. If post-depositional burndown (i.e., diagenetic remobilization) removed a substantial fraction of U_{auth} after the time of initial deposition, the magnitude of the correction for ingrown ^{230}Th may be too small (Jacobel et al., 2017a). Loss of U_{auth} is primarily problematic in cores with low sedimentation rates (< 2 cm/kyr, Costa et al., 2018; Mangini et al., 2001). The number of records in which it has been clearly demonstrated as problematic is thus far small and restricted to regions which have experienced large changes in bottom water oxygen and/or organic matter fluxes (Hayes et al., 2014; Jacobel et al., 2017a).

2.4. *^{230}Th normalization*

After scavenging from the water column and deposition on the seafloor, the excess ^{230}Th activity in the sediment decreases with a half-life of 75.584 kyr (Cheng et al., 2013). In order to calculate the $^{230}Th_{xs}$ activity at the time of initial sediment deposition, $^{230}Th_{xs}{}^{0}$, this decay must be accounted for by using independent chronological constraints (such as oxygen isotope stratigraphy or radiocarbon dates) and the classic radio-decay equation:

$$A_{230Thxs}^{0} = A_{230Thxs} * \ e^{\lambda_{230}*t} \quad (6)$$

The long half-life of ^{230}Th allows utilization of the proxy as far back as 500,000 years, although the errors expand in increasingly older sediments. These errors are largely due to uncertainties in the lithogenic and authigenic corrections. A big advantage of ^{230}Th-normalization over fluxes derived using stratigraphic age control points is that ^{230}Th-normalized fluxes are relatively insensitive to errors in the age model (<1% error in flux for a 1 kyr error in age). Altogether, propagated uncertainties on $^{230}Th_{xs}{}^0$ activities are typically less than 5% for the 30 kyr, and often less than 2%, including analytical uncertainties, authigenic corrections, lithogenic corrections, and decay corrections.

The ^{230}Th-normalized mass flux (or preserved rain rate) of sediment (g/cm^{2}kyr) may then be calculated (Bacon, 1984; Suman & Bacon, 1989):

$$Mass\ Flux = \frac{\beta_{230} * z}{A^0_{230Thxs}} \tag{7}$$

where β_{230} is the production rate (as in Section 2.1), z is the water depth in centimeters, and the term β*z is equivalent to the integrated ^{230}Th production (P) in the overlying water column. At relatively shallow sites (<1200 m water depth), it may be important to consider glacial-interglacial changes in sea level (e.g., Grant et al., 2014), but this adjustment is generally only necessary when the change in sea level (-120 m, on average, during the LGM) comprises 10% or more of the modern water column depth (e.g., in the Bahamas, Slowey & Curry, 1991; Williams et al., 2016; and in the Red Sea, Palchan & Torfstein, 2019). At deeper sites, the compensatory increase in salinity driven by reduced ocean volume at sea level low stands (e.g., Adkins et al., 2002) largely negates any change in P driven by changes in water column depth (z) by increasing the production rate (β_{230}, see section 2.1), and the effects essentially cancel at the mean depth of the ocean (McManus et al., 1998). For example, at Bermuda Rise, modern P at 4584m water depth and S=34.885 is 11.70 dpm/cm^{2}kyr. During the LGM, assuming 120 m lower water depth (4464 m) and S=35.84 (Adkins et al., 2002), glacial P was 11.75 dpm/cm^{2}kyr, a negligible difference of only 0.4%.

The ^{230}Th-normalized flux of any sedimentary component *j* (e.g., calcium carbonate) can be determined from the fraction of *j* in the bulk sediments (f_j) by:

$$Mass\ Flux(j) = f_j * Mass\ Flux \tag{8}$$

2.5 Calculating focusing factors (Ψ)

If the accumulation rate of scavenged ^{230}Th differs substantially from its inferred production rate (P) in the overlying water column, then the deposited sediment is likely to have been affected by lateral addition/removal (focusing/winnowing) of ^{230}Th and the associated sediment by bottom currents or downslope redistribution, from a local to larger spatial scale. The degree of sediment focusing (Ψ) can be calculated by comparing the inventory of ^{230}Th in a dated sediment horizon with the inferred production of ^{230}Th in the overlying water column over the same time interval (Suman & Bacon, 1989):

$$\Psi = \frac{\rho \int_{z1}^{z2} A^0_{230Thxs} dz}{P(\Delta t)} \approx \frac{\rho\ \overline{A^0_{230Thxs}(\Delta z)}}{P\ (\Delta t)} \tag{9}$$

where ρ is the sediment dry bulk density (in g/cm^3), Δt is the time elapsed (in kyr), and Δz is the sediment accumulation (in cm). Where available, sediment density in this compilation is obtained from previously published sources, generally derived from calibrated gamma ray attenuation as determined from a core scanning multi-sensor track system. Where unspecified, sediment density is arbitrarily set to 0.75 g/cm^3, which at least limits the contributed uncertainty to a systematic bias. If the amount of ^{230}Th buried in the sediment is equal to the amount produced in the water column, then $\Psi = 1$. Otherwise Ψ will vary with the addition (focusing, $\Psi > 1$) or loss (winnowing, $\Psi < 1$) of sedimentary material.

2.6. *Data compilation*

Over 50 years (1966-2019) worth of data have been compiled to create the global thorium database (*n*=1167) presented here (Adkins et al., 2006; Anderson et al., 2006, 2009, 2014, 2019; Bausch, 2018; Böhm et al., 2015; Bohrmann, 2013; Borole, 1993; Bradtmiller et al., 2006, 2007, 2009; Broecker, 2008; Broecker et al., 1993; Brunelle et al., 2007, 2010; Causse & Hillaire-Marcel, 1989; Chase et al., 2003, 2014; Chong et al., 2016; Costa et al., 2017a; Costa et al., 2017b; Costa & McManus, 2017; Crusius et al., 2004; Dekov, 1994; Denis et al., 2009; Dezileau et al., 2000, 2004; Durand et al., 2017; Fagel et al., 2002; François et al., 1990, 1993; Frank et al., 1995, 1996; Fukuda et al., 2013; Galbraith et al., 2007; Geibert et al., 2005; Gherardi et al., 2005, 2009; Gottschalk et al., 2016; Hickey, 2010; Hillaire-Marcel et al., 2017; Hoffmann et al., 2013, 2018; Jaccard et al., 2009, 2013; Jacobel et al., 2017a; Jonkers et al., 2015; Kienast et al., 2007; Ku & Broecker, 1966; Kumar et al., 1995; Lam et al., 2013; Lamy et al., 2014; Lao et al., 1992; Lippold et al., 2009, 2011, 2012, 2016; Loubere et al., 2004; Loveley et al., 2017; Lund et al., 2019; Mangini & Dominik, 1978; Marcantonio et al., 1996, 2001, 2014; Martínez-Garcia et al., 2009; McGee et al., 2007, 2010, 2013; McManus et al., 1998, 2004; Meier, 2015; Middleton et al., 2020; Missiaen et al., 2018; Mohamed et al., 1996; Mollenhauer et al., 2011; Moran et al., 2005; Mulitza et al., 2008, 2017; Muller et al., 2012; Nave et al., 2007; Negre et al., 2010; Neimann & Geibert, 2003; Ng et al., 2018; Not & Hillaire-Marcel Claude, 2010; Nuttin, 2014; Nuttin & Hillaire-Marcel, 2015; Paetsch, 1991; Palchan & Torfstein, 2019; Pichat et al., 2004, 2014; Plain, 2004; Pourmand et al., 2004, 2007; Purcell, 2019; Roberts et al., 2014; Robinson et al., 2008; Rowland et al., 2017; Ruhlemann et al., 1996; Sarin et al., 1979; Saukel, 2011; Scholten et al., 1990, 1994, 2005, 2008; Serno et al., 2014, 2015; Shiau et al., 2012; Shimmield et al., 1986; Shimmield & Mowbray, 1991; Shimmield & Price, 1988; Singh et al., 2011; Skonieczny et al., 2019; Studer et al., 2015; Sukumaran, 1994; Thiagarajan & McManus, 2019; Thöle et al., 2019; Thomas et al., 2007; Thomson et al., 1993, 1995, 1999; Vallieres, 1997; Veeh et al., 1999, 2000; Veiga-Pires & Hillaire-Marcel, 1999; Voigt et al., 2017; Waelbroeck et al., 2018; Walter et al., 1997; Wengler et al., 2019; Williams et al., 2016; Winckler et al., 2008; Yang & Elderfield, 1990; Yang et al., 1995; Yu, 1994; Zhou & McManus, 2020).

Ideally, data were contributed as primary ^{230}Th, ^{232}Th, and ^{238}U activities so that $^{230}Th_{xs}{}^{0}$, mass fluxes, and focusing factors could all be re-calculated using consistent formulas and constants (e.g. ^{230}Th half-life, ^{230}Th production rate) as described above. However, a substantial portion of the data were only reported as $^{230}Th_{xs}{}^{0}$ (*n*=196, ~17% of the database), or only as mass flux (*n*=25, ~2% of the database), in which case the values may have been calculated using different constants. In an effort towards inclusivity, we have included these records in favor of greater spatial coverage at the expense of some small degree of inconsistency. Variability in constants has been relatively small, with the ^{230}Th half-life changing by less than 10% (80,000 years, Hyde, 1946; vs. 75,587 years, Cheng et al., 2013) and the production rate changing by less than 5% ($2.67*10^{-5}$ dpm/cm^3kyr, Francois et al., 2004; vs. $2.562*10^{-5}$ dpm/cm^3kyr, calculated in Section 2.1). As we focus on two relatively young time periods, the combined effect of these inconsistencies should yield only minor deviations between the reported values and those that would have been determined using the updated constants applied here.

All data are presented using the age models in the original publications. Generally, the ages are derived from radiocarbon or $\delta^{18}O$ stratigraphy, but some data (particularly core-tops) have no or only basic age information based on assumed constant sedimentation rates. As the associated uncertainties do not permit precision at millennial time scales, we focus only on the Late Holocene (LH) and the Last Glacial Maximum (LGM) and do not consider deglacial events such as Heinrich Stadial 1, for which more stringent age constraints would be required. We conducted sensitivity tests to determine the optimal time frame for the Holocene (0-3, 0-5, 0-10 ka) and the LGM (19-23 ka, 18-24 ka, 18.5-23.5 ka) (Supplementary Figure 2). The majority of records show only minimal deviation amongst the different time windows; the main effect of reducing the time window is to limit the number of cores included.

For example, defining the Holocene as 0-3 ka results in 825 cores (71% of the database) whereas defining the Holocene as 0-5 ka yields 982 cores (84% of the database) and 0-10 ka includes 1068 cores (92% of the database). Although by definition the Holocene spans 0-11.7 ka, we focus here on the late Holocene (0-5ka) in order to (i) avoid intra-Holocene climatic variations, (ii) minimize potential incorporation of deglacial values due to age model uncertainties, and (iii) better align the duration (5kyrs) integrated for both time slices.

For the LGM time slice, we tested three different chronozones based on the recommendations from Mix et al. (2001). The effect on the database for the three different time windows is minimal: 297 cores (25% of the database) for 18-24 ka vs. 266 cores for 19-23 ka (23% of the database). We select the intermediate option (18.5-23.5 ka, 281 cores, 24% of the database) as the best compromise between sustaining adequate spatial coverage and limiting the potential incorporation of data from the bounding Heinrich events due to age model uncertainties. Henceforth, we define the Late Holocene time slice as 0-5 ka and the LGM time slice as 18.5-23.5 ka.

Finally, all data have been screened for quality control, where records were passed when they positively met the criteria described below (Table 1). In addition to raw radionuclide concentrations and age model constraints, we considered whether stated uncertainties were available, the associated magnitude of those errors, and the specified lithogenic corrections. A total of 6 cores (0.5% of the database) were excluded from our analysis because the data failed to pass our criteria. Lithogenic corrections (Section 2.3.1) were applied using the $(A_{238U}/A_{232Th})_{lith}$ reported in the original publication (Supplementary Figure 1), generally ranging between 0.4 and 0.7, but three cores were excluded due to high reported $(A_{238U}/A_{232Th})_{lith}$ (greater than 0.8). An additional three coretops without age control were excluded because the resulting calculated fluxes were anomalously high (e.g., by an order of magnitude) compared to neighboring cores with better age constraints.

Overall quality levels were computed by summing each record's scores on the individual criteria. A record is optimal if it is based on a chronology that is constrained by $\delta^{18}O$ or ^{14}C and it provides both the raw nuclide concentrations and the associated errors. About one quarter of the records in the database achieved this highest quality level. The large majority of the records in the database are good, passing 2 of the 3 criteria, while the remaining quarter are fair or poor quality. Restricting the database by quality level primarily reduces the spatial coverage, with little impact on the overall data patterns observed (Supplementary Figure 3). Time slice data (LH and LGM) and quality screening for all sites are provided in Supplementary Table 1. Maps of raw $^{230}Th_{xs}^{0}$ are provided in Supplementary Figure 4.

3. ^{230}Th Global Database Results

3.1 Atlantic Ocean

Holocene mass fluxes in the Atlantic (Figure 1A, Table 2, Supplementary Figure 5) are highest in the northwestern basin, particularly Baffin Bay and the Labrador Sea, where fluxes reach values as high as ~12 g/cm^{2}kyr. In the Nordic Seas, mass fluxes range from <1 g/cm^{2}kyr to 2.3 g/cm^{2}kyr, and are generally lower than fluxes in the central northern basin to the south of Iceland, which range from 1-5 g/cm^{2}kyr. Most equatorial Atlantic sites show mass fluxes between 1 and 2 g/cm^{2}kyr, except near the mouth of the Amazon River. Mass fluxes are lower in the South Atlantic than in the North, almost all below 2 g/cm^{2}kyr.

During the LGM (Figure 1B), mass fluxes are high (5-20 g/cm^{2}kyr) in Baffin Bay, the Labrador Sea, and in the western North Atlantic subtropical gyre, all sites that likely received glaciogenic sediment from the Laurentide Ice Sheet. Mass fluxes at sites off western Europe fall between 3 and 5 g/cm^{2}kyr, while subtropical sites near the Mid-Atlantic Ridge have the lowest fluxes (1-2 g/cm^{2}kyr) in the North Atlantic. Nordic Seas mass fluxes in the LGM range between 2-4 g/cm^{2}kyr, up to double the Holocene fluxes at these locations. Much of the North Atlantic basin thus shows higher LGM mass flux relative to the Holocene (Figure 1C). South Atlantic LGM fluxes are lower than those in the northern basin: almost all fall below 2 g/cm^{2}kyr, with a few exceptions near the equator or the Southern Ocean. LGM/Holocene mass flux ratios in the South Atlantic are mostly less than or equal to 1, except for a handful of sites showing a doubling to tripling of mass fluxes during the LGM off southern Brazil and in the southern Cape Basin. There is no significant trend in LGM/Holocene mass flux ratios with core site water depth.

Holocene focusing factors tend to be >1 in the western Atlantic (Figure 2A), as well as near continental margins in the Eastern Atlantic. A few sites in the Nordic Seas, southeast of the Labrador Sea and in the equatorial Atlantic show focusing factors <1, but sites with positive focusing factors are much more common, reflecting intentional sampling bias towards regions with rapidly accumulating sediments. LGM focusing factors are lower than 1 in broad regions of the North Atlantic, with focusing only occurring at a few sites in the central western Atlantic or at continental margins in the Eastern Atlantic. There appears to be a latitudinal divide in the

North Atlantic, with all but one site north of 50˚N having LGM/Hol <1, indicating less focusing in the LGM relative to the Holocene in this region.

3.2 Pacific Ocean

Holocene mass fluxes in the Pacific (Figure 1A, Table 2, Supplementary Figure 5) are highest along the continental margins and in the Bering Sea, where fluxes reach up to ~8 g/cm^{2}kyr. The lowest mass fluxes occur in the North and South Pacific gyres (<0.5 g/cm^{2}kyr). It is possible that even lower mass fluxes may exist in the centers of the gyres that have not yet been sampled, and where accumulation rates are so low (0.5 cm/kyr or less, Schmitz et al., 1986) that LGM and Holocene sediments are mixed by bioturbation. Mass fluxes are generally higher in the western Pacific (120 to 180˚E, >1 g/cm^{2}kyr) than in the eastern Pacific (-180 to -70˚E, <1 g/cm^{2}kyr). Along the equatorial Pacific, Holocene mass fluxes average about 1 g/cm^{2}kyr, with a latitudinal gradient that mirrors the decreasing productivity trend with increasing distance from the nutrient-rich zone of equatorial upwelling. For example, at the Line Islands (approximately -160˚E), Holocene mass fluxes along a latitudinal transect of 9 sites steadily decrease from ~1.8 g/cm^{2}kyr at the equator (0.2˚S) to 0.8 g/cm^{2}kyr at the northernmost site (7.0˚N) (Costa et al., 2016, 2017a; Jacobel et al., 2017b), a trend that is not captured in age-model based mass accumulation rates. The equatorial Pacific also manifests a distinct zonal distance effect (Supplementary Figure 6), with the lowest mass fluxes occurring in the central equatorial Pacific (~0.5 g/cm^{2}kyr) and increasing more or less monotonically towards the continental margins.

The existing data show that LGM mass fluxes (Figure 1B) were high along the continental margins and low within the North and South Pacific gyres. Unlike in the Atlantic, proximity to ice sheets had only a minor impact on adjacent marine mass fluxes, specifically in the northeastern Pacific near the Cordilleran Ice Sheet (Figure 1B). A more systematic shift in mass fluxes occurred in the Okhotsk Sea and western Subarctic Pacific, where glacial mass fluxes were generally >2 g/cm^{2}kyr and as high as 5.8 g/cm^{2}kyr. Along the equator, glacial mass fluxes averaged 1.3 g/cm^{2}kyr and displayed the same zonal and meridional mass flux trends as in the Holocene. The LGM/Holocene mass flux ratio was greater than 1.1 for the majority of the Pacific Basin (Figure 1C). Only parts of the South Pacific and western equatorial Pacific have LGM/Holocene mass flux ratios that are less than or equal to 1. There is no significant trend in LGM/Holocene mass flux ratios with core site water depth.

Constraints on focusing factors in the Pacific are spatially limited, with coverage of the subtropical gyres practically absent. Holocene focusing factors are generally greater than 1 (Figure 2A), and only five sites record winnowing (Ψ=0.67-0.98) in the Holocene, on the Ontong Java Plateau, the Sulu Basin, and the eastern Japanese coast. Sites in the equatorial Pacific have slightly higher average rates of focusing during the Holocene (Ψ=2.8) than in the LGM (Ψ=2.4), but zonal and/or meridional trends in focusing appear less pronounced than those of mass fluxes. In fact, almost all sites in the Pacific show lower rates of sediment focusing during the LGM relative to the Holocene (Figure 2C).

3.3 Indian Ocean

Data coverage in the Indian Ocean is relatively low compared to other ocean basins (Figures 1-2, Table 2, Supplementary Figure 5). Coverage in this region is also 4 times greater for the Holocene (n = 83) than the LGM (n = 21). Holocene mass fluxes increase near the continental margin in the northern Indian Ocean, in the eastern Indian Ocean along the coast of Australia, and in the western Indian Ocean near the southeast coast of Africa (Figure 1A). The few sites that approach the subtropical gyre suggest Holocene mass fluxes are quite low there, down to 0.15 g/cm^{2}kyr. LGM mass fluxes generally show similar spatial patterns, albeit with far fewer data (Figure 1B). High glacial mass fluxes occurred in the Red Sea (up to 3.46 g/cm^{2}kyr) and Arabian Sea (4.03 g/cm^{2}kyr), while low glacial mass fluxes still characterized the sites off Madagascar (0.90 g/cm^{2}kyr) and near the subtropical gyre (0.23 g/cm^{2}kyr). Of the sites with both LGM and Holocene data, about half experienced lower mass fluxes during the LGM relative to the Holocene (LGM/Hol<1, Figure 1C), with the possible exception of the core near the subtropical gyre.

Sediment focusing in the Indian Ocean is poorly constrained (Figure 2) and thus it is difficult to draw any robust conclusions about the remobilization of sediment along the seafloor and how it affects ^{230}Th burial in this region as a whole. In the Red Sea, sediment focusing is between 1 and 2.2 in the Holocene, and two of the three records have high sediment focusing (Ψ=3.9-6.5) during the LGM. Extreme winnowing (Ψ=0.25) is calculated during the Holocene for one site just to the north of Madagascar. During the LGM, several sites along the west coast of Australia showed no or relatively low degrees of sediment focusing (Ψ=0.95-1.9).

3.4 Southern Ocean

The Southern Ocean is defined here as regions south of the Subantarctic Front, comprising all records south of 55˚S in the Pacific sector and 50˚S in the Atlantic and Indian sectors. Holocene mass fluxes in the Southern Ocean (Figure 1A, Table 2, Supplementary Figure 5) are fairly low, with over half of the sites having values greater than or equal to 1 g/cm^{2}kyr. The highest mass fluxes in the Holocene occur in the Indian sector, at 4.9 g/cm^{2}kyr. Within the Atlantic sector, adjacent sites sometimes show inconsistent results. For example, at 5-6˚E, 50-53˚S, three different mass fluxes are reported: 3.30 g/cm^{2}kyr at ODP1094 (Jaccard et al., 2013; Robinson et al., 2009), 1.64 g/cm^{2}kyr at TN57-13PC4 (Anderson et al., 2009), and 0.66 g/cm^{2}kyr at PS1759 (Geibert et al., 2005; Walter et al., 1997).

Data coverage during the LGM is considerably reduced, dropping to about 13% of what is available for the Holocene (Figure 1B, Table 2). Most of these records (26 of 35) are in the Pacific sector, with only one in the Indian sector. Mass fluxes are highest (up to 5.7 g/cm^{2}kyr) in the Atlantic sector, particularly at the sites near the Weddell Sea (within 500 km), which may have received enhanced delivery of ice rafted debris during the glacial period. Many sites in the Atlantic sector had higher LGM mass flux relative to the Holocene (Figure 1C). In the Pacific sector, glacial mass fluxes were generally lower in the Antarctic Zone (LGM/Hol = 0.70-0.97, 95% confidence) and higher in the Subantarctic Zone (LGM/Hol = 0.93-2.10, 95% confidence).

As in the Indian Ocean, sediment focusing in the Southern Ocean is poorly constrained (Figure 2). In the Holocene (Figure 2A), sediment focusing is generally above 1, with particularly high values ($\Psi \geq 10$) at two sites in the Atlantic sector and two sites in the Indian sector. The three sites with sediment winnowing (Ψ = 0.34-0.86) in the Holocene are all in the Pacific sector, and they range from the margin of the Southern Ocean (50˚S) into the Antarctic zone (64˚S). In the LGM, sediment focusing ($\Psi > 1$) occurs everywhere but the Weddell Sea (Ψ = 0.13) and south of New Zealand (Ψ = 0.88). This same site from New Zealand is the only one that shows greater sediment focusing during the LGM (LGM/Hol of 1.3). The other five sites that have focusing factors in both the Holocene and the LGM all show substantially lower rates of sediment focusing during the glacial period (LGM/Hol= 0.09-0.52).

3.5 Arctic

In the Arctic Ocean, mass flux varies from 0.13 to 7.24 g/cm^{2}kyr during the Holocene (Figure 1A, Table 2, Supplementary Figure 5), and the highest mass fluxes are located close to the coast in the Canadian Arctic shelf. In contrast, cores located in the central Arctic ocean have mass fluxes ranging from 0.2 to 1.5 g/cm^{2}kyr, with no distinction between Amerasian and Eurasian basins. Variations in mass flux within the central Arctic appear to be linked to both water depth and physiographic features of the core location (e.g. proximity to ridge). The spatial difference in mass fluxes between central Arctic and coastal area reflects the large difference of sediment input within the different parts of the Arctic Ocean.

Sedimentation in the Arctic Ocean during the LGM was limited (Figure 1B), and several cores may even contain a hiatus during this period (Not & Hillaire-Marcel, 2012; Poore et al., 1999). Therefore mass flux data for the LGM are quite sparse. Generally lower mass fluxes (0.12-0.80 g/cm^{2}kyr) occurred during the LGM in comparison with the Holocene, which is consistent with a slow-down of the sedimentation process in the Arctic Ocean during colder periods characterized by extended ice cover. Near the Canadian Arctic Shelf, where Holocene mass fluxes are relatively high for the Arctic, the resulting LGM/Hol mass flux ratios are all below one (LGM/Hol=0.37-0.92, Figure 1C).

Sediment focusing in the Arctic is poorly constrained (Figure 2) and thus it is difficult to draw any robust conclusions about the remobilization of sediment along the seafloor and how it affects ^{230}Th burial in this region as a whole. At 140-150˚E, sediment focusing in the Holocene is minimal (Ψ=1.09-1.38, Figure 2A), but higher degrees of focusing (Ψ=1.46-3.34) are found near the Bering Strait (-175 to 175˚E). Only one site, north of western Greenland (-61˚E), contained sufficient data to assess sediment focusing in the LGM (Figure 2B), during which this site demonstrated sediment focusing (Ψ=2.03) within the range observed in the Holocene.

4. <u>Sediment fluxes under Last Glacial Maximum climate conditions</u>

The response in sedimentary mass fluxes to glacial climate conditions varied amongst individual ocean basins (Table 2). The Atlantic is the only ocean with significantly higher mass fluxes during the LGM (2.42-4.39 g/cm^{2}kyr; all ranges are at the 95% confidence level) relative to the Holocene (1.77-2.05 g/cm^{2}kyr). The Pacific, Indian, and Southern Oceans also had higher mass fluxes during the LGM relative to the Holocene, but they were not significantly greater. In contrast to the other basins, the Arctic is the only ocean with significantly lower mass fluxes during the LGM (0.13-0.63 g/cm^{2}kyr) relative to the Holocene (1.34-3.44 g/cm^{2}kyr).

This basin-specific variability in glacial mass flux suggests that multiple mechanisms were simultaneously active but heterogeneously distributed in altering mass fluxes. For example, in the North Atlantic, mass fluxes were likely high due to enhanced glacial terrigenous input including ice-rafted debris (e.g., McManus et al., 1998) that more than compensated for lower $CaCO_3$ burial (e.g., Crowley, 1985). Lower glacial sea level may have allowed more efficient transport of sediments to the deep sea rather than storage on the continental shelves (Francois et al., 1991). This process would have been more effective at increasing basin-wide mass fluxes in the Atlantic, where the narrow basin width would concentrate these "additional" sediments into a more confined region than in, e.g., the Pacific. Globally higher dust flux (e.g., Kohfeld & Harrison, 2001; Kienast et al., 2016) also may have contributed to higher mass fluxes in the Atlantic, particularly downwind of the Sahara. In other ocean basins, windblown dust deposition is only a small net contributor to sediment fluxes. In the equatorial Pacific, mass fluxes were likely higher due to enhanced glacial $CaCO_3$ preservation (e.g., Anderson et al., 2008; Farrell & Prell, 1989, Cartapanis et al., 2018), and in the western Pacific warm pool, due to land exposure and erosion. Mass fluxes may have been lower in the Arctic and certain sites in the Southern Ocean due to the inhibiting effects of sea ice formation on the biological production of particles. Generally, glacial sediment fluxes were higher almost everywhere in the northern hemisphere, possibly because of the erosive presence of continental ice sheets. Large portions of the south Pacific, south Atlantic, Southern Ocean and Indian Ocean have few if any constraints during the LGM. Whether or not mass fluxes in these regions may have changed in the past is still an open question for future research.

5. Modeling ^{230}Th: State of the Art

5.1. From simple 1D scavenging models to integration of ^{230}Th into Earth System models

Modeling ^{230}Th in the ocean began with 1-D analytical models (Bacon & Anderson, 1982; Clegg et al., 1991; Nozaki et al., 1981; Nozaki & Horibe, 1983; Roy-Barman et al., 1996), which demonstrated that only reversible scavenging was able to reproduce the observations of both the dissolved and particulate vertical profiles. To explain more complex (nonlinear) ^{230}Th profiles, more elaborate box models were developed that could account for different transport conditions and particle regimes under different ocean conditions, such as upwelling of deep water masses in the Southern Ocean (Rutgers van der Loeff & Berger, 1993; Chase et al., 2003; Venchiarutti et al., 2011; Rutgers van der Loeff et al., 2016; Roy-Barman et al., 2019), convection of deep water masses in the North Atlantic (Moran et al., 1995, 1997; Vogler et al., 1998) and lateral exchange between open-ocean and ocean-margin regimes (Anderson et al., 1983, Lao et al., 1992; Roy-Barman, 2009). More recently, ^{230}Th has also been integrated into complex geographic schemes in 2-D models (Luo et al., 2010; Marchal et al., 2000), in 3-D models of intermediate complexity (Henderson et al., 1999; Missiaen et al., 2019; Rempfer et al., 2017; Siddall et al., 2007, 2005), and in global climate models (GCMs) (Dutay et al., 2009; Rogan et al., 2016; Gu & Liu, 2017; Van Hulten et al., 2018). The models of intermediate complexity are generally computationally efficient (i.e. able to produce 1000 years of simulations in a few hours), but their spatial resolution is rather coarse (e.g., Henderson et al., 1999; Siddall et al., 2005) and/or the particle representation contains strong simplifications (e.g., Missiaen et al., 2019; Siddall et al., 2005). Conversely, the GCMs embed more sophisticated particle computation (Van Hulten et al., 2018), but their use is restricted to shorter simulations (hundreds of years).

Thorium removal to sediments is primarily driven by two major parameters 1) the particle fluxes (concentrations and settling speed) and 2) the partition coefficients, or the affinity of each particle type for scavenging Th. Most early models did not parameterize different particle types but instead used a homogeneous particle field (Henderson et al., 1999; Luo et al., 2010). Now, most 3-D models at least consider 3 different biogenic particle types: calcium carbonate ($CaCO_3$), particulate organic carbon (POC), and opal. Some models also include lithogenic (dust and fluvial) particles (Siddall et al., 2005; Van Hulten et al., 2018) or other aerosols like volcanic ash (Rogan et al., 2016), but uncertainty regarding their influence on Th scavenging has justified their omission in other models (e.g., Gu & Liu, 2017; Missiaen et al., 2019). At the same time, all models face challenges in reproducing the observed particle size spectrum. Many models still employ one single particle size class with a uniform settling speed of 1000 m/yr, which is consistent with estimates derived from observed particulate ^{230}Th profiles (Anderson et al., 2016; Gdaniec et al., 2018; Krishnaswami et al., 1976). NEMO-PISCES (Dutay et al., 2009; Van Hulten et al., 2018) accounts for 2 particle size classes: fast (18,200 m/yr) and slow (730 m/yr) sinking particles, while HAMOCC has a parametrization of the scavenging coefficients that implicitly accounts for the observed variability in particle sizes (Heinze et al., 2006; Henderson et al., 1999).

Thorium scavenging has been represented in two distinct ways in models. The first method considers only one tracer, the total ^{230}Th activity for transport (advection and diffusion), and partitions it into dissolved and particulate activities using equilibrium partition coefficients (e.g. Dutay et al., 2009; Gu & Liu, 2017; Siddall et al., 2005, 2007). The second method considers dissolved and particulate ^{230}Th activities as two tracers transported by the model and regulates the exchange between the two phases using adsorption and desorption rate constants (e.g. Marchal et al., 2000; Missiaen et al., 2019; Rempfer et al., 2017) or partition coefficients (Henderson et al., 1999; van Hulten et al, 2018). Most models (Gu & Liu, 2017; Rempfer et al., 2017; Siddall et al., 2005, 2007) initiate with partition coefficients (K_d) that were determined on the JGOFS campaigns in the Pacific Ocean (Chase et al., 2002), but due to the large uncertainties on these observations (Chase et al., 2002; Chase and Anderson, 2004; Hayes et al., 2015a; Luo & Ku, 2004; Roy-Barman et al., 2005), the models subsequently treat the K_d as tunable parameters. HAMOCC (Heinze et al., 2018) is the only model currently updated with the newer scavenging coefficients from the Atlantic GEOTRACES section (Hayes et al., 2015b). In NEMO-PISCES

(Dutay et al., 2009; Van Hulten et al., 2018) and iLOVECLIM (Missiaen et al., 2019), the ^{230}Th scavenging coefficients are scaled to the particle fluxes rather than based on data from either JGOFS or GEOTRACES.

Incorporation of additional scavenging processes (such as described in Section 6.2 and 6.3) is only just beginning. To date, only Bern 3D (Rempfer et al., 2017) accounts for particle resuspension in benthic nepheloid layers, which they found improved their model-data agreement for dissolved and particulate water column ^{230}Th activities. The impacts of hydrothermal scavenging have not yet been considered in any ^{230}Th models. Finally, all the above cited studies mostly focus on reproducing the modern dissolved and particulate water column ^{230}Th. Although some studies also performed sensitivity tests for changes in settling speed (Siddall et al., 2005), scavenging coefficients (Gu & Liu, 2017; Siddall et al., 2005) or circulation strength (e.g., Missiaen et al., 2019; Rempfer et al., 2017; Gu & Liu, 2017; Siddall et al., 2007), no simulations are yet available for ^{230}Th scavenging under past climate conditions.

5.2. Modern Th flux to the sediments in models

In this section we compare the pre-industrial outputs of two GCMs (Figure 3): NEMO-PISCES (Dutay et al., 2009; Van Hulten et al., 2018) and CESM (Gu & Liu, 2017), and two models of intermediate complexity: iLOVECLIM (Missiaen et al., 2019) and HAMOCC (Heinze et al., 2006, 2018). We evaluate the ^{230}Th flux to the sediments (F) normalized by the production of ^{230}Th in the overlying water column (P). F/P values equal to 1 would indicate that ^{230}Th is buried in the sediments at the rate at which it is produced, whereas F/P values above or below 1 indicate that ^{230}Th has been transported away from its production site, either by ocean circulation or by diffusive fluxes along concentration gradients. Observations of F/P are sparse as they require independent flux calculations, either from bottom moored sediment traps (below 2000m) or an independent constant flux proxy (such as ^{3}He) in sediments. We compare the model output data with bottom moored sediment traps primarily in the North Pacific and North Atlantic (Yu et al., 2001), the Equatorial Pacific (Lyle et al., 2014), Southern Ocean (Chase et al., 2003), and in the Arabian Sea (Scholten et al., 2005).

iLOVECLIM, CESM, and NEMO-PISCES (Figure 3A, 3C, and 3D) produce a consistent pattern for F/P, in which ^{230}Th is transported and accumulated (F/P > 1) at the equator and in coastal areas, especially along the east coast of Japan, on the west African coast, and along the American coasts. Conversely, ^{230}Th is removed (F/P < 1) from the basin interiors and subtropical gyres. In these 3 models, the ^{230}Th burial patterns closely resemble primary productivity, with excess ^{230}Th burial in high productivity areas and deficit ^{230}Th burial in oligotrophic and low productivity areas. Interestingly, HAMOCC (Figure 3B) is the only model that displays a completely different pattern with spatially homogenous F/P except in the North Atlantic and in the Southern Ocean, where ^{230}Th is preferentially removed. This difference may be related to the choice of the scavenging coefficients, which are similar in iLOVECLIM, CESM and NEMO-PISCES and different in HAMOCC, and/or to the particle fields themselves. Modelled F/P broadly agree with sediment trap observations (Figure 3E), in that continental margins tend to have high values and oligotrophic values have low values. The best correlation between data and model occurs in NEMO-PISCES, although the skill remains modest (Figure 3D, R^2=0.22). Substantial divergence between estimates is more likely at shallow depths (< 2.5 km, Figure 3E); otherwise the models tend to slightly overestimate the F/P relative to the sediment traps. Overall, iLOVECLIM and HAMOCC have F/P ratios that are closest to 1, suggesting minimal deviation of ^{230}Th burial from ^{230}Th production, while NEMO-PISCES has the largest divergence from 1.

This brief model comparison raises a few questions:

- How do particle parameterization, settling speed, and scavenging coefficients influence the inter-model agreement or disagreement?
- Are the models too sensitive to scavenging by biogenic particles vs lithogenic particles?
- How do the particulate and dissolved concentrations at the bottom ocean grid-cell compare to individual GEOTRACES profiles including anomalous features like benthic nepheloid layers or hydrothermal scavenging?

Answering those questions would require a full model intercomparison project comparing the fields of dissolved and particulate activities to the available GEOTRACES data as well as coretop measurements, which is beyond the scope of this paper. Yet, the work presented here highlights the diversity in ^{230}Th modeling and demonstrates that modeling studies can be helpful in evaluating the assumptions and determining the spatial efficacy of ^{230}Th-normalization.

6. Uncertainties and limits of the constant ^{230}Th flux model

6.1 Boundary Scavenging

The application of ^{230}Th as a constant flux proxy relies on the assumption that net lateral transport by eddy diffusion and advection in the water column are negligible components of the local ^{230}Th mass balance. This assumption is often presumed to be justified *a priori* (François et al., 2004), since the residence time of ^{230}Th averaged over the full water column is 20-40 years, while the timescale for basin-scale mixing and deep-ocean ventilation is on the order of centuries (Sarmiento & Gruber, 2006). However, spatial gradients in scavenging intensity throughout the ocean (Bacon, 1988) may more efficiently remove scavenging-prone elements from the water column in a high particle flux zone compared to an adjacent low particle flux zone (Anderson et al., 1983; Roy-Barman et al., 2009). This situation creates a concentration gradient in the water column that in turn generates a dispersive transport (advection + eddy diffusion) of the affected element toward the high particle flux zone, a process called *boundary scavenging* as it was first identified at continental boundaries (Bacon et al., 1976). Boundaries are now defined more broadly, and they can include productivity gradients such as those driven by upwelling in the central equatorial Pacific (e.g., Costa et al., 2017a), which can occur far from any continental margin.

Where boundary scavenging can be quantified, the offset between ^{230}Th burial flux (F) and its overlying production (P) can be estimated. A simple particle flux module incorporated into a general circulation model suggested that 70% of the seafloor receives a ^{230}Th flux that is within 30% of the overlying production (Henderson et al., 1999). In other words, in most of the ocean, ^{230}Th-estimated mass fluxes are within 30% of their true value (F/P = 0.7-1.3). Furthermore, the deviations from overlying production are not simply a spatially uniform random error but a predictable property dependent on other oceanographic conditions, such as surface productivity and local particle composition, for example. There was relatively little water column data available to assess this model result at the time of its publication, but the annually averaged flux of ^{230}Th into deep sediment traps (Bacon et al., 1985; Scholten et al., 2005; Yu et al., 2001) have tended to support the roughly 30% uncertainty in the assumption of deep sea ^{230}Th flux.

With higher precision and sample throughput of seawater thorium measurements afforded by modern mass spectrometry techniques, the GEOTRACES era allowed quantification of spatial concentration gradients in ^{230}Th and lateral redistribution of ^{230}Th associated with boundary scavenging. In the upwelling zone off the coast of west Africa, where lateral gradients in export flux are among the steepest globally (DeVries & Weber, 2017), it was concluded that roughly 40% of the water column ^{230}Th production was being transported from the lower particle flux region around the Cape Verde Islands (F/P = 0.59) toward the high particle flux Mauritanian margin (F/P = 1.41) (Hayes et al., 2015a). In the Atlantic sector of the Southern Ocean, a scavenging gradient results in a net transport of ^{230}Th from the ice-covered, low particle-flux Weddell Sea (F/P = 0.4) towards the productive and particle-rich Antarctic Circumpolar Current region (F/P = 1.4) (Walter et al. 2000; Rutgers van der Loeff et al., 2016; Roy-Barman et al., 2019). In the highly productive eastern equatorial Pacific, it was concluded that roughly 25% of the water column ^{230}Th production was being transported from the low scavenging area in the Peru Basin (F/P = 0.76) toward the high scavenging area in the Panama Basin (F/P = 1.23) (Singh et al., 2013). All of these estimates are in qualitative agreement with the modelled transport of ^{230}Th. Future efforts to quantify boundary scavenging more precisely would benefit from more abundant observations of seawater ^{230}Th variations across gradients in scavenging intensity in addition to more precise constraints on lateral eddy diffusivity constants, which are also spatially variable.

As a consequence of boundary scavenging, sedimentary ^{230}Th accumulation may deviate from constant production in the overlying water column. High particle flux may yield surplus sedimentary ^{230}Th, in which case the mass fluxes calculated using equation 7 would be biased low. In low particle flux zones, too little ^{230}Th may be buried, and mass fluxes may be biased high. The net effect is to reduce the gradient in mass fluxes observed near a boundary. For example, ^{230}Th-normalized opal fluxes measured along a transect off west Africa would likely underestimate the difference in productivity between a near shore site and an offshore site. This systematic bias in regions where boundary scavenging is active is likely to make comparison of absolute fluxes difficult to interpret between multiple sites across the boundary. Fortunately, boundary scavenging regions are largely defined by biogeographical provinces, which are unlikely to vary relative to one another in the past (e.g., marginal sites are likely to always have had higher absolute export productivity than gyre sites). Thus mass fluxes may adequately capture relative trends in local fluxes at any one site over time (e.g., LGM to Holocene changes in opal flux), retaining sufficient efficacy in ^{230}Th normalization for many paleoceanographic inquiries.

6.2 Nepheloid layers

Nepheloid layers are regions of increased concentrations of suspended sediments near the seafloor. They are generated by high near-seafloor current velocities (>20 cm/s) that exceed the critical shear stress necessary for resuspension of particulates (Gardner et al., 2017; McCave, 1986). Persistent nepheloid layers were found to extend as much as 1000 meters above the seafloor at several stations along the GEOTRACES Section GA03 between Cape Cod and Bermuda (Lam et al., 2015). Because the nepheloid layer particles in this region are primarily of lithogenic composition (Lam et al., 2015), particulate ^{232}Th can be used as a tracer of these particles (Figure 4). Near-bottom concentrations of particulate ^{232}Th within the nepheloid layer are two orders of magnitude greater than concentrations measured at mid depth (Figure 4D). ^{230}Th activities also demonstrate anomalous behaviors in the nepheloid layer. While dissolved ^{230}Th activities increase in a near-linear fashion throughout the upper water column (Figure 4A), as expected for removal of dissolved ^{230}Th by reversible scavenging (Bacon & Anderson, 1982), ^{230}Th activity profiles then exhibit a sharp reversal just above the upper extent of the nepheloid layer at each station. This reversal indicates enhanced scavenging and removal of dissolved ^{230}Th by nepheloid layer particles, and it is accompanied, in part, by increased concentrations of particulate ^{230}Th through the same depth interval (Figure 4B).

If nepheloid layers consisted exclusively of locally resuspended sediment for which adsorbed ^{230}Th remained fully exchangeable with dissolved ^{230}Th in the surrounding seawater, then nepheloid layers would not be expected to enhance the removal of dissolved ^{230}Th from bottom water. Yet there is clear evidence that enhanced removal of dissolved ^{230}Th does occur within nepheloid layers (Figure 4A and 4B). Similar effects of nepheloid layers on dissolved and particulate ^{230}Th profiles have also been observed in the Nansen basin (GEOTRACES central Arctic section, GN04, Gnadiec et al., 2019). One possible mechanism to enhance removal of dissolved ^{230}Th within nepheloid layers would involve reduced exchangeability of sediment-bound ^{230}Th. For example, ^{230}Th could be immobilized on the sea bed due to the growth of diagenetic coatings of Fe-Mn oxides or other authigenic phases that lock adsorbed ^{230}Th into the particle structure. This diagenetic generation of fresh particle surfaces would also enable resuspended sediment to scavenge additional dissolved ^{230}Th from the water column, consistent with the observed reduction of dissolved ^{230}Th concentrations to levels well below those predicted by extrapolating trends from shallower depths (Figure 4A). Alternatively, nepheloid layers may consist of sediment resuspended from nearby topographic highs and transported laterally to the sampling locations over a time scale too short to achieve adsorption-desorption equilibrium with dissolved ^{230}Th in ambient seawater. The observation that the specific activity (dpm/g of particles) of ^{230}Th on particles within nepheloid layers is substantially less than for particles above the nepheloid layers (Figure 4C) would be consistent with this mechanism.

Lower specific activity of ^{230}Th on nepheloid layer particles would also be consistent with sources involving erosion of older sediment from which ^{230}Th had decayed, as has been observed in the Pacific Ocean (Kadko, 1983). These conditions are not mutually exclusive.

Although the processes occurring within nepheloid layers that enhance the scavenging and removal of dissolved Th remain incompletely defined, results from these stations provide compelling evidence that these processes may impose a strong bias on ^{230}Th -normalized fluxes. This bias can be illustrated by calculating the ^{230}Th-normalized flux of lithogenic particles, traced using ^{232}Th. In regions of the ocean far from continents where the lithogenic material in the water column is supplied mainly as dust, the ^{230}Th-normalized flux of particulate ^{232}Th is expected to be uniform throughout the water column (Anderson et al., 2016). This expectation is clearly violated within the nepheloid layers of the NW Atlantic Ocean, where ^{230}Th-normalized fluxes of particulate ^{232}Th increase through the nepheloid layer by an order of magnitude at Station 8, and by about a factor of 40 at Station 10 (Figure 4E). Whether this reflects lateral supply of lithogenic particles or an as-yet unidentified violation of the assumptions inherent in ^{230}Th normalization remains unknown. However, interpreting ^{232}Th fluxes from the deepest particulate samples collected by in situ filtration (Figure 4E) as recording dust fluxes would greatly overestimate the local supply of ^{232}Th by dust. Fully assessing the merits of ^{230}Th normalization in regions of nepheloid layers will require identification of 1) the source(s) of the particles (resuspension of surface sediments locally, erosion and suspension of older sediments, or lateral transport from nearby topographic highs), 2) the diagenetic processes that affect the surface-adsorption properties of resuspended particles, 3) the propagated effects of variability in nepheloid thickness and particle concentration on ^{230}Th scavenging, and 4) the 3-D mass budget of ^{230}Th within regions of nepheloid layers. Until then, we recommend consulting global compilations of information about nepheloid layers (Gardner et al., 2018a, 2018b, 2018c) and interpreting ^{230}Th-normalized fluxes in these regions with caution.

6.3 Hydrothermal scavenging

In boundary scavenging regions, rapid ^{230}Th removal creates concentration gradients that drive lateral diffusion of ^{230}Th towards areas of high particle flux (Section 6.1). Similar concentration gradients are found near mid-ocean ridges, where hydrothermal plumes laden with highly reactive metalliferous particles scavenge ^{230}Th from the water column (Hayes et al., 2015b; Pavia et al., 2018, 2019; Valk et al., 2018; Gdaniec et al., 2019). In sediment traps within 1 km of an active vent on the northern East Pacific Rise (EPR), ^{230}Th fluxes were 2-10x higher than the water column production rate (German et al., 2002), suggesting the possibility of high ^{230}Th burial rates in near-ridge environments. If a similar process occurs at other locations along the global mid-ocean ridge system, it is possible that ridges act as an important boundary sink for ^{230}Th in the open ocean (German et al., 2002). While early efforts to quantify ^{230}Th burial rates in sediments were limited by a lack of independent flux constraints (Dymond & Veeh, 1975; Shimmield & Price, 1988), more recently, the use of extraterrestrial ^{3}He to determine sedimentary ^{230}Th fluxes has permitted the independent assessment of ^{230}Th scavenging by hydrothermal plumes. ^{3}He-normalized ^{230}Th fluxes, when compared to production in the water column, provide flux to production ratios (F/P) similar to sediment traps but with the unique ability to record changes in ^{230}Th burial over geologic timescales.

On the southern EPR, F/P values in ridge crest sediments are highly variable (Figure 5). Although most F/P ratios fall in the range of 1.0-1.5, values as high as 4 were found at stratigraphic levels corresponding to the highest hydrothermal iron fluxes (Lund et al., 2019). The strong correlation between ^{230}Th and Fe fluxes indicates that hydrothermal fallout was the primary driver of the ^{230}Th signal. The data also imply that scavenging of ^{230}Th may vary over millennial time scales, with maximum ^{230}Th burial rates occurring during the last deglaciation. Elevated deglacial burial fluxes of ^{230}Th occurred at all three southern EPR sites examined thus far, which are located 8 to 28 km from the ridge crest. If the surplus ^{230}Th associated with hydrothermal scavenging originated from off-axis locations, the flanks of the southern EPR may have experienced ^{230}Th deficits during the deglaciation (Lund et al., 2019).

Hydrothermal scavenging can also influence ^{230}Th burial on mid-ocean ridges with substantially less plume coverage than the southern EPR. For example, on the Juan de Fuca Ridge (JdFR), ^{230}Th burial rates are lower than the water column production rate (F/P < 1) within 10 km of the ridge crest, while ^{230}Th burial is similar to the production rate (F/P ~ 1) in cores located more than 10 km off-axis (Figure 5A) (Middleton et al., 2020; Costa et al., 2017b). Furthermore, surplus F/P values (i.e., F/P > 1) are not as high on the JdFR as on the southern EPR, with F/P values not exceeding ~2 in samples deposited within 18 km of the ridge crest. The most important result from the JdFR, however, is the clear documentation of ^{230}Th deficits (F/P <1), presumably due to lateral diffusion of ^{230}Th from the water column at the core site location towards areas of high hydrothermal particle flux on the ridge axis (Middleton et al., 2020). Hydrothermally-influenced sediment cores recovered within the axial valley of the Mid-Atlantic Ridge also exhibit deficit ^{230}Th burial rates (F/P < 1), as observed on the JdFR (Middleton et al., 2020). However, ^{230}Th systematics in the Mid-Atlantic Ridge environment may be additionally complicated by along-axis currents and bottom scavenging induced by the unique bathymetry of slow spreading ridges (Middleton et al., 2020).

Interestingly, the hydrothermal threshold for surplus F/P ratios appears to occur at Fe fluxes of ~20 mg/cm^{2}kyr at both the JdFR and the southern EPR. F/P values greater than 1 correspond to hydrothermal Fe fluxes >20 mg/cm^{2}kyr, while F/P values less than 1 correspond to Fe fluxes <20 mg/cm^{2}kyr (Figure 5B). Whether or not this observed threshold is coincidental or meaningful will be borne out through continued research into ^{230}Th burial in a range of mid-ocean ridge settings. The JdFR and southern EPR data capture two primary consequences of hydrothermal scavenging for ^{230}Th, including higher than expected fluxes near the ridge axis and lower than expected fluxes at more distal locations.

Based on the results from each ridge, we present a conceptual model for how hydrothermal activity modifies ^{230}Th burial rates (Figure 5C) (Lund et al., 2019; Middleton et al., 2020). Surplus ^{230}Th burial where hydrothermal particle flux is high must be supplied by lateral diffusion from further off-axis, which creates ^{230}Th deficits where Fe fluxes are relatively low. Reduced ^{230}Th burial is clearly observed on the JdFR, at distances of approximately 5 to 12 km off-axis. On the southern EPR, the magnitude and spatial footprint of ridge flank ^{230}Th deficits remains unknown, and it would require analyzing ^{230}Th burial fluxes from an array of sites from the ridge crest and flanks. We suggest that a full quantitative model for the effects of hydrothermal scavenging on ^{230}Th burial be developed that combines ^{230}Th and ^{3}He analyses from a range of hydrothermal environments with variable Fe flux, plume incidence, spreading rate, and ridge geometry. In the interim, we suggest that both ^{230}Th and ^{3}He-normalization be used to assess the potential influence of hydrothermal scavenging on bulk sedimentation rates in ridge proximal locations.

6.4 Grain size effects and focusing: *Does particle size bias ^{230}Th-normalized sedimentary fluxes?*

Because small particles (<10 μm) have a large specific surface area relative to their mass, they tend to bear higher ^{230}Th concentrations relative to other particle classes in sediment (Kretschmer et al., 2010; Loveley et al., 2017; McGee et al., 2010). For example, in sediments from the Southern Ocean and southeast Atlantic, it was found that ^{230}Th concentrations were 1.6-2.2 times higher in the <2 μm fraction than in the bulk sediment (Kretschmer et al., 2010), while in the Eastern Equatorial Pacific, ^{230}Th concentrations in the <4 μm fraction ranged from 0.7-2.1 times the ^{230}Th concentrations in the bulk sediment (Loveley et al., 2017). Any process that preferentially affects fine grain size classes thus has the potential to decouple bulk sedimentary ^{230}Th concentrations from the overlying integrated water column inventory.

One such process is sediment redistribution along the seafloor, during which near bottom flow speeds >10-15 cm/s will preferentially remove fine grains (<16 μm) from areas of winnowing and re-deposit them further downstream in areas of focusing (e.g., Law et al., 2008; McCave et al., 1995, 2017). The consequences of such fine-fraction redistribution on ^{230}Th-normalized fluxes have been modeled by Kretschmer et al. (2010), with the assumptions that (i) the original vertical flux is coarser than the lateral sediment flux; (ii) lateral sediment flux is controlled by preferential transport of fines; (iii) both vertical and lateral fluxes contain the same ^{230}Th activity in the fine fraction. This model demonstrated that, in the Southern Ocean, the particle size effect may lead to an underestimation of vertical fluxes in areas of focusing and an overestimation of vertical fluxes in areas of winnowing. The estimated bias scales with both the degree of sediment focusing and the mean grain size of the focused sediment, ranging from as low as a 6% underestimation of true mass fluxes to as much as 80% underestimation (Kretschmer et al., 2010). Similarly, in the Eastern Equatorial Pacific, preferential focusing of fine grain size classes has been suggested to affect the ^{230}Th derived vertical flux at focused sites (Marcantonio et al., 2014), causing underestimations of 30% or less in most cases but maximally 70% underestimation in one sample (Loveley et al., 2017).

Importantly, in both the Southern Ocean and eastern equatorial Pacific, even the most extreme particle size effects (e.g., up to 80% underestimation) are still considerably lower than errors associated with age-model based flux estimates in these areas. In most pelagic settings, the particle size effect is likely to be less than 30% under- or over-estimation of mass fluxes, which is within the range of other errors associated with the ^{230}Th normalization technique (e.g., see Section 2). In fact, at other sites in the eastern equatorial Pacific, no positive relationship was found between the amount of cohesive silt (< 10-μm) and the ^{230}Th activity of the bulk sediment in focused cores, corroborating that the grain size effect on Th-normalized flux estimates in this area is likely small (Bista et al., 2016). This insensitivity to sediment focusing may arise because most pelagic sediment is already relatively fine (<35% coarse, McGee et al., 2010), so that there may not be any conspicuous grain size discrepancy in the lateral sediment flux relative to the vertical sediment flux, in contrast to the first assumption of the sediment remobilization model of Kretschmer (2010). Furthermore, in many places sediment focusing occurs via syndepositional transport of phytodetritus "fluff" material (Smith et al., 1996; Beaulieu et al., 2002; Nodder et al., 2007) that may incorporate particles of all size classes, so that size fractionation during winnowing and transport would not be minimal. In a practical sense, the application of ^{230}Th-normalization in paleoceanographic contexts does not appear to be particularly sensitive to the degree of sediment focusing that occurs in pelagic settings.

This resilience can be demonstrated by comparing mass fluxes of bulk sediment, fine material, and coarse material from multiple cores that experience different degrees of sediment remobilization (Figure 6), including both focusing and winnowing. A common proxy for lithogenic material, ^{232}Th is primarily carried in the fine fraction, so that any grain size fractionation of ^{230}Th will be compensated by the inverse effect on ^{232}Th activities. In contrast, coarse material (>63 μm) will be particularly sensitive to sediment remobilization, as focusing and winnowing generally do not act on these larger grain sizes. The Juan de Fuca Ridge, in the northeast Pacific (~45˚N, -135˚E, 2655-2794 m), contains 6 sites within 50 km of one another and suffers from a range of sediment focusing caused by the rough bathymetry of the mid-ocean ridge (Costa et al., 2016a; Costa & McManus, 2017). The Line Islands, in the central equatorial Pacific (~0-7˚N, -160˚E, 2798-3542 m), contain 9 sites along a rough carbonate ridge (Lyle et al., 2016), and although the core transect spans over 1000km, their extremely low dust content leads to only minor spatial trends in dust flux on glacial-interglacial timescales (Costa et al., 2016b; Jacobel et al., 2017a). Focusing factors were calculated within Marine Isotope Stages (MIS, e.g., Lisiecki & Raymo, 2005). Flux anomalies were calculated by first averaging (mean) fluxes over each MIS at each site, and then calculating the regional average flux of all sites (n = 6 for Juan de Fuca Ridge, n = 9 for Line Islands) for each MIS, subtracting this regional average from the flux at each site, and then dividing the site difference by the regional average to obtain the percent anomaly. The same procedure was applied for ^{232}Th fluxes and coarse fluxes. Samples with uncertainties (1 s.e.) greater than ±100% have been excluded.

Theoretically, focused sites (Ψ >1) would contain excess ^{230}Th, creating a negative flux anomaly and plotting in the lower right quadrant (Figure 6). Winnowed sites (Ψ <1) would have a deficit of ^{230}Th, creating a positive flux anomaly and plotting in the upper left quadrant. These deviations are expected to be damped in the ^{232}Th (fine) flux (Figure 6B) and pronounced in the coarse flux (Figure 6C). Yet, no systematic bias in any of the three fluxes - bulk, fine, or coarse - emerges as a function of focusing factors, in either region. Total fluxes, fine fluxes, and coarse fluxes may be over or underestimated at winnowed sites. Total fluxes, fine fluxes, and coarse fluxes may be over or underestimated at focused sites. In other words, the degree of sediment focusing does not appear to be a reliable predictor of flux anomalies in the sediment. Previous studies have demonstrated the resiliency of fine fraction fluxes against grain size fractionation (e.g., McGee et al., 2010), in accordance with theoretical expectations, but we demonstrate here that ^{230}Th-normalization may function adequately in coarse fraction fluxes as well. Thus, even though fine sediment may be more susceptible to sediment redistribution, its preferential mobility along the seafloor does not appear to significantly bias ^{230}Th systematics.

6.5 Diagenesis and calcium carbonate dissolution

One key assumption of ^{230}Th normalization is that the ^{230}Th adsorbed onto particles is unaltered by sediment dissolution. If, for example, 50% of the particles reaching the seafloor subsequently dissolve, then the affiliated ^{230}Th, which is highly particle-reactive, would be predicted to re-adsorb onto the remaining fraction of sediment. The sedimentary ^{230}Th concentration would then increase by a factor of two, since the same inventory of ^{230}Th is distributed over half the sediment mass, and the preserved ^{230}Th-normalized mass flux would halve. But what if the ^{230}Th did not fully re-adsorb onto adjacent particles? If instead, some or all of the newly dissolved ^{230}Th were permanently 'lost' from the sediment by advection or diffusion, then sediment dissolution would bias ^{230}Th concentrations too low and subsequent calculations of mass fluxes too high. Where systematic patterns of sediment dissolution occur, as they do for carbonate, especially below the lysocline, ^{230}Th normalized mass fluxes may be particularly susceptible to biases from loss of ^{230}Th out of the sediment.

The influence of calcium carbonate ($CaCO_3$) dissolution on ^{230}Th-normalized mass fluxes may be investigated by looking at coretop depth transects, for example in a study from seamounts across the tropical Atlantic (Rowland et al., 2017). These sites are primarily composed of $CaCO_3$ and lithogenic components, and they are proximally located such that the principle deviations in apparent preserved mass flux with depth should result from increasing carbonate dissolution with increasing depth. For each seamount, depth-dependent $CaCO_3$ concentration and ^{230}Th-normalized mass flux anomalies can be calculated relative to the shallowest coretop available (Figure 7). If ^{230}Th is conserved in the sediment as $CaCO_3$ dissolves, then the change in mass flux and the change in $CaCO_3$ should scale in a coherent manner (Figure 7, red line). Instead the data scatter broadly, with little to no relation to the expected behavior ($R^2 = 0.09$, $p = 0.22$). Some of this inconsistency may be due to loss of ^{230}Th during $CaCO_3$ dissolution, which has resulted in mass fluxes lower than predicted (Figure 7, red arrows), but most of the data do not deviate in the manner predicted by ^{230}Th loss. The comparison is unfortunately imperfect, as scatter may have also been introduced by unrelated processes, such as differential bioturbation, inconsistent coretop ages, or downward sediment transport along steep seamount slopes. A more rigorous assessment of the effects of dissolution on ^{230}Th loss would require additional data from similarly clustered sites along $CaCO_3$ preservation gradients and, ideally, independent mass flux constraints from ^{3}He.

A different approach to investigating the effects of $CaCO_3$ dissolution on ^{230}Th retention in the sediment was conducted in the equatorial Pacific. Without a shallow site to benchmark the initial $CaCO_3$ content, it is impossible to infer the absolute extent of $CaCO_3$ dissolution from the sedimentary $CaCO_3$ content. Instead, the degree of dissolution would need to be estimated using an independent $CaCO_3$ dissolution proxy, for example the fragmentation of fragile foraminiferal shells, such as those of *Globorotalia menardii* (*Menardii* Fragmentation Index, or MFI; Mekik et al., 2002, 2010). In the equatorial Pacific, a comparison of MFI-based $CaCO_3$ dissolution and ^{230}Th-normalized mass flux showed that for core tops with less than ~64% dissolution, the relationship between ^{230}Th-normalized mass fluxes and % $CaCO_3$ dissolution (Mekik & Anderson, 2018) is consistent with reasonable ^{230}Th retention in the sediment. As a consequence, the small variability mean glacial $CaCO_3$ (~86%) and interglacial $CaCO_3$ (~83%) in the equatorial Pacific (Anderson et al., 2008) is unlikely to cause glacial-interglacial biases in sediment ^{230}Th retention, even if that retention is incomplete in either time period. More extreme variability in $CaCO_3$ preservation, such as during transitional events from glacial to interglacial periods of the late Pleistocene (Anderson et al., 2008), would suggest much higher rates of $CaCO_3$ dissolution, which may be more likely to have an effect on ^{230}Th retention in sediments on millennial timescales.

In summary, ^{230}Th concentrations are observed to increase with increasing $CaCO_3$ dissolution, which confirms that some portion of ^{230}Th previously associated with the dissolved sediment is indeed retained on the remainder of the sediment. Therefore the assumption that ^{230}Th becomes re-adsorbed is at least partly valid. Additionally, the wealth of water column data now available from GEOTRACES (e.g. Hayes et al., 2015) and other work, shows no definitive indication of increased concentrations of dissolved ^{230}Th near the seafloor that would be expected if significant loss of ^{230}Th from the seabed occurred (Francois et al., 2007), arguing against the widespread loss of ^{230}Th from sediments to the water column. As yet, the scarcity of appropriate data (e.g., high-resolution depth transects and ^{3}He-normalized ^{230}Th fluxes) currently precludes a robust test of the extent of ^{230}Th loss and the conditions under which it may be problematic for the application of ^{230}Th as a constant flux proxy, which remains an outstanding question for further investigation.

7. Outlook on a new development: ^{230}Th-normalization in the water column

In addition to quantifying fluxes at the seafloor, ^{230}Th can also be used to estimate the sinking flux of particles in the water column (e.g., Figure 4E). Sinking particles can be expected to carry all of the overlying production of ^{230}Th due to U decay at any depth level in the water column. The flux of a particulate component or element can be estimated simply by measuring the ratio of that component to ^{230}Th in sinking particles. This approach is equivalent to the application of ^{230}Th normalization to sediments, except that particles collected from the water column by filters are used instead (Hirose, 2006). Thanks to advances in analytical capabilities under GEOTRACES, particulate ^{230}Th-normalization in filter samples has now been used to generate flux profiles of trace elements (Hayes et al. 2018), particulate organic carbon (Pavia et al. 2019, Hayes et al. 2018) and lithogenic dust (Anderson et al. 2016).

While this method shows considerable promise to provide unprecedented constraints on regeneration rates of marine particulate constituents, there remain assumptions that require further testing. First, similar to sedimentary ^{230}Th-normalization, model estimates and more regional measurements (e.g. in annually-averaged sediment traps) of ^{230}Th burial fluxes at different depths will be required to validate where ^{230}Th flux is equal to its integrated water column production, comparable to previous studies on sediment traps (Walter et al. 2000; Scholten et al., 2001). Second, water column ^{230}Th-normalization to date has been applied to suspended (0.8-51 μm) particles rather than sinking (e.g. >51 μm) particles due to sampling constraints on filters. Provided that the aggregation and disaggregation of small and large particles are in equilibrium (Bacon et al., 1985), fluxes determined on suspended particles will still be valid. Results from a limited number of measurements using large (>51 μm) particles indicates an offset from results obtained using the smaller size class of only a few tens of percent (Anderson et al., 2016; Pavia et al., 2019); however, additional measurements of ^{230}Th on larger, sinking particles will ultimately be needed to shed light on the particle dynamics involved in Th removal.

Provided that the assumptions inherent to the method can be validated, water column ^{230}Th-normalization on filtered particles could ultimately function as a more cost-effective, higher-resolution method than bottom-moored sediment traps for determining annual to multi-annual particulate fluxes. These fluxes would constitute an extremely powerful tool for studying upper water column biogeochemistry (e.g. the spatial pattern of organic carbon fluxes and regeneration, Pavia et al., 2019), and for providing near-bottom fluxes of material arriving to the seafloor in studies of early diagenesis.

8. Takeaways & future recommendations: The utility of ^{230}Th-normalization on a global scale

As proxies mature, the continued evaluation of their inherent assumptions is necessary to retain their relevance to the oceanographic community. In this review, we have compiled all existing ^{230}Th data and explored existing and new caveats to the proxy's functionality. Based on this discussion, we can summarize 1) the applicability of ^{230}Th as a constant flux proxy and 2) useful directions for future research.

The main takeaway of this work is that ^{230}Th-normalization, as it is typically applied in paleoceanographic research, performs sufficiently well to serve the purpose for which it is intended. That is, as yet, we have no strong evidence for significantly aberrant ^{230}Th behavior that would make age-model based mass accumulation rates or other approaches preferable. We do note, however, that there are several regions or circumstances (Figure 8) under which special consideration is recommended when interpreting ^{230}Th-normalized mass fluxes:

- *Shallow waters (<1000m)*: Low ^{230}Th inventories produced in the shallow water column may make application of ^{230}Th normalization analytically challenging.
- *Continental margins, particularly in eastern boundary current regions of high biological productivity and downwind of major dust sources (e.g., NW Africa and the Arabian Sea)*: High particle fluxes can create concentration gradients that lead to the burial of more ^{230}Th than is produced in the overlying water column (F/P >1). Absolute mass fluxes in such locations may thus be underestimated, but relative changes in mass fluxes are still likely to be robust.

- *Polar oceans*: Models and water column data suggest that boundary scavenging may be quite active in the Arctic and Antarctic seas, suggesting that ^{230}Th-normalized mass fluxes in these regions may be overestimated. We note, however, that these regions, particularly the Arctic, are the least well constrained by sedimentary data, and that the complex circulation of the Southern Ocean is notoriously difficult to capture in model simulations. Future work to improve model skill and to provide better data coverage of these regions will greatly enhance our understanding of ^{230}Th systematics in the polar oceans.
- *Hydrothermal vents*: Scavenging by hydrothermal Fe-Mn particles can lead to the enhanced burial of ^{230}Th close to active vents (F/P > 1) and reduced ^{230}Th burial on the ridge flanks (F/P < 1). The spatial domain of these effects is poorly constrained, but it may be a function of ridge-specific hydrothermal iron flux. Mass fluxes derived using ^{230}Th normalization are likely to be underestimated near vents and overestimated on ridge flanks, but as yet these effects have only been observed within ~30 km of the ridge axis. Future work in a range of hydrothermal settings with different particulate fluxes and chemistry will help establish more specific guidelines for the use of ^{230}Th as a constant flux proxy on mid-ocean ridges.
- *Benthic nepheloid layers*: Resuspension of particles from the seafloor may scavenge ^{230}Th from the water column. Although enhanced near-bottom scavenging by resuspended sediment by itself does not violate the assumptions inherent in ^{230}Th normalization, provided that 1-D mass balance remains intact, empirical evidence from the northwestern Atlantic nepheloid layers indicates a strong bias in ^{230}Th-normalized fluxes. The effects of benthic nepheloid layers on the assumptions of ^{230}Th normalization are poorly constrained, and basic questions about the processes involved remain unanswered. Future work in this area may include the incorporation of benthic nepheloid layers in modeling efforts and the application of ^{3}He-normalization to calculate F/P ratios in regions afflicted with these nepheloid layers.

Acknowledgments
We thank Zanna Chase and one anonymous reviewer for valuable feedback. K.M.C. was supported by a Post-Doctoral Scholarship at WHOI. L.M. acknowledges funding from the Australian Research Council grant DP180100048. The contribution of C.T.H., J.F.M., and R.F.A were supported in part by the US National Science Foundation (US-NSF). G.H.R. was supported by the Natural Environment Research Council [grant number NE/L002434/1]. S.L.J. acknowledges support from the Swiss National Science Foundation (grants PP002P2_144811 and PP00P2_172915). This study was supported by the Past Global Changes (PAGES) project, which in turn received support from the Swiss Academy of Sciences and the US-NSF. This work grew out of a 2018 workshop in Aix-Marseille, France, funded by PAGES, GEOTRACES, SCOR, US-NSF, Aix-Marseille Université and John Cantle Scientific. All data are publicly available as supplementary information to this document, on the National Center for Environmental Information (NCEI), and on Pangaea (links to be provided upon acceptance).

Words: 14,423
References: 272
Figures: 8
Tables: 2
Supp Figures: 7
Supp Tables: 1

References

Adams, J. A. S., Weaver, C. E. (1958). Thorium-to-Uranium ratios as indicators of sedimentary processes: Example of concept of geochemical facies. Am. Assoc. Pet. Geol. Bull., 42, 387–430.

Adkins, J. F., DeMenocal, P., Eshel, G. (2006). The "African humid period" and the record of marine upwelling from excess 230 Th in Ocean Drilling Program Hole 658C. Paleoceanography, 21(4), PA4203. https://doi.org/10.1029/2005PA001200

Adkins, J. F., McIntyre, K., Schrag, D. P. (2002). The salinity, temperature, and δ18O of the glacial deep ocean. Science, 298(5599), 1769–1773. https://doi.org/10.1126/science.1076252

Allegre, C. J., Dupre, B., Lewin, E. (1986). Thorium/Uranium ratio of the Earth. Chem. Geol., 56, 219–227.

Andersen, M. B., Stirling, C. H., Zimmermann, B., Halliday, A. N. (2010). Precise determination of the open ocean 234U/238U composition. Geochemistry Geophys. Geosystems, 11. https://doi.org/10.1029/2010GC003318

Anderson, R. F. (1982). Concentration, vertical flux, and remineralization of particulate uranium in seawater. Geochim. Cosmochim. Acta, 46, 1293–1299.

Anderson, R. F., Ali, S., Bradtmiller, L. I., Nielson, S. H. H., Fleisher, M. Q., Anderson, B. E., Burckle, L. H. (2009). Wind-driven upwelling in the Southern Ocean and the deglacial rise in atmospheric CO2. Science, 323, 1443–1448. https://doi.org/10.1126/science.1167441

Anderson, R. F., Bacon, M. P., Brewer, P.G. (1983). Removal of 230Th and 231Pa at ocean margins. Earth and Planetary Science Letters, 66, 73-90.

Anderson, R. F., Barker, S., Fleisher, M., Gersonde, R., Goldstein, S. L., Kuhn, G., Mortyn, P. G., Pahnke, K., Sachs, J. P. (2014). Biological response to millennial variability of dust and nutrient supply in the Subantarctic South Atlantic Ocean. Philosophical Transactions of the Royal Society of London, 372, 20130054. https://doi.org/20130054

Anderson, R. F., Cheng, H., Edwards, R. L., Fleisher, M. Q., Hayes, C. T., Huang, K., Kadko, D. C., Lam, P. J., Landing, W. M., Lao, Y., Lu, Y. (2016). How well can we quantify dust deposition to the ocean? Philos. Trans. A. Math. Phys. Eng. Sci., 374.

Anderson, R. F., Fleer, A. P. (1982). Determination of Natural Actinides and Plutonium in Marine Particulate Material. Analytical Chemistry, 54(7), 1142–1147. https://doi.org/10.1021/ac00244a030

Anderson, R. F., Fleisher, M. Q., Biscaye, P. E., Kumar, N., Dittrich, B., Kubik, P. W., Suter, M. (1994). Anomalous boundary scavenging in the Middle Atlantic Bight: evidence from 230Th, 231Pa, 10Be and 210Pb. Deep Sea Res. II, 41, 537–561.

Anderson, R. F., Fleisher, M. Q., Lao, Y. (2006). Glacial–interglacial variability in the delivery of dust to the central equatorial Pacific Ocean. Earth and Planetary Science Letters, 242(3–4), 406–414. https://doi.org/10.1016/j.epsl.2005.11.061

Anderson, R. F., Fleisher, M. Q., Lao, Y., Winckler, G. (2008). Modern CaCO3 preservation in equatorial Pacific sediments in the context of late-Pleistocene glacial cycles. Mar. Chem., 111, 30–46. https://doi.org/10.1016/j.marchem.2007.11.011

Anderson, R. F., LeHuray, A. P., Fleisher, M. Q., Murray, J. W. (1989). Uranium deposition in Saanich Inlet sediments, Vancouver Island. Geochim. Cosmochim. Acta 53, 2205–2213.

Anderson, R. F., Sachs, J. P., Fleisher, M. Q., Allen, K. A., Yu, J., Koutavas, A., Jaccard, S. L. (2019). Deep-Sea Oxygen Depletion and Ocean Carbon Sequestration During the Last Ice

Age. Global Biogeochemical Cycles, 33. https://doi.org/10.1029/2018GB006049

Bacon, M. P. (1984). Glacial to interglacial changes in carbonate and clay sedimentation in the Atlantic Ocean estimated from 230Th measurements. Isot. Geosci. 2, 97–111.

Bacon, M. P. (1988). Tracers of chemical scavenging in the ocean: boundary effects and large-scale chemical fractionation. Philos. Trans. R. Soc. London, 325, 147–160.

Bacon, M. P., Anderson, R. F. (1982). Distribution of thorium isotopes between dissolved and particulate forms in the deep sea. J. Geophys. Res., 87, 2045–2056.

Bacon, M. P., Huh, C.-A., Fleer, A. P., Deuser, W. G. (1985). Seasonality in the flux of natural radionuelides and plutonium in the deep Sargasso Sea. Deep Sea Res. 32, 273–286.

Bacon, M. P., Spencer, D. W., Brewer, P. G. (1976) 210Pb-226Ra and 210Po-210Pb disequilibria in seawater and suspended particulate matter. Earth and Planetary Science Letters, 32, 277-296.

Barnes, C. E., Cochran, J. K. (1990). Uranium removal in oceanic sediments and the oceanic U balance. Earth Planet. Sci. Lett. 97, 94–101. https://doi.org/10.1016/0012-821X(90)90101-3

Bausch, A. (2018). Interactive effects of ocean acidification with other environmental drivers on marine plankton. Columbia University. https://doi.org/10.7916/D81278PZ

Beaulieu, S. E. (2002) Accumulation and fate of phytodetritus on the sea floor, Oceanography and Marine Biology, Vol 40, pp. 171-232.

Biscaye, P. E., Anderson, R. F. (1988). Fluxes of particles and constituents to the eastern United States continental slope and rise: SEEP-I. Cont. Shelf Res., 8, 855–904.

Biscaye, P. E., Eittreim, S. L. (1977). Suspended particulate loads and transports in the nepheloid layer of the abyssal Atlantic ocean. Mar. Geol., 23, 155–172.

Bista, D., Kienast, S. S., Hill, P. S., Kienast, M. (2016). Sediment sorting and focusing in the eastern equatorial Pacific. Mar. Geol., 382, 151–161. https://doi.org/10.1016/j.margeo.2016.09.016

Böhm, E., Lippold, J., Gutjahr, M., Frank, M., Blaser, P., Antz, B., Fohlmeister, J., Frank, N., Andersen, M. B., Deininger, M. (2015). Strong and deep Atlantic meridional overturning circulation during the last glacial cycle. Nature, 517, 73–76. https://doi.org/10.1038/nature14059

Bohrmann, H. (2013). Radioisotope stratigraphy, sedimentology and geochemistry of Late Quaternary sediments from the Eastern Arctic Ocean. https://doi.org/10.1594/PANGAEA.809032

Borole, D. V. (1993). Late pleistocene sedimentation: a case study of the central Indian Ocean Basin. Deep-Sea Research Part I, 40(4), 761–775. https://doi.org/10.1016/0967-0637(93)90070-J

Bourdon, B., Sims, K. W. W. (2003). U-series constraints on intraplate basaltic magmatism. Rev. Mineral. Geochemistry 52, 215–254.

Bourne, M. D., Thomas, A. L., Mac Niocaill, C., Henderson, G. M. (2012). Improved determination of marine sedimentation rates using 230Thxs. Geochemistry, Geophys. Geosystems 13, Q09017. https://doi.org/10.1029/2012GC004295

Bradtmiller, L. I., Anderson, R. F., Fleisher, M. Q., Burckle, L. H. (2006). Diatom productivity in the equatorial Pacific Ocean from the last glacial period to the present: A test of the silicic acid leakage hypothesis. Paleoceanography, 21(4), PA4201. https://doi.org/10.1029/2006PA001282

Bradtmiller, L. I., Anderson, R. F., Fleisher, M. Q., Burckle, L. H. (2007). Opal burial in the equatorial Atlantic Ocean over the last 30 ka: Implications for glacial-interglacial changes in the ocean silicon cycle. Paleoceanography, 22(4), n/a-n/a. https://doi.org/10.1029/2007PA001443

Bradtmiller, L. I., Anderson, R. F., Fleisher, M. Q., Burckle, L. H. (2009). Comparing glacial and Holocene opal fluxes in the Pacific sector of the Southern Ocean. Paleoceanography, 24(2), 1–20. https://doi.org/10.1029/2008PA001693

Broecker, W. S. (1971). Calcite accumulation rates and glacial to interglacial changes in oceanic mixing, in: Turekian, K.K. (Ed.), The Late Cenozoic Glacial Ages. Yale University Press, New Haven, CT, pp. 239–265.

Broecker, W. S. (2008). Excess sediment 230Th: Transport along the sea floor or enhanced water column scavenging? Global Biogeochemical Cycles, 22(1), n/a-n/a. https://doi.org/10.1029/2007GB003057

Broecker, W. S., Lao, Y., Klas, M., Clark, E., Bonani, G., Ivy, S., Chen, C. (1993). A search for an early Holocene CaCO3 preservation event. Paleoceanography, 8(3), 333–339.

Brunelle, B. G., Sigman, D. M., Cook, M. S., Keigwin, L. D., Haug, G. H., Plessen, B., Schettler, G., Jaccard, S.L. (2007). Evidence from diatom-bound nitrogen isotopes for subarctic Pacific stratification during the last ice age and a link to North Pacific denitrification changes. Paleoceanography, 22(1), 1–17. https://doi.org/10.1029/2005PA001205

Brunelle, B. G., Sigman, D. M., Jaccard, S. L., Keigwin, L. D., Plessen, B., Schettler, G., Cook, M. S., Haug, G.H. (2010). Glacial/interglacial changes in nutrient supply and stratification in the western subarctic North Pacific since the penultimate glacial maximum. Quaternary Science Reviews, 29(19–20), 2579–2590. https://doi.org/10.1016/j.quascirev.2010.03.010

Buesseler, K. O., Antia, A. N., Chen, M., Fowler, S. W., Gardner, W. D., Gustafsson, O., Harada, K., Michaels, A. F., Rutgers van der Loeff, M., Sarin, M., Steinberg, D. K., Trull, T. (2007). An assessment of the use of sediment traps for estimating upper ocean particle fluxes. J. Mar. Res. 65, 345–416.

Buesseler, K. O., Bacon, M. P., Cochran, J. K., Livingston, H. D. (1992). Carbon and nitrogen export during the JGOFS North Atlantic Bloom experiment estimated from 234Th:238U disequilibria. Deep Sea Research Part A, Oceanographic Research Papers, 39(7–8), 1115–1137. https://doi.org/10.1016/0198-0149(92)90060-7

Burckel, P., Waelbroeck, C., Luo, Y., Roche, D. M., Pichat, S., Jaccard, S. L., Gherardi, J., Govin, A., Lippold, J., Thil, F. (2016). Changes in the geometry and strength of the Atlantic meridional overturning circulation during the last glacial (20-50 ka). Clim. Past 12, 2061–2075. https://doi.org/10.5194/cp-12-2061-2016

Cartapanis, O., Galbraith, E. D., Bianchi, D., Jaccard, S. L. (2018). Carbon burial in deep-sea sediment and implications for oceanic inventories of carbon and alkalinity over the last glacial cycle. Climate of the Past, 14(11), 1819–1850. https://doi.org/10.5194/cp-14-1819-2018

Causse, C., Hillaire-Marcel, C. (1989). Thorium and uranium isotopes in Upper Pleistocene sediments of ODP Sites 645 (Baffin Bay), 646, and 647 (Labrador Sea). In S. Srivastava, M. Arthur, & B. Clement (Eds.), Proceedings of the Ocean Drilling Program, Scientific Results (105th ed., pp. 551–560). College Station, TX: Ocean Drilling Program. https://doi.org/10.2973/odp.proc.sr.105.155.1989

Chase, Z., Anderson, R. F. (2004). Comment on “On the importance of opal, carbonate, and lithogenic clays in scavenging and fractionating 230 Th, 231 Pa and 10 Be in the ocean” by S. Luo and T.-L. Ku. Earth Planet. Sci. Lett. 220, 213–222. https://doi.org/10.1016/S0012-821X(04)00028-7

Chase, Z., Anderson, R. F., Fleisher, M. Q., Kubik, P. W. (2002). The influence of particle composition and particle flux on scavenging of Th, Pa and Be in the ocean. Earth Planet. Sci. Lett. 204, 215–229.

Chase, Z., Anderson, R. F., Fleisher, M. Q., Kubik, P. W. (2003). Scavenging of 230Th, 231Pa and 10Be in the Southern Ocean (SW Pacific sector): The importance of particle flux and advection. Deep Sea Res. Part II Top. Stud. Oceanogr. 50, 739–768.

Cheng, H., Lawrence Edwards, R., Shen, C. C., Polyak, V. J., Asmerom, Y., Woodhead, J., Hellstrom, J., Wang, Y., Kong, X., Spötl, C., Wang, X., Calvin Alexander, E. (2013). Improvements in 230Th dating, 230Th and 234U half-life values, and U-Th isotopic measurements by multi-collector inductively coupled plasma mass spectrometry. Earth Planet. Sci. Lett. 371–372, 82–91. https://doi.org/10.1016/j.epsl.2013.04.006

Chong, L. S., Berelson, W. M., Hammond, D. E., Fleisher, M. Q., Anderson, R. F., Rollins, N. E., Lund, S. (2016). Biogenic sedimentation and geochemical properties of deep-sea sediments of the Demerara Slope/Abyssal Plain: Influence of the Amazon River Plume. Marine Geology, 379, 124–139. https://doi.org/10.1016/j.margeo.2016.05.015

Clegg, S. L., Bacon, M. P., Whitfield, M. (1991). Application of a generalized scavenging model to thorium isotope and particle data at equatorial and high-latitude sites in the Pacific Ocean. J. Geophys. Res. 96, 20655. https://doi.org/10.1029/91jc01784

Coale, K. H., Bruland, K. W. (1987). Oceanic stratified euphotic zone as elucidated by 234Th:238U disequilibria. Limnol. Oceanogr. 32, 189–200.

Costa, K. M., Anderson, R. F., McManus, J. F., Winckler, G., Middleton, J. L., Langmuir, C. H. (2018). Trace element (Mn, Zn, Ni, V) and authigenic uranium (aU) geochemistry reveal sedimentary redox history on the Juan de Fuca Ridge, North Pacific Ocean. Geochim. Cosmochim. Acta 236, 79–98. https://doi.org/10.1016/j.gca.2018.02.016

Costa, K. M., Jacobel, A. W., McManus, J. F., Anderson, R. F., Winckler, G., Thiagarajan, N. (2017a). Productivity patterns in the Equatorial Pacific over the last 30,000 years. Global Biogeochem. Cycles 31. https://doi.org/10.1002/2016GB005579

Costa, K. M., McManus, J. F., Anderson, R. F., Ren, H., Sigman, D. M., Winckler, G., Fleisher, M. Q., Marcantonio, F., Ravelo, A. C. (2016b). No iron fertilization in the equatorial Pacific Ocean during the last ice age. Nature 529, 519–522. https://doi.org/10.1038/nature16453

Costa, K. M., McManus, J. F., Boulahanis, B., Carbotte, S. M., Winckler, G., Huybers, P., & Langmuir, C. H. (2016a). Sedimentation, stratigraphy and physical properties of sediment on the Juan de Fuca Ridge. Marine Geology, 380, 163–173.

Costa, K. M., McManus, J. F., Middleton, J. L., Langmuir, C. H., Huybers, P. J., Winckler, G., Mukhopadhyay, S. (2017b). Hydrothermal deposition on the Juan de Fuca Ridge over multiple glacial-interglacial cycles. Earth Planet. Sci. Lett. 479, 120–132. https://doi.org/10.1016/j.epsl.2017.09.006

Costa, K.M., McManus, J.F. (2017). Efficacy of 230Th normalization in sediments from the Juan de Fuca Ridge, northeast Pacific Ocean. Geochim. Cosmochim. Acta 197, 215–225. https://doi.org/10.1016/j.gca.2016.10.034

Crowley, T. J. (1985). Late Quaternary carbonate dissolution changes in the North Atlantic and Atlantic/Pacific Comparisons, in: Sundquist, E., Broecker, W.S. (Eds.), The Carbon Cycle and Atmospheric CO2: Natural Variations Archean to Present. American Geophysical Union, Washington, D.C., pp. 271–284.

Crusius, J., Pedersen, T. F., Kienast, S., Keigwin, L., Labeyrie, L. (2004). Influence of northwest Pacific productivity on North Pacific Intermediate Water oxygen concentrations during the

Bolling-Allerod interval (14.7-12.9 ka). Geology, 32(7), 633–636. https://doi.org/10.1130/G20508.1

Dekov, V. M. (1994). Contents of calcium carbonate, iron, uranium and thorium isotopes and their ratios in metalliferous sediments from the axial zone of the East Pacific Rise. https://doi.org/10.1594/PANGAEA.737081

Denis, D., Crosta, X., Schmidt, S., Carson, D. S., Ganeshram, R. S., Renssen, H., Bout-Roumazeilles, V., Zaragosi, S., Martin, B., Cremer, M., Giraudeau J. (2009). Holocene glacier and deep water dynamics, Adélie Land region, East Antarctica. Quaternary Science Reviews, 28(13–14), 1291–1303. https://doi.org/10.1016/j.quascirev.2008.12.024

DePaolo, D. J., Lee, V. E., Christensen, J. N., Maher, K. (2012). Uranium comminution ages: Sediment transport and deposition time scales. Comptes Rendus - Geosci. 344, 678–687. https://doi.org/10.1016/j.crte.2012.10.014

DeVries, T., Weber, T. (2017). The export and fate of organic matter in the ocean: New constraints from combining satellite and oceanographic tracer observations. Global Biogeochem. Cycles 31, 535–555. https://doi.org/10.1002/2016GB005551

Dezileau, L., Bareille, G., Reyss, J. L., Lemoine, F. (2000). Evidence for strong sediment redistribution by bottom currents along the southeast Indian ridge. Deep-Sea Research Part I: Oceanographic Research Papers, 47(10), 1899–1936. https://doi.org/10.1016/S0967-0637(00)00008-X

Dezileau, L., Ulloa, O., Hebbeln, D., Lamy, F., Reyss, J. L., Fontugne, M. (2004). Iron control of past productivity in the coastal upwelling system off the Atacama Desert, Chile. Paleoceanography, 19(3). https://doi.org/10.1029/2004PA001006

Durand, A., Chase, Z., Noble, T. L., Bostock, H., Jaccard, S. L., Kitchener, P., Townsend A. T., Jansen, N., Kinsley, L., Jacobsen, G., Johnson, S., Neil, H. (2017). Export production in the New-Zealand region since the Last Glacial Maximum. Earth and Planetary Science Letters, 469, 110–122. https://doi.org/10.1016/j.epsl.2017.03.035

Dutay, J.-C., Lacan, F., Roy-Barman, M., Bopp, L. (2009). Influence of particle size and type on 231Pa and 230Th simulation with a global coupled biogeochemical-ocean general circulation model: A first approach. Geochemistry Geophys. Geosystems 10, 1–26. https://doi.org/10.1029/2008GC002291

Dymond, J., Veeh, H. H. (1975). Metal accumulation rates in the southeast Pacific and the origin of metalliferous sediments. Earth Planet. Sci. Lett. 28, 13–22. https://doi.org/10.1038/251465a0

Edwards, R. L., Gallup, C. D., Cheng, H. (2003). Uranium-series dating of marine and lacustrine carbonates. Reviews in Mineralogy and Geochemistry, 52, 363–405. https://doi.org/10.2113/0520363

Fagel, N., Dehairs, F., André, L., Bareille, G., Monnin, C. (2002). Ba distribution in surface Southern Ocean sediments and export production estimates. Paleoceanography, 17(2), 1-1-1–20. https://doi.org/10.1029/2000pa000552

Farrell, J. W., Prell, W. L. (1989). Climatic change and CaCO3 Preservation: An 800,000 year bathymetric reconstruction from the Central Equatorial Pacific Ocean. Paleoceanography 4, 447–466.

Finneran, K. T., Anderson, R. T., Nevin, K. P., Lovley, D. R. (2002). Potential for bioremediation of Uranium-contaminated aquifers with microbial U(VI) reduction. Soil Sediment Contam. 11, 339–357.

Fleisher M. Q., Anderson R. F. (2003) Assessing the collection efficiency of Ross Sea sediment traps using 230Th and 231Pa. Deep Sea Res. Part II Top. Stud. Oceanogr. 50, 693–712.

Francis, A. J., Dodge, C. J., Lu, F., Halada, G. P., Clayton, C. R. (1994). XPS and XANES studies of uranium reduction by Clostridium sp. Environ. Sci. Technol. 28, 636–639.

Francois, R., Bacon, M. P. (1991). Variations in terrigenous input to the deep equatorial Atlantic during the past 24,000 years. Science, 251, 1473–1476.

Francois, R., Bacon, M. P., Altabet, M. A., Labeyrie, L. D. (1993). Glacial/Interglacial changes in sediment rain rate in the SW Indian sector of Subantarctic waters as recorded by 230Th, 231Pa, U, and d15N. Paleoceanography, 8(5), 611–629. https://doi.org/10.1029/93pa00784

Francois, R., Bacon, M. P., Suman, D. O. (1990). Thorium230 profiling in deep-sea sediments: High resolution records of flux and dissolution of carbonate in the Equatorial Atlantic during the last 24,000 years. Paleoceanography 5, 761–787.

Francois, R., Frank, M., Rutgers van der Loeff, M., Bacon, M. P. (2004). 230Th normalization: An essential tool for interpreting sedimentary fluxes during the late Quaternary. Paleoceanography 19, PA1018. https://doi.org/10.1029/2003PA000939

Francois, R., Frank, M., Rutgers van der Loeff, M., Bacon, M. P., Geibert, W., Kienast, S., Anderson, R. F., Bradtmiller, L. I., Chase, Z., Henderson, G. M., Marcantonio, F., Allen, S. E. (2007). Comment on “Do geochemical estimates of sediment focusing pass the sediment test in the equatorial Pacific?” by M. Lyle et al. Paleoceanography 22, PA1216. https://doi.org/10.1029/2005PA001235

Frank, M., Eisenhauer, A., Bonn, W. J., Walter, P., Grobe, H., Kubik, P. W., Dittrich-Hannen, B., Mangini, A. (1995). Sediment redistribution versus paleoproductivity change: Weddell Sea margin sediment stratigraphy and biogenic particle flux of the barium profiles. Earth and Planetary Science Letters, 136(95), 559–573.

Frank, M., Mangini, A., Gersonde, R., Rutgers van der Loeff, M., Kuhn, G. (1996). Late Quaternary sediment dating and quantification of lateral sediment redistribution applying230Thex: a study from the eastern Atlantic sector of the Southern Ocean. Geologische Rundschau, 85(3), 554–566. https://doi.org/10.1007/BF02369010

Fukuda, M., Harada, N., Sato, M., Lange, C. B., Ahagon, N., Kawakami, H., Miyashita, W., Pantoja, S., Matsumoto, T., Motoyama, I. (2013). Th-normalized fluxes of biogenic components from the central and southernmost Chilean margin over the past 22 , 000 years. Geochemical Journal, 47, 119–135. https://doi.org/10.2343/geochemj.2.0230

Galbraith, E. D., Jaccard, S. L., Pedersen, T. F., Sigman, D. M., Haug, G. H., Cook, M. S., Southon, J. R., Francois, R. (2007). Carbon dioxide release from the North Pacific abyss during the last deglaciation. Nature, 449(7164), 890–893. https://doi.org/10.1038/nature06227

Ganesh, R., Robinson, K. G., Reed, G. D. (1997). Reduction of Hexavalent Uranium from Organic Complexes by Sulfate- and Iron-Reducing Bacteria. Appl. Environ. Microbiol. 63, 4385–4391.

Gardner, W. D. (2000). Sediment trap sampling in surface water, in: Hanson, R.B., Ducklow, H.W., Field, J.G. (Eds.), The Changing Ocean Carbon Cycle, a Midterm Synthesis of the Joint Global Ocean Flux Study. Cambridge University Press, pp. 240–284.

Gardner, W. D., Mishonov, A. V., Richardson, M. J. (2018a). Decadal comparisons of particulate matter in repeat transects in the Atlantic, Pacific, and Indian Ocean basins. Geophys. Res. Lett. 45, 277–286. https://doi.org/10.1002/2017GL076571

Gardner, W. D., Richardson, M. J., Mishonov, A. V. (2018b). Global assessment of benthic nepheloid layers and linkage with upper ocean dynamics. Earth Planet. Sci. Lett. 482, 126–

134. https://doi.org/10.1016/j.epsl.2017.11.008

Gardner, W. D., Richardson, M. J., Mishonov, A. V., Biscaye, P. E. (2018c). Global comparison of benthic nepheloid layers based on 52 years of nephelometer and transmissometer measurements. Prog. Oceanogr. 168, 100–111. https://doi.org/10.1016/j.pocean.2018.09.008

Gardner, W. D., Tucholke, B. E., Richardson, M. J., Biscaye, P. E. (2017). Benthic storms, nepheloid layers, and linkage with upper ocean dynamics in the western North Atlantic. Mar. Geol. 385, 304–327. https://doi.org/10.1016/j.margeo.2016.12.012

Gdaniec, S., Roy-Barman, M., Foliot, L., Thil, F., Dapoigny, A., Burckel, P., Garcia-Orellana, J., Masqué, P., Mörth, C.-M., Andersson, P. S. (2018). Thorium and protactinium isotopes as tracers of marine particle fluxes and deep water circulation in the Mediterranean Sea. Mar. Chem. 199, 12–23. https://doi.org/10.1016/j.marchem.2017.12.002

Gdaniec, S., Roy-Barman, M., Levier M., Valk O., Rutgers van der Loeff M., Foliot, L., Dapoigny, A., Morth, M., Andersson, P. S. (2019). 231Pa and 230Th in the Arctic Ocean: implications for Boundary Scavenging and 231Pa-230Th fractionation in the Eurasian Basin. Chemical Geology, 533, 119380. https://doi.org/10.1016/j.chemgeo.2019.119380

Geibert, W., Rutgers van der Loeff, M. M., Usbeck, R., Gersonde, R., Kuhn, G., Seeberg-Elverfeldt, J. (2005). Quantifying the opal belt in the Atlantic and southeast Pacific sector of the Southern Ocean by means of 230Th normalization. Global Biogeochem. Cycles 19. https://doi.org/10.1029/2005GB002465

German, C. R., Colley, S., Palmer, M. R., Khripounoff, A., Klinkhammer, G. P. (2002). Hydrothermal plume-particle fluxes at 13 degrees N on the East Pacific Rise. Deep. Res. Part I-Oceanographic Res. Pap. 49, 1921–1940. https://doi.org/10.1016/S0967-0637(02)00086-9

Gherardi, J. M., Labeyrie, L., McManus, J. F., Francois, R., Skinner, L. C., Cortijo, E. (2005). Evidence from the Northeastern Atlantic basin for variability in the rate of the meridional overturning circulation through the last deglaciation. Earth and Planetary Science Letters, 240(3–4), 710–723. https://doi.org/10.1016/j.epsl.2005.09.061

Gherardi, J.-M., Labeyrie, L., Nave, S., Francois, R., McManus, J. F., Cortijo, E. (2009). Glacial-interglacial circulation changes inferred from 231 Pa/ 230 Th sedimentary record in the North Atlantic region. Paleoceanography, 24(2), PA2204. https://doi.org/10.1029/2008PA001696

Gottschalk, J., Skinner, L. C., Lippold, J., Vogel, H., Frank, N., Jaccard, S. L., Waelbroeck, C. (2016). Biological and physical controls in the Southern Ocean on past millennial-scale atmospheric CO2 changes. Nature Communications, https://doi.org/10.1038/ncomms11539

Gu, S., Liu, Z. (2017). 231Pa and 230Th in the ocean model of the Community Earth System Model (CESM1.3). Geosci. Model Dev. 10.

Guihou, A., Pichat, S., Nave, S., Govin, A., Labeyrie, L., Michel, E., Waelbroeck, C. (2010). Late slowdown of the Atlantic Meridional Overturning Circulation during the Last Glacial Inception: New constraints from sedimentary (231Pa/230Th). Earth Planet. Sci. Lett. 289, 520–529. https://doi.org/10.1016/j.epsl.2009.11.045

Hayes, C. T., Anderson, R. F., Fleisher, M. Q., Huang, K., Robinson, L. F., Lu, Y., Cheng, H., Edwards, R. L., Moran, S. B. (2015a). 230Th and 231Pa on GEOTRACES GA03, the U. S. GEOTRACES North Atlantic transect, and implications for modern and paleoceanographic chemical fluxes. Deep. Res. Part II 116, 29–41. https://doi.org/10.1016/j.dsr2.2014.07.007

Hayes, C. T., Anderson, R. F., Fleisher, M. Q., Vivancos, S. M., Lam, P. J., Ohnemus, D. C., Huang, K. F., Robinson, L. F., Lu, Y., Cheng, H., Edwards, R. L., Moran, S. B. (2015b). Intensity of Th and Pa scavenging partitioned by particle chemistry in the North Atlantic Ocean. Mar. Chem. 170, 49–60. https://doi.org/10.1016/j.marchem.2015.01.006

Hayes, C. T., Martínez-García, A., Hasenfratz, A. P., Jaccard, S. L., Hodell, D. A., Sigman, D. M., Haug, G. H., Anderson, R. F. (2014). A stagnation event in the deep South Atlantic during the last interglacial period. Science. 346, 1514–1517.

Heinze, C., Gehlen, M., Land, C. (2006). On the potential of 230Th , 231Pa , and 10Be for marine rain ratio determinations: A modeling study. Global Biogeochem. Cycles 20, GB2018. https://doi.org/10.1029/2005GB002595

Heinze, C., Ilyina, T., Gehlen, M. (2018). The potential of 230Th for detection of ocean acidification impacts on pelagic carbonate production. Biogeosciences 15, 3521–3539. https://doi.org/10.5194/bg-15-3521-2018

Henderson, G. M. (2002) Seawater (234U/238U) during the last 800 thousand years. Earth and Planetary Science Letters 199, 97-110.

Henderson, G. M., Anderson, R. F. (2003). The U-series Toolbox for Paleoceanography. Rev. Mineral. Geochemistry 52, 493–531.

Henderson, G. M., Heinze, C., Anderson, R. F., Winguth, A. M. E. (1999). Global distribution of the 230Th flux to ocean sediments constrained by GCM modelling. Deep Sea Res. I 46, 1861–1893.

Hickey, B. J. (2010). Reconstructing past flow rates of southern component water masses using sedimentary 231Pa/230Th (PhD thesis).

Hillaire-Marcel, C., Ghaleb, B., de Vernal, A., Maccali, J., Cuny, K., Jacobel, A. W., Le Duc, C., McManus, J. F. (2017). A New Chronology of Late Quaternary Sequences From the Central Arctic Ocean Based on “Extinction Ages” of Their Excesses in 231Pa and 230Th. Geochemistry, Geophysics, Geosystems, 18(12), 4573–4585. https://doi.org/10.1002/2017GC007050

Hirose, K. (2006). A new method to determine depth-dependent carbon export fluxes using vertical 230Th profiles. Geophysical Research Letters, 33(5), 9–12. https://doi.org/10.1029/2005GL025129

Hoffmann, S. S., McManus, J. F., Curry, W. B., Brown-Leger, L. S. (2013). Persistent export of 231Pa from the deep central Arctic Ocean over the past 35,000 years. Nature, 497(7451), 603–606. https://doi.org/10.1038/nature12145

Hoffmann, S. S., McManus, J. F., Swank, E. (2018). Evidence for Stable Holocene Basin-Scale Overturning Circulation Despite Variable Currents Along the Deep Western Boundary of the North Atlantic Ocean. Geophys. Res. Lett. 45. https://doi.org/10.1029/2018GL080187

Hyde, E. K. (1946). Determination of the half-life of ionium. No. AECD-2468.

Jaccard, S. L., Galbraith, E. D., Sigman, D. M., Haug, G. H., Francois, R., Pedersen, T. F., Dulski, P., Thierstein, H. R. (2009). Subarctic Pacific evidence for a glacial deepening of the oceanic respired carbon pool. Earth and Planetary Science Letters, 277(1–2), 156–165. https://doi.org/10.1016/j.epsl.2008.10.017

Jaccard, S. L., Hayes, C. T., Hodell, D. A., Anderson, R. F., Sigman, D. M., Haug, G. H. (2013). Two modes of change in Southern Ocean productivity over the past million years. Science. 339, 1419–1423.

Jacobel, A. W., McManus, J. F., Anderson, R. F., Winckler, G. (2017a). Repeated storage of respired carbon in the equatorial Pacific Ocean over the last three glacial cycles. Nat. Commun. 8. https://doi.org/10.1038/s41467-017-01938-x

Jacobel, A. W., McManus, J. F., Anderson, R. F., Winckler, G. (2017b). Climate-related response of dust flux to the central equatorial Pacific over the past 150 kyr. Earth Planet. Sci. Lett. 457, 160–172. https://doi.org/10.1016/j.epsl.2016.09.042

Johnson, D. A., Johnson, T. C. (1970). Sediment redistribution by bottom currents in the central Pacific. Deep Sea Res. 17, 157–169. https://doi.org/10.1016/0011-7471(70)90094-X

Jonkers, L., Zahn, R., Thomas, A., Henderson, G. M., Abouchami, W., François, R., Masque, P., Hall, I. R., Bickert, T. (2015). Deep circulation changes in the central South Atlantic during the past 145 kyrs reflected in a combined 231Pa/230Th, Neodymium isotope and benthic d13C record. Earth and Planetary Science Letters, 419, 14–21. https://doi.org/10.1016/j.epsl.2015.03.004

Kadko, D. (1983), A Multitracer Approach to the Study of Erosion in the Northeast Equatorial Pacific, Earth and Planetary Science Letters, 63(1), 13-33

Kienast, S. S., Kienast, M., Mix, A. C., Calvert, S. E., François, R. (2007). Thorium-230 normalized particle flux and sediment focusing in the Panama Basin region during the last 30,000 years. Paleoceanography, 22(2), n/a-n/a. https://doi.org/10.1029/2006PA001357

Kienast, S. S., Winckler, G., Lippold, J., Albani, S., Mahowald, N. M. (2016). Tracing dust input to the global ocean using thorium isotopes in marine sediments: ThoroMap. Global Biogeochem. Cycles 30, 1526–1541. https://doi.org/10.1002/2016GB005408

Klinkhammer, G .P., Palmer, M. R. (1991). Uranium in the oceans: Where it goes and why. Geochim. Cosmochim. Acta 55, 1799–1806.

Kohfeld K. E., Harrison S. P. (2001) DIRTMAP: the geological record of dust. Earth Sci. Rev. 54, 81-114,

Kretschmer, S., Geibert, W., Rutgers van der Loeff, M.M., Mollenhauer, G. (2010). Grain size effects on 230Thxs inventories in opal-rich and carbonate-rich marine sediments. Earth Planet. Sci. Lett. 294, 131–142. https://doi.org/10.1016/j.epsl.2010.03.021

Krishnaswami, S., Lal, D., Somayajulu, B. L. K., Weiss, R. F., Craig, H. (1976). Large-volume in-situ filtration of deep Pacific waters: Mineralogical and radioisotope studies. Earth Planet. Sci. Lett. 32, 420–429. https://doi.org/10.1192/bjp.111.479.1009-a

Ku, T.-L. (1965). An evaluation of the 234U/238U method as a tool for dating pelagic sediments. J. Geophys. Res., 3457-3474.

Ku, T.-L., Broecker, W. S. (1966). Atlantic deep-sea stratigraphy: Extension of absolute chronology to 320,000 years. Science, 151, 448–450.

Kumar, N., Anderson, R. F., Mortlock, R. A., Froelich, P. N., Kubik, P. W., Dittrich-Hannen, B., Suter, M. (1995). Increased biological productivity and export production in the glacial Southern Ocean. Nature, 378, 675–680.

Lam, P. J., Ohnemus, D. C., Auro, M. E. (2015). Size-fractionated major particle composition and concentrations from the US GEOTRACES North Atlantic Zonal Transect. Deep. Res. Part II 116, 303–320. https://doi.org/10.1016/j.dsr2.2014.11.020

Lam, P. J., Robinson, L. F., Blusztajn, J., Li, C., Cook, M. S., McManus, J. F., Keigwin, L. D. (2013). Transient stratification as the cause of the North Pacific productivity spike during deglaciation. Nature Geoscience, 6(8), 622–626. https://doi.org/10.1038/ngeo1873

Lamy, F., Gersonde, R., Winckler, G., Esper, O., Jaeschke, A, Kuhn, G., Ullermann, J., Martinez-Garcia, A, Lambert, F., Kilian, R. (2014). Increased dust deposition in the Pacific Southern Ocean during glacial periods. Science (New York, N.Y.), 343(6169), 403–7. https://doi.org/10.1126/science.1245424

Lao, Y., Anderson, R. F., Broecker, W. S. (1992). Boundary scavenging and deep-sea sediment dating: Constraints from excess 230Th and 231Pa. Paleoceanography, 7(6), 783–798.

Law, B. A., Hill, P. S., Milligan, T. G., Curran, K. J., Wiberg, P. L., Wheatcroft, R. A. (2008). Size sorting of fine-grained sediments during erosion: Results from the western Gulf of Lions. Cont. Shelf Res. 28, 1935–1946. https://doi.org/10.1016/j.csr.2007.11.006

Lippold, J., Gherardi, J. M., Luo, Y. (2011). Testing the 231Pa/230Th paleocirculation proxy: A data versus 2D model comparison. Geophysical Research Letters, 38(20), 1–7. https://doi.org/10.1029/2011GL049282

Lippold, J., Grützner, J., Winter, D., Lahaye, Y., Mangini, A., Christl, M. (2009). Does sedimentary 231Pa/ 230Th from the Bermuda Rise monitor past Atlantic Meridional Overturning Circulation? Geophys. Res. Lett. 36, L12601. https://doi.org/10.1029/2009GL038068

Lippold, J., Gutjahr, M., Blaser, P., Christner, E., de Carvalho Ferreira, M. L., Mulitza, S., Christl, M., Wombacher, F., Böhm, E., Antz, B., Cartapanis, O., Vogel, H., Jaccard, S. L. (2016). Deep water provenance and dynamics of the (de)glacial Atlantic meridional overturning circulation. Earth and Planetary Science Letters, 445, 68–78. https://doi.org/10.1016/j.epsl.2016.04.013

Lippold, J., Mulitza, S., Mollenhauer, G., Weyer, S., Heslop, D., Christl, M. (2012). Boundary scavenging at the East Atlantic margin does not negate use of 231Pa/230Th to trace Atlantic overturning. Earth Planet. Sci. Lett. 334, 317–331. https://doi.org/10.1016/j.epsl.2012.04.005

Loubere, P., Mekik, F., Francois, R., Pichat, S. (2004). Export fluxes of calcite in the eastern equatorial Pacific from the Last Glacial Maximum to present. Paleoceanography, 19(2), PA2018. https://doi.org/10.1029/2003PA000986

Loveley, M. R., Marcantonio, F., Lyle, M., Ibrahim, R., Hertzberg, J. E., Schmidt, M. W. (2017). Sediment redistribution and grain size effects on 230Th-normalized mass accumulation rates and focusing factors in the Panama Basin. Earth Planet. Sci. Lett. 480, 107–120. https://doi.org/10.1016/j.epsl.2017.09.046

Lovley, D. R., Phillips, E. J. P., Gorby, Y. A., Landa, E. R. (1991). Microbial reduction of Uranium. Nature 350, 413–416.

Lund, D. C., Pavia, F. J., Seeley, Eß. I., McCart, S. E., Rafter, P. A., Farley, K. A., Asimow, P. D., Anderson, R. F. (2019). Hydrothermal scavenging of 230Th on the Southern East Pacific Rise during the last deglaciation. Earth Planet. Sci. Lett. 510, 64–72. https://doi.org/10.1016/j.epsl.2018.12.037

Luo, S., Ku, T. L. (2004). On the importance of opal, carbonate, and lithogenic clays in scavenging and fractionating 230Th, 231Pa and 10Be in the ocean. Earth Planet. Sci. Lett. 220, 201–211. https://doi.org/10.1016/S0012-821X(04)00027-5

Luo, Y., Francois, R., Allen, S. E. (2010). Sediment 231Pa/230Th as a recorder of the rate of the Atlantic meridional overturning circulation: Insights from a 2-D model. Ocean Sci. 6, 381–400. https://doi.org/10.5194/os-6-381-2010

Lyle, M., Marcantonio, F., Moore, W. S., Murray, R. W., Huh, C., Finney, B .P., Murray, D. W., Mix, A. C. (2014). Sediment size fractionation and focusing in the equatorial Pacific: Effect on 230Th normalization and paleo flux measurements. Paleoceanography 29, 747–763. https://doi.org/10.1002/2014PA002616.Received

Lyle, M., Mitchell, N., Pisias, N., Mix, A., Martinez, J. I., Paytan, A. (2005). Do geochemical estimates of sediment focusing pass the sediment test in the equatorial Pacific? Paleoceanography 20. https://doi.org/10.1029/2004PA001019

Mangini, A., Dominik, J. (1978). Uranium, Thorium and ionium content of the bulk samples and amount of EDTA extracted Th-isotopes in sediment core M22_48, Ionian Sea. https://doi.org/10.1594/PANGAEA.527935

Mangini, A., Jung, M., Laukenmann, S. (2001). What do we learn from peaks of uranium and of manganese in deep sea sediments? Mar. Geol. 177, 63–78.

Marcantonio, F., Anderson, R. F., Higgins, S. M., Stute, M., Schlosser, P., Kubik, P. W. (2001). Sediment focusing in the central equatorial Pacific Ocean. Paleoceanography, 16(3), 260–267.

Marcantonio, F., Anderson, R. F., Stute, M., Kumar, N., Schlosser, P., Mix, A. (1996). Extraterrestrial 3He as a tracer of marine sediment transport and accumulation. Nature 383, 705–707.

Marcantonio, F., Lyle, M., Ibrahim, R. (2014). Particle sorting during sediment redistribution processes and the effect on 230Th-normalized mass accumulation rates. Geophys. Res. Lett. 41, 5547–5554. https://doi.org/10.1002/2014GL060477.Received

Marchal, O., Francois, R., Stocker, T. F., Joos, F. (2000). Ocean thermohaline circulation and sedimentary 231Pa/230Th ratio. Paleoceanography 15, 625–641.

Martínez-Garcia, A., Rosell-Melé, A., Geibert, W., Gersonde, R., Masqué, P., Gaspari, V., Barbante, C. (2009). Links between iron supply, marine productivity, sea surface temperature, and CO2 over the last 1.1 Ma. Paleoceanography, 24, doi:10.1029/2008PA001657. https://doi.org/10.1029/2008PA001657

McCave, I. N. (1986). Local and global aspects of the bottom nepheloid layers in the world ocean. Netherlands J. Sea Res. 20, 167–181.

McCave, I. N., Manighetti, B., Robinson, S. G. (1995). Sortable silt and fine sediment size/composition slicing: Parameters for palaeocurrent speed and palaeoceanography. Paleoceanography 10, 593–610.

McCave, I. N., Thornalley, D. J. R., Hall, I. R. (2017). Relation of sortable silt grain-size to deep-sea current speeds: Calibration of the 'Mud Current Meter.' Deep. Res. Part I 127, 1–12. https://doi.org/10.1016/j.dsr.2017.07.003

McGee, D., Marcantonio, F., Lynch-Stieglitz, J. (2007). Deglacial changes in dust flux in the eastern equatorial Pacific. Earth and Planetary Science Letters, 257(1–2), 215–230. https://doi.org/10.1016/j.epsl.2007.02.033

McGee, D., Marcantonio, F., McManus, J. F., Winckler, G. (2010). The response of excess 230Th and extraterrestrial 3He to sediment redistribution at the Blake Ridge, western North Atlantic. Earth Planet. Sci. Lett. 299, 138–149. https://doi.org/10.1016/j.epsl.2010.08.029

McGee, D., Mukhopadhyay, S. (2013) Extraterrestrial He in sediments: From recorder of asteroid collisions to timekeeper of global environmental changes, The Noble Gases as Geochemical Tracers. Springer-Verlag, Hiedelberg, Heidelberg, pp. 155-176.

McManus, J. F., Anderson, R. F., Broecker, W. S., Fleisher, M. Q., Higgins, S. M (1998). Radiometrically determined sedimentary fluxes in the sub-polar North Atlantic during the last 140,000 years. Earth Planet. Sci. Lett. 155, 29–43.

McManus, J. F., Francois, R., Gherardi, J.-M., Keigwin, L. D., Brown-Leger, S. (2004). Collapse and rapid resumption of Atlantic meridional circulation linked to deglacial climate changes. Nature, 428(6985), 834–7. https://doi.org/10.1038/nature02494

McManus, J., Berelson, W. M., Klinkhammer, G. P., Hammond, D. E., Holm, C. (2005). Authigenic uranium: relationship to oxygen penetration depth and organic carbon rain. Geochim. Cosmochim. Acta 69, 95–108. https://doi.org/10.1016/j.gca.2004.06.023

Meier, B. (2015). Evolution of the southwest Pacific across the last glacial cycle: Insights from a multi-proxy approach to biological export production. University of Bern, Master's Thesis, 57 pp.

Mekik, F., Anderson, R. F. (2018). Is the core top modern? Observations from the eastern equatorial Pacific. Quat. Sci. Rev. 186, 156–168. https://doi.org/10.1016/j.quascirev.2018.01.020

Mekik, F., Loubere, P. W., Archer, D. E. (2002). Organic carbon flux and organic carbon to calcite flux ratio recorded in deep-sea carbonates: Demonstration and a new proxy. Global Biogeochem. Cycles 16, 25-1-25–15. https://doi.org/10.1029/2001GB001634

Mekik, F., Noll, N., Russo, M. (2010). Progress toward a multi-basin calibration for quantifying deep sea calcite preservation in the tropical/subtropical world ocean. Earth Planet. Sci. Lett. 299, 104–117. https://doi.org/10.1016/J.EPSL.2010.08.024

Middleton, J. L., Mukhpoadhyay, S., Costa, K. M., Pavia, F. J., Winckler, G., McManus, J. F., D'Almeida, M., Langmuir, C. H., Huybers, P. J. (2020). The spatial footprint of hydrothermal scavenging on 230ThXS-derived mass accumuation rates. Geochimica et Cosmochimica Acta. *(in press)*.

Missiaen, L., Bouttes, N., Roche, D. M., Dutay, J., Waelbroeck, C., Pichat, S., Peterschmitt, J.-Y. (2019). Carbon isotopes and Pa / Th response to forced circulation changes : a model perspective 1–26.

Missiaen, L., Pichat, S., Waelbroeck, C., Douville, E., Bordier, L., Dapoigny, A., Thil, F., Foliot, L., Wacker, L. (2018). Downcore Variations of Sedimentary Detrital (238U/232Th) Ratio: Implications on the Use of 230Thxs and 231Paxs to Reconstruct Sediment Flux and Ocean Circulation. Geochemistry Geophys. Geosystems 19, 2560–2573. https://doi.org/10.1029/2017GC007410

Mix, A. C., Bard, E., Schneider, R. (2001). Environmental processes of the ice age: land, oceans, glaciers (EPILOG). Quaternary Science Reviews, 20, 627–657.

Mohamed, C. A. R., Narita, H., Harada, K., Tsunogai, S. (1996). Sedimentation of natural radionuclides on the seabed across the northern Japan Trench. Geochemical Journal, 30, 217–229.

Mollenhauer, G., McManus, J. F., Wagner, T., McCave, I. N., Eglinton, T. I. (2011). Radiocarbon and 230Th data reveal rapid redistribution and temporal changes in sediment focussing at a North Atlantic drift. Earth and Planetary Science Letters, 301(1–2), 373–381. https://doi.org/10.1016/j.epsl.2010.11.022

Moran, S. B., Charette, M. A., Hoff, J. A., Edwards, R. L., Landing, W. M. (1997) Distribution of 230Th in the Labrador Sea and its relation to ventilation. Earth and Planetary Science Letters 150, 151-160.

Moran, S. B., Hoff, J. A., Buesseler, K. O., Edwards, R.L. (1995) High-Precision 230Th-230 and 232Th in the Norwegian Sea and Denmark by Thermal Ionization Mass-Spectrometry. Geophysical Research Letters 22, 2589-2592.

Moran, S. B., Kelly, R. P., Hagstrom, K., Smith, J. N., Grebmeier, J. M., Cooper, L. W., Cota, G. F., Walsh, J. J., Bates, N. R., Hansell, D. A., Maslowski, W., Nelson, R. P., Mulsow, S. (2005). Seasonal changes in POC export flux in the Chukchi Sea and implications for water column-benthic coupling in Arctic shelves. Deep-Sea Research Part II: Topical Studies in Oceanography, 52(24–26), 3427–3451. https://doi.org/10.1016/j.dsr2.2005.09.011

Mulitza, S., Chiessi, C. M., Schefuß, E., Lippold, J., Wichmann, D., Antz, B., Mackensen, A., Paul, A., Prange, M., Rehfeld, K., Werner, M., Bickert, T., Frank, N., Kuhnert, H., Lynch-

Stieglitz, J., Portilho-Ramos, R. C., Sawakuchi, A. O., Schulz, M., Schwenk, T., Tiedemann, R., Vahlenkamp, M., Zhang, Y. (2017). Synchronous and proportional deglacial changes in Atlantic meridional overturning and northeast Brazilian precipitation. Paleoceanography 32, 622–633. https://doi.org/10.1002/2017PA003084

Mulitza, S., Prange, M., Stuut, J. B., Zabel, M., Von Dobeneck, T., Itambi, A. C., Nizou, J., Schulz, M., Wefer G. (2008). Sahel megadroughts triggered by glacial slowdowns of Atlantic meridional overturning. Paleoceanography, 23(4), 1–11. https://doi.org/10.1029/2008PA001637

Muller, J., McManus, J. F., Oppo, D. W., Francois, R. (2012). Strengthening of the Northeast Monsoon over the Flores Sea, Indonesia, at the time of Heinrich event 1. Geology, 40(7), 635–638. https://doi.org/10.1130/G32878.1

Nave, S., Labeyrie, L., Gherardi, J., Caillon, N., Cortijo, E., Kissel, C., Abrantes, F. (2007). Primary productivity response to Heinrich events in the North Atlantic Ocean and Norwegian Sea. Paleoceanography, 22(3), 1–18. https://doi.org/10.1029/2006PA001335

Negre, C., Zahn, R., Thomas, A. L., Masqué, P., Henderson, G. M., Martínez-Méndez, G., Hall, I. R., Mas, J. L. (2010). Reversed flow of Atlantic deep water during the Last Glacial Maximum. Nature, 468(7320), 84–88. https://doi.org/10.1038/nature09508

Neimann, S., Geibert, W. (2003). 231Pa ex and 230Th ex at the southeast South American continental margin - Is the 231Pa ex / 230Th ex ratio a proxy for particle flux or ocean circulation? Freie Universit√§t Berlin.

Ng, H. C., Robinson, L. F., McManus, J. F., Mohamed, K. J., Jacobel, A. W., Ivanovic, R. F., Gregoire, L. J., Chen, T. (2018). Coherent deglacial changes in western Atlantic Ocean circulation. Nature Communications, 9, 2947. https://doi.org/10.1038/s41467-018-05312-3

Nodder, S. D., Duineveld, G. C. A., Pilditch, C. A., Sutton, P. J., Probert, P. K., Lavaleye, M. S. S., Witbaard, R., Chang, F. H., Hall, J. A., Richardson, K.M. (2007) Focusing of phytodetritus deposition beneath a deep-ocean front, Chatham Rise, New Zealand. Limnology and Oceanography 52, 299-314.

Not, C., Hillaire-Marcel Claude, C. (2010). Time constraints from 230Th and 231Pa data in late Quaternary, low sedimentation rate sequences from the Arctic Ocean: An example from the northern Mendeleev Ridge. Quaternary Science Reviews, 29(25–26), 3665–3675. https://doi.org/10.1016/j.quascirev.2010.06.042

Not, C., Hillaire-Marcel, C. (2012). Enhanced sea-ice export from the Arctic during the Younger Dryas. Nat. Commun. 3. https://doi.org/10.1038/ncomms1658

Nozaki, Y., Horibe, Y. (1983). Alpha-emitting thorium isotopes in northwest Pacific deep waters. Earth Planet. Sci. Lett. 65, 39–50. https://doi.org/10.1016/0012-821X(83)90188-7

Nozaki, Y., Horibe, Y., Tsubota, H. (1981). The water column distributions of thorium isotopes in the western North Pacific. Earth Planet. Sci. Lett. 54, 203–216. https://doi.org/10.1016/0012-821X(81)90004-2

Nozaki, Y., Yang, H.-S., Yamada, M. (1987). Scavenging of thorium in the ocean. J. Geophys. Res. 92, 772. https://doi.org/10.1029/jc092ic01p00772

Nuttin, L. (2014). LES ISOTOPES DES FAMILLES U & Th: UN REGARD SUR LA DYNAMIQUE SÉDIMENTAIRE DE LA BAIE DE BAFFIN ET DU NORD-OUEST DE LA MER DU LABRADOR AU COURS DU DERNIER CYCLE GLACIAIRE. University of Quebec at Montreal.

Nuttin, Laurence, Hillaire-Marcel, C. (2015). U- and Th-series isotopes in deep Baffin Bay sediments: Tracers of detrital sources and of contrasted glacial/interglacial sedimentary processes. Marine Geology, 361, 1–10. https://doi.org/10.1016/j.margeo.2015.01.003

Okubo, A., Obata, H., Gamo, T., Yamada, M. (2012). 230Th and 232Th distributions in mid-latitudes of the North Pacific Ocean: effect of bottom scavenging. Earth and Planetary Science Letters, 339, 139-150.

Owens, S. A., Buesseler, K. O., & Sims, K. W. W. (2011). Re-evaluating the 238U-salinity relationship in seawater: Implications for the 238U–234Th disequilibrium method. Marine Chemistry, 127(1–4), 31–39. https://doi.org/10.1016/j.marchem.2011.07.005

Paetsch, H. (1991). Sedimentation im Europäischen Nordmeer. Berichte aus dem Sonderforschungsbereich 313, Christian-Albrechts-Universität, Kiel, 29, 102 pp, https://doi.org/10.2312/reports-sfb313.1991.29.

Palchan, D., Torfstein, A. (2019). A drop in Sahara dust fluxes records the northern limits of the African Humid Period. Nature Communications, 10(1). https://doi.org/10.1038/s41467-019-11701-z

Pavia, F. J., Anderson, R. F., Black, E. E., Kipp, L. E., Vivancos, S. M., Fleisher, M. Q., Charette, M. A., Sanial, V., Moore, W. S., Hult, M., Lu, Y., Cheng, H., Zhang, P., Edwards, R. L. (2019). Timescales of hydrothermal scavenging in the South Pacific Ocean from 234Th, 230Th, and 228Th. Earth and Planetary Science Letters, 506, 146–156. https://doi.org/10.1016/j.epsl.2018.10.038

Pavia, F. J., Anderson, R. F., Vivancos, S., Fleisher, M., Lam, P., Lu, Y., Cheng, H., Zhang, P., Lawrence Edwards, R. (2018). Intense hydrothermal scavenging of230Th and231Pa in the deep Southeast Pacific. Mar. Chem. 201, 212–228. https://doi.org/10.1016/j.marchem.2017.08.003

Pichat, S., Abouchami, W., Galer, S. J. G. (2014). Lead isotopes in the Eastern Equatorial Pacific record Quaternary migration of the South Westerlies. Earth and Planetary Science Letters, 388, 293–305. https://doi.org/10.1016/j.epsl.2013.11.035

Pichat, S., Sims, K. W. W., Francois, R., McManus, J .F., Brown-Leger, S., Albarede, F. (2004). Lower export production during glacial periods in the equatorial Pacific derived from (231Pa/230Th)xs,0 measurements in deep-sea sediments. Paleoceanography 19, PA4023. https://doi.org/10.1029/2003PA000994

Plain, C. (2004). INCIDENCE OF GRAIN-SIZE. MINERALOGY AND DIAGENETIC PROCESSES ON THE CALCULATION OF 230ThXS IN LATE QUATERNARY DEEP SEA SEDIMENTS -EXAMPLE FROM THE IRMINGER SEA. University of Quebec at Montreal.

Poore, R. Z., Osterman, L., Curry, W. B., Phillips, R. L. (1999). Late Pleistocene and Holocene meltwater events in the western Arctic Ocean. Geology 27, 759–762. https://doi.org/10.1130/0091-7613(1999)027<0759:LPAHME>2.3.CO;2

Pourmand, A., Marcantonio, F., Bianchi, T. S., Canuel, E. A., Waterson, E. J. (2007). A 28-ka history of sea surface temperature, primary productivity and planktonic community variability in the western Arabian Sea. Paleoceanography, 22(4), n/a-n/a. https://doi.org/10.1029/2007PA001502

Pourmand, A., Marcantonio, F., Schulz, H. (2004). Variations in productivity and eolian fluxes in the northeastern Arabian Sea during the past 110 ka. Earth and Planetary Science Letters, 221(1–4), 39–54. https://doi.org/10.1016/S0012-821X(04)00109-8

Purcell, K. (2019). Masters Thesis. University of Quebec in Montreal.

Rempfer, J., Stocker, T. F., Joos, F., Lippold, J., Jaccard, S. L. (2017). New insights into cycling of 231Pa and 230Th in the Atlantic Ocean. Earth Planet. Sci. Lett. 468, 27–37.

https://doi.org/10.1016/j.epsl.2017.03.027
Roberts, N. L., McManus, J. F., Piotrowski, A. M., McCave, I. N. (2014). Advection and scavenging controls of Pa/Th in the northern NE Atlantic. Paleoceanography, 29(6), 668–679. https://doi.org/10.1002/2014PA002633
Robinson, L. F., Noble, T., McManus, J. F. (2008). Measurement of adsorbed and total 232Th/230Th ratios from marine sediments. Chemical Geology, 252(3–4), 169–179. https://doi.org/10.1016/j.chemgeo.2008.02.015
Robinson, R. S., Martinez, P., Pena, L. D., Cacho, I. (2009). Nitrogen isotopic evidence for deglacial changes in nutrient supply in the eastern equatorial Pacific. Paleoceanography 24, PA4213. https://doi.org/10.1029/2008PA001702
Rogan, N., Achterberg, E. P., Le Moigne, F. A. C., Marsay, C. M., Tagliabue, A., Williams, R. G. (2016), Volcanic ash as an oceanic iron source and sink, Geophys. Res. Lett., 43, 2732–2740, doi:10.1002/2016GL067905.
Rowland, G. H., Chin, H., Robinson, L. F., McManus, J. F., Mohamed, K. J., McGee, D. (2017). Investigating the use of 232Th/230Th as a dust proxy using co-located seawater and sediment samples from the low-latitude North Atlantic. Geochim. Cosmochim. Acta 214, 143–156. https://doi.org/10.1016/j.gca.2017.07.033
Roy-Barman M., Thill, F., Bordier, L., Dapoigny, A., Foliot, L., Ayrault, S., Lacan, F., Pradoux, C., Jeandel, C., Garcia Solsona, E. (2019) Thorium isotopes in the Southeast Atlantic Ocean: Tracking scavenging during water mass mixing along neutral density surfaces. Deep Sea Res. Part I. 149, 103042.
Roy-Barman, M., Chen, J. H., Wasserburg, G. J. (1996). 230Th-232Th systematics in the central Pacific Ocean: The sources and the fates of thorium. Earth Planet. Sci. Lett. 139, 351–363.
Roy-Barman, M., Jeandel, C., Souhaut, M., Rutgers van der Loeff, M., Voege, I., Leblond, N., Freydier, R. (2005). The influence of particle composition on thorium scavenging in the NE Atlantic ocean (POMME experiment). Earth Planet. Sci. Lett. 240, 681–693. https://doi.org/10.1016/j.epsl.2005.09.059
Roy-Barman, M., Lemaître, C., Ayrault, S., Jeandel, C., Souhaut, M., Miquel, J. (2009). The influence of particle composition on Thorium scavenging in the Mediterranean Sea. Earth Planet. Sci. Lett. 286, 526–534. https://doi.org/10.1016/j.epsl.2009.07.018
Ruhlemann, C., Frank, M., Hale, W., Mangini, A., Mulitza, S., Muller, P. J., Wefer, G. (1996). Late Quaternary productivity changes in the western equatorial Atlantic: Evidence from Th-230-normalized carbonate and organic carbon accumulation rates. Marine Geology, 135(1–4), 127–152. https://doi.org/Doi 10.1016/S0025-3227(96)00048-5
Rutgers van der Loeff, M. M., Berger, G. W. (1993) Scavenging of 230Th and 231Pa near the Antarctic Polar Front in the South-Atlantic. Deep-Sea Research Part I-Oceanographic Research Papers 40, 339-357.
Rutgers van der Loeff, M. M., Venchiarutti, C., Stimac, I., van Ooijen, J., Huhn, O., Rohardt, G., Strass, V. (2016) Meridional circulation across the Antarctic Circumpolar Current serves as a double 231Pa and 230Th trap. Earth and Planetary Science Letters 455, 73-84.
Sani, R. K., Peyton, B. M., Amonette, J. E., Geesey, G. G. (2004). Reduction of uranium (VI) under sulfate-reducing conditions in the presence of Fe (III)-(hydr)oxides. Geochim. Cosmochim. Acta 68, 2639–2648. https://doi.org/10.1016/j.gca.2004.01.005
Sarin, M. M., Borole, D. V., Krishnaswami, S. (1979). Geochemistry and geochronology of sediments from the Bay of Bengal and the equatorial Indian Ocean. Proceedings of the Indian Academy Of Sciences - Earth And Planetary Sciences, 88A(2), 131–154.

Sarmiento, J. L., Gruber, N. (2006). Ocean biogeochemical dynamics. Princeton University Press.
Saukel, C. (2011). Tropical Southeast Pacific Continent-Ocean-Atmosphere Linkages Since the Pliocene Inferred from Eolian Dust. University of Bremen. https://doi.org/10.1594/PANGAEA.811988
Schlosser, P. and Winckler, G. (2002). Noble gases in ocean waters and sediments. Reviews in mineralogy and geochemistry 47, 701-730
Schmitz, W., Mangini, A., Stoffers, P., Glasby, G. P., Pluger, W. L. (1986) Sediment Accumulation Rates in the Southwestern Pacific Basin and Aitutaki Passage. Marine Geology 73, 181-190.
Scholten, J. C., Bohrmann, H., Botz, R., Mangini, A., Paetsch, H., Stoffers, P., Vogelsang, E. (1990). High Resolution Stratigraphy of Sediments from High Latidute areas (Norwegian Sea, Framstrait). Earth Planet. Sci. Lett, 101, 54–62.
Scholten, J. C., Botz, R., Paetsch, H., Stoffers, P. (1994). 230Thex flux into Norwegian-Greenland Sea sediments: Evidence for lateral sediment transport during the past 300,000 years. Earth and Planetary Science Letters, 121(1–2), 111–124. https://doi.org/10.1016/0012-821X(94)90035-3
Scholten, J. C., Fietzke, J., Mangini, A., Stoffers, P., Rixen, T., Gaye-Haake, B., Blanz, T., Ramaswamy, V., Sirocko, F., Schulz, H., Ittekkot, V. (2005). Radionuclide fluxes in the Arabian Sea: The role of particle composition. Earth Planet. Sci. Lett. 230, 319–337. https://doi.org/10.1016/j.epsl.2004.11.003
Scholten, J. C., Fietzke, J., Mangini, A., Garbe-Schönberg, C. D., Eisenhauer, A., Schneider, R., Stoffers, P. (2008). Advection and scavenging: Effects on 230Th and 231Pa distribution off Southwest Africa. Earth and Planetary Science Letters, 271(1–4), 159–169. https://doi.org/10.1016/j.epsl.2008.03.060
Scholten, J. C., Fietzke, J., Vogler, S., Rutgers van der Loeff, M., Mangini, A., Koeve, W., Waniek, J., Stoffers, P., Antia, A., Kuss, J. (2001). Trapping efficiencies of sediment traps from the deep Eastern North Atlantic:: the 230Th calibration. *Deep Sea Research Part II: Topical Studies in Oceanography*, *48*(10), pp.2383-2408.
Serno, S., Winckler, G., Anderson, R. F., Hayes, C. T., McGee, D., Machalett, B., Ren, H., Straub, S. M., Gersonde, R., Haug, G. H. (2014). Eolian dust input to the Subarctic North Pacific. Earth and Planetary Science Letters, 387, 252–263. https://doi.org/10.1016/j.epsl.2013.11.008
Serno, S., Winckler, G., Anderson, R. F., Maier, E., Ren, H., Gersonde, R., Haug, G. H. (2015). Comparing dust flux records from the Subarctic North Pacific and Greenland: Implications for atmospheric transport to Greenland and for the application of dust as a chronostratigraphic tool. Paleoceanography, 30(6), 583–600. https://doi.org/10.1002/2014PA002748
Shiau, L.-J., Chen, M.-T., Huh, C.-A., Yamamoto, M., Yokoyama, Y. (2012). Insolation and cross-hemispheric controls on Australian monsoon variability over the past 180 ka: new evidence from offshore southeastern Papua New Guinea. Journal of Quaternary Science, 27(9), 911–920. https://doi.org/10.1002/jqs.2581
Shimmield, G. B., Mowbray, S. R. (1991). U-series disequilibrium, particle scavenging, and sediment accumulation during the late Pleistocene on the Owen Ridge, Site 722. In W. Prell & N. Niitsuma (Eds.), Proceedings of the Ocean Drilling Program, Scientific Results (pp. 465–472). College Station, TX.

Shimmield, G. B., Murray, J. W., Bacon, M. P., Anderson, R. F., Price, N. B. (1986). The distribution and behaviour of 230Th and 231Pa at an ocean margin, Baja California, Mexico. Geochimica et Cosmochimica Acta, 50, 2499–2507.

Shimmield, G. B., Price, N. B. (1988). The scavenging of U, 230Th, and 231Pa during pulsed hydrothermal activity at 20˚S, East Pacific Rise. Geochim. Cosmochim. Acta 52, 669–677.

Siddall, M., Henderson, G.M., Edwards, N.R., Frank, M., Müller, S. A., Stocker, T.F., Joos, F. (2005). 231Pa/230Th fractionation by ocean transport, biogenic particle flux and particle type. Earth Planet. Sci. Lett. 237, 135–155. https://doi.org/10.1016/j.epsl.2005.05.031

Siddall, M., Stocker, T. F., Henderson, G. M., Joos, F., Frank, M., Edwards, N. R., Ritz, S. P., Müller, S. A. (2007). Modeling the relationship between 231Pa/230Th distribution in North Atlantic sediment and Atlantic meridional overturning circulation. Paleoceanography 22, 1–14. https://doi.org/10.1029/2006PA001358

Singh, A. K., Marcantonio, F., Lyle, M. (2011). Sediment focusing in the panama basin, eastern equatorial pacific ocean. Earth and Planetary Science Letters, 309(1–2), 33–44. https://doi.org/10.1016/j.epsl.2011.06.020

Singh, A. K., Marcantonio, F., Lyle, M. (2013). Water column 230Th systematics in the eastern equatorial Pacific Ocean and implications for sediment focusing. Earth Planet. Sci. Lett. 362, 294–304. https://doi.org/10.1016/j.epsl.2012.12.006

Skonieczny, C., McGee, D., Winckler, G., Bory, A., Bradtmiller, L. I., Kinsley, C. W., Polissar, P. J., De Pol-Holz, R., Rossignol, L., Malaizé, B. (2019). Monsoon-driven Saharan dust variability over the past 240,000 years. Science Advances, 5(1), 1–9. https://doi.org/10.1126/sciadv.aav1887

Slowey, N. C., Curry, W. B. (1991), Using 230Th in Marine Sediments to Reconstruct the Late Quaternary History of Sea Level: Paleoceanography, v. 6, no. 5, p. 609-619.

Smith, C. R., Hoover, D. J., Doan, S. E., Pope, R. H., DeMaster, D. J., Dobbs, F. C., Altabet, M. A. (1996) Phytodetritus at the abyssal seafloor across 10 degrees of latitude in the central equatorial Pacific. Deep-Sea Research Part II-Topical Studies in Oceanography 43, 1309-1338.

Studer, A. S., Sigman, D. M., Martínez-García, A., Benz, V., Winckler, G., Kuhn, G., Esper, O., Lamy, F., Jaccard, S. L., Wacker, L., Oleynik, S., Gersonde, R., Haug, G. H. (2015). Antarctic Zone nutrient conditions during the last two glacial cycles. Paleoceanography, 30(7), 845–862. https://doi.org/10.1002/2014PA002745

Sukumaran, N. P. (1994). Some aspects on the variations in depositional flux of excess thorium-230 in the central Indian basin during late quaternary. Proceedings Of The Indian Academy Of Sciences - Earth And Planetary Sciences, 103(4), 489–497.

Suman, D. O., Bacon, M. P. (1989). Variations in Holocene sedimentation in the North American Basin determined from 230Th measurements. Deep Sea Res. 36, 869–878.

Taylor, S. R., McLennan, S. M. (1995). The geochemical evolution of the continental crust. Rev. Geophys. 33, 241–265.

Thiagarajan, N., McManus, J. F. (2019). Productivity and sediment focusing in the Eastern Equatorial Pacific during the last 30,000 years. Deep-Sea Research Part I: Oceanographic Research Papers, 147(March), 100–110. https://doi.org/10.1016/j.dsr.2019.03.007

Thöle, L. M., Amsler, H. E., Moretti, S., Auderset, A., Gilgannon, J., Lippold, J., Vogel, H., Crosta, X., Mazaud, A., Michel, E., Martínez-García, A., Jaccard, S. L. (2019). Glacial-interglacial dust and export production records from the Southern Indian Ocean. Earth and Planetary Science Letters, 525, 115716. https://doi.org/10.1016/j.epsl.2019.115716

Thomas, A. L., Henderson, G. M., McCave, I. N. (2007). Constant bottom water flow into the Indian Ocean for the past 140 ka indicated by sediment 231 Pa/ 230 Th ratios. Paleoceanography, 22(4), n/a-n/a. https://doi.org/10.1029/2007PA001415

Thomson, J., Cook, G. T., Anderson, R. F., MacKenzie, A. B., Harkness, D. D., McCave, I. N. (1995). Radiocarbon age offsets in different-sized carbonate components of deep-sea sediments. Radiocarbon, 37(2), 91–101.

Thomson, J., Higgs, N. C., Croudace, I. W., Colley, S., Hydes, D. J. (1993). Redox zonation of elements at an oxic/post-oxic boundary in deep-sea sediments. Geochimica et Cosmochimica Acta, 57, 579–595.

Thomson, J., Schonfeld, J., Zahn, R., Grootes, P., Nixon, S., Summerhayes, C. P. (1999). Implications for sedimentation changes on the Iberian margin over the last two glacial/interglacial transitions from (230Th(excess))0 systematics. Earth and Planetary Science Letters, 165(3–4), 255–270. https://doi.org/10.1016/S0012-821X(98)00265-9

Valk, O., Rutgers van der Loeff, M. M., Geibert, W., Gdaniec, S., Rijkenberg, M. J. A., Moran, S. B., Lepore, K., Edwards, R. L., Lu, Y., Puigcorbé, V. (2018). Importance of hydrothermal vents in scavenging removal of 230Th in the Nansen Basin. Geophys. Res. Lett. 1–10. doi:10.1029/2018GL079829

Vallieres, S. (1997). Flux d'uranium et excès de 230Th dans les sédiments de la mer du Labrador: relation avec les conditions paléocéanographiques et la paléoproductivité du bassin. Université du Québec à Chicoutimi.

Van Hulten, M., Dutay, J.-C., Roy-Barman, M. (2018). A global scavenging and circulation ocean model of thorium-230 and protactinium-231 with realistic particle dynamics (NEMO-ProThorP 0.1). Geosci. Model Dev. 1–32. https://doi.org/doi:10.5194/gmd-2017-274

Veeh, H. H., Heggie, D. T., Crispe, A. J. (1999). Biogeochemistry of southern Australian continental slope sediments. Aust. J. Earth Sci., 46, 563–575. https://doi.org/10.1046/j.1440-0952.1999.00729.x

Veeh, H. H., McCorkle, D., Heggie, D. (2000). Glacial/interglacial variations of sedimentation on the West Australian continental margin: constraints from excess 230Th. Marine Geology, 166(1–4), 11–30. https://doi.org/10.1016/S0025-3227(00)00011-6

Veiga-Pires, C. C., Hillaire-Marcel, C. (1999). U and Th isotope constraints on the duration of Heinrich events H0-H4 in the southeastern Labrador Sea. Paleoceanography 14, 187–199.

Venchiarutti, C., Rutgers van der Loeff, M. M., Stimac, I. (2011) Scavenging of 231Pa and thorium isotopes based on dissolved and size-fractionated particulate distributions at Drake Passage (ANTXXIV-3). Deep Sea Research Part II: Topical Studies in Oceanography 58, 2767-2784.

Vogler, S., Rutgers van der Loeff, M. M., Mangini, A. (1998) 230Th in the eastern North Atlantic: the importance of water mass ventilation in the balance of 230Th. Earth and Planetary Science Letters 156, 61-74.

Voigt, I., Cruz, A. P. S., Mulitza, S., Chiessi, C. M., Mackensen, A., Lippold, J., Antz, B., Zabel, M., Zhang, Y., Barbosa, C. F., Tisserand, A. A. (2017). Variability in mid-depth ventilation of the western Atlantic Ocean during the last deglaciation. Paleoceanography, 32(9), 948–965. https://doi.org/10.1002/2017PA003095

Waelbroeck, C., Pichat, S., Böhm, E., Lougheed, B. C., Faranda, D., Vrac, M., Missiaen, L., Vazquez Riveiros, N., Burckel, P., Lippold, J., Arz, H. W., Dokken, T., Thil, F., Dapoigny, A. (2018). Relative timing of precipitation and ocean circulation changes in the western equatorial Atlantic over the last 45 kyr. Climate of the Past, 14(9), 1315–1330.

https://doi.org/10.5194/cp-14-1315-2018

Walter, H. J., Hegner, E., Diekmann, B., Luhn, G., Rutgers, M. M. (2000). Provenance and transport of terrigenous sediment in the South Atlantic Ocean and their relations to glacial and interglacial cycles: Nd and Sr isotopic evidence. Geochimica et Cosmochimica Acta, 64(22), 3813–3827.

Walter, H., Rutgers van der Loeff, M .M., Hoeltzen, H. (1997). Enhanced scavenging of 231Pa relative to 230Th in the South Atlantic south of the polar front: Implications for the use of 231Pa/230Th ratio as a paleoproductivity proxy. Earth Planet. Sci. Lett. 149, 85–100.

Wengler, M., Lamy, F., Struve, T., Borunda, A., Böning, P., Geibert, W., Kuhn, G., Pahnke, K., Roberts, J., Tiedemann, R., Winckler, G. ((2019). A geochemical approach to reconstruct modern dust fluxes and sources to the South Pacific. Geochimica et Cosmochimica Acta, 264, 205–223. https://doi.org/10.1016/j.gca.2019.08.024

Williams, R. H., McGee, D., Kinsley, C. W., Ridley, D. A., Hu, S., Fedorov, A., Tal, I., Murray, R. W., DeMenocal, P. B (2016). Glacial to Holocene changes in trans-Atlantic Saharan dust transport and dust-climate feedbacks. Science Advances, 2(11), 1–12. https://doi.org/10.1126/sciadv.1600445

Winckler, G., Anderson, R. F., Fleisher, M. Q., McGee, D., Mahowald, N. (2008). Covariant glacial-interglacial dust fluxes in the equatorial Pacific and Antarctica. Science (New York, N.Y.), 320(5872), 93–96. https://doi.org/10.1126/science.1150595

Winckler, G., Anderson, R. F., Stute, M., Schlosser, P. (2004) Does interplanetary dust control 100kyr glacial cycles? Quaternary Science Reviews 23, 1873-1878.

Yang, Y.-L., Elderfield, H. (1990). Glacial to Holocene changes in carbonate and clay sedimentation in the equatorial Pacific Ocean estimated from thorium 230 profiles. Paleoceanography, 5(5), 789–809.

Yang, Y.-L., Elderfield, H., Pedersen, T. F., Ivanovich, M. (1995). Geochemical record of the Panama Basin during the Last Glacial Maximum carbon event shows that the glacial ocean was not suboxic. Geology, 23(12), 1115–1118. https://doi.org/10.1130/0091-7613(1995)023<1115:GROTPB>2.3.CO

Yong, L., Anderson, R. F., Broecker, W. S., Trumbore, S. E., Hofmann, H. J., Wolfli, W. (1992) Transport and burial rates of 10Be and231Pa in the Pacific Ocean during the Holocene period. Earth and Planetary Science Letters 113, 173-189.

Yu, E. (1994). Variations in the Particulate Flux of 230Th and 231Pa and Paleoceanographic Applications of the 231Pa/230Th Ratio.

Yu, E. F., Francois, R., Bacon, M. P., Fleer, A.P. (2001). Fluxes of 230Th and 231Pa to the deep sea: Implications for the interpretation of excess 230Th and 231Pa/230Th profiles in sediments. Earth Planet. Sci. Lett. 191, 219–230. https://doi.org/10.1016/S0012-821X(01)00410-1

Zhou, Y., McManus, J. F. (2020). Enhanced iceberg discharge in the western North Atlantic during all Heinrich events of the last glaciation. EarthArXiv. https://doi.org/10.31223/osf.io/yn57z

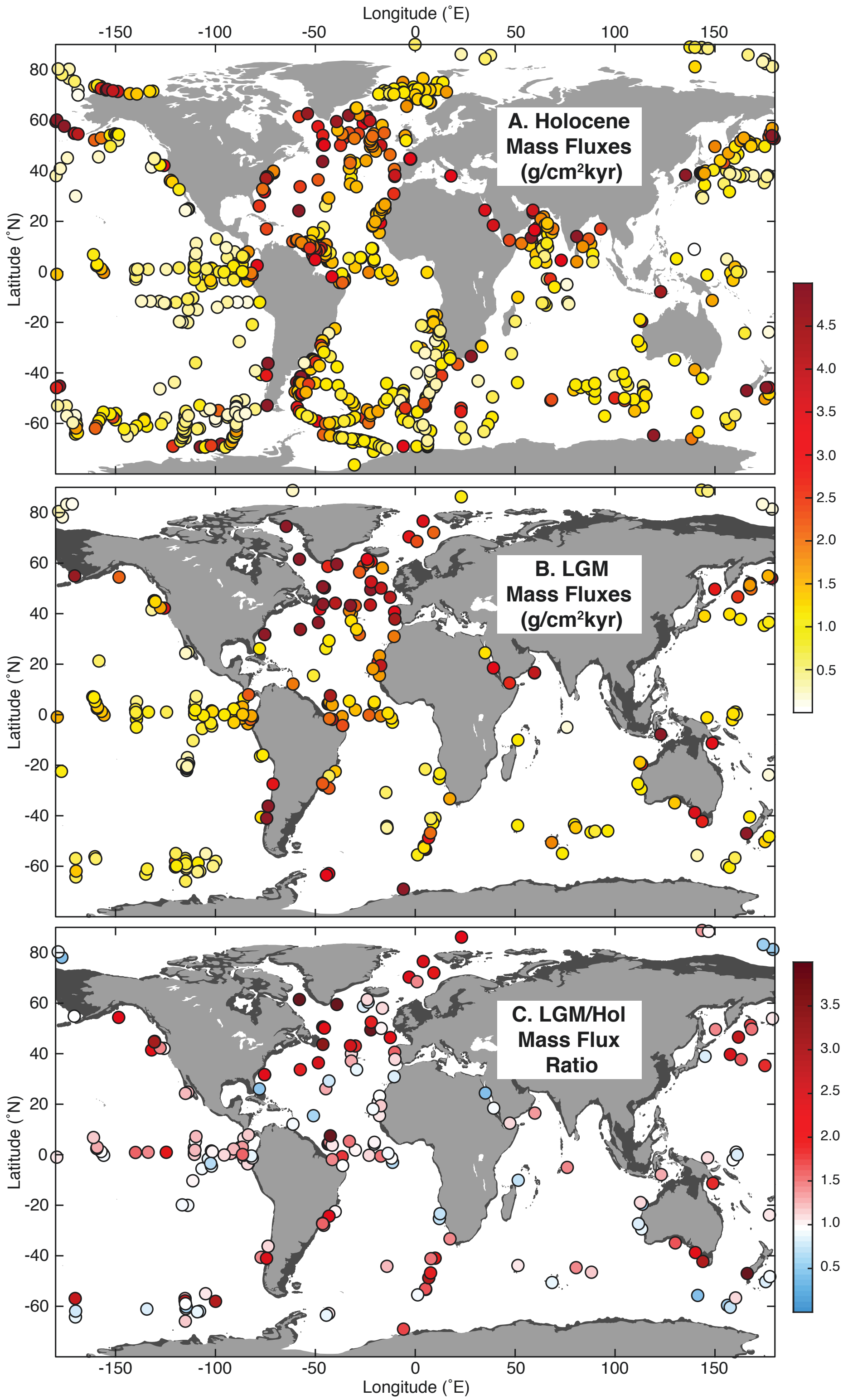

Figure 1. Compiled ^{230}Th-normalized mass fluxes for the Holocene (0-5 ka, A), the Last Glacial Maximum (LGM, 18.5-23.5 ka, B), and the LGM/Holocene mass flux ratio (C). Dark gray shaded area in (B) and (C) shows exposed land when sea level is 120 m lower. All data and references are provided in Supplementary Table 1. Raw $^{230}Th_{xs}{}^{0}$ concentrations maps are provided in Supplementary Figure 4.

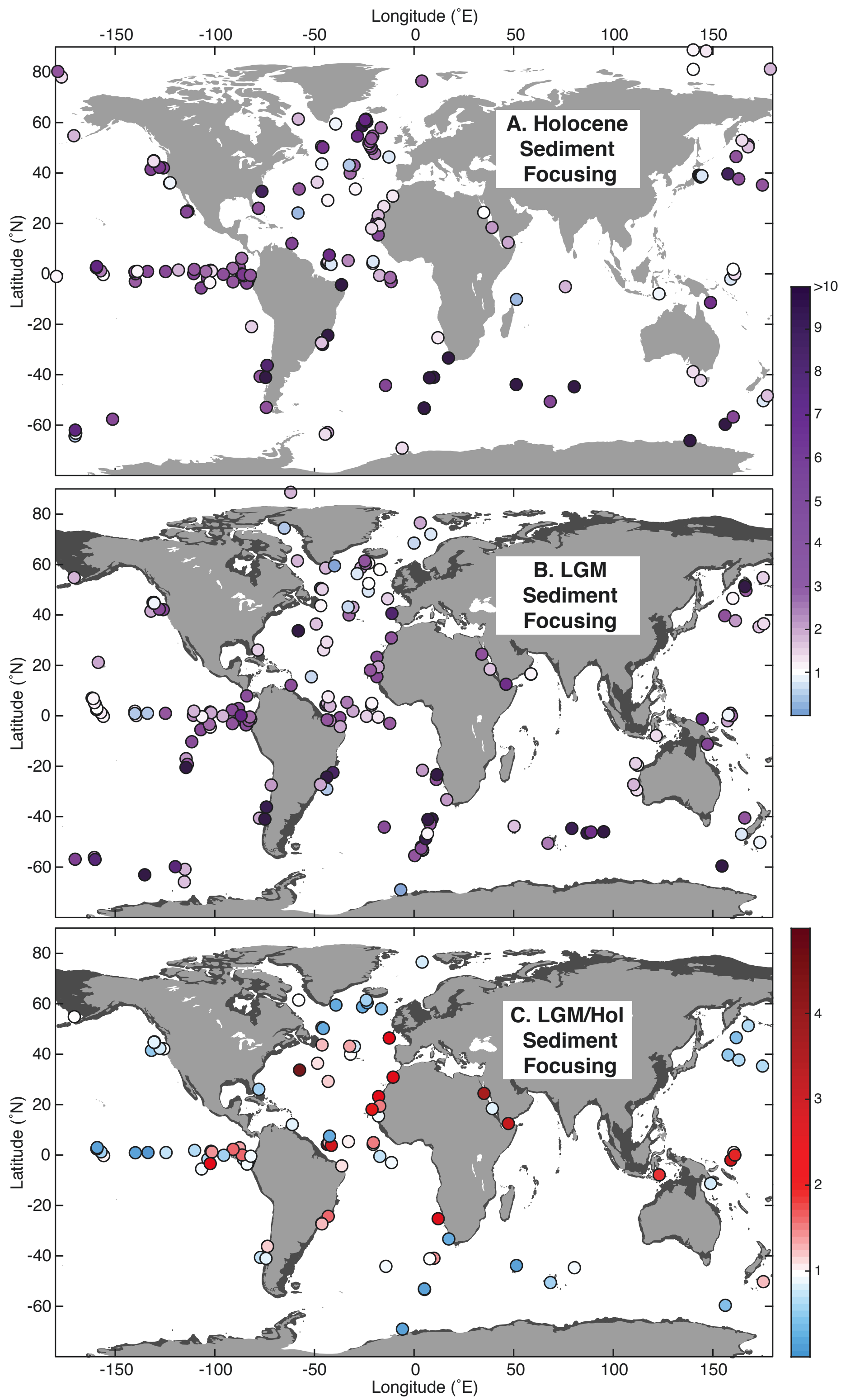

Figure 2. Sediment focusing for the Holocene (0-5 ka, A) and the Last Glacial Maximum (LGM, 18.5-23.5 ka, B), and the LGM/Holocene ratio of sediment focusing ratio (C). The generally high rates of focusing (>1) are largely due to the sampling bias towards high-accumulation rate sites. Dark gray shaded area in (B) and (C) shows exposed land when sea level is 120 m lower.

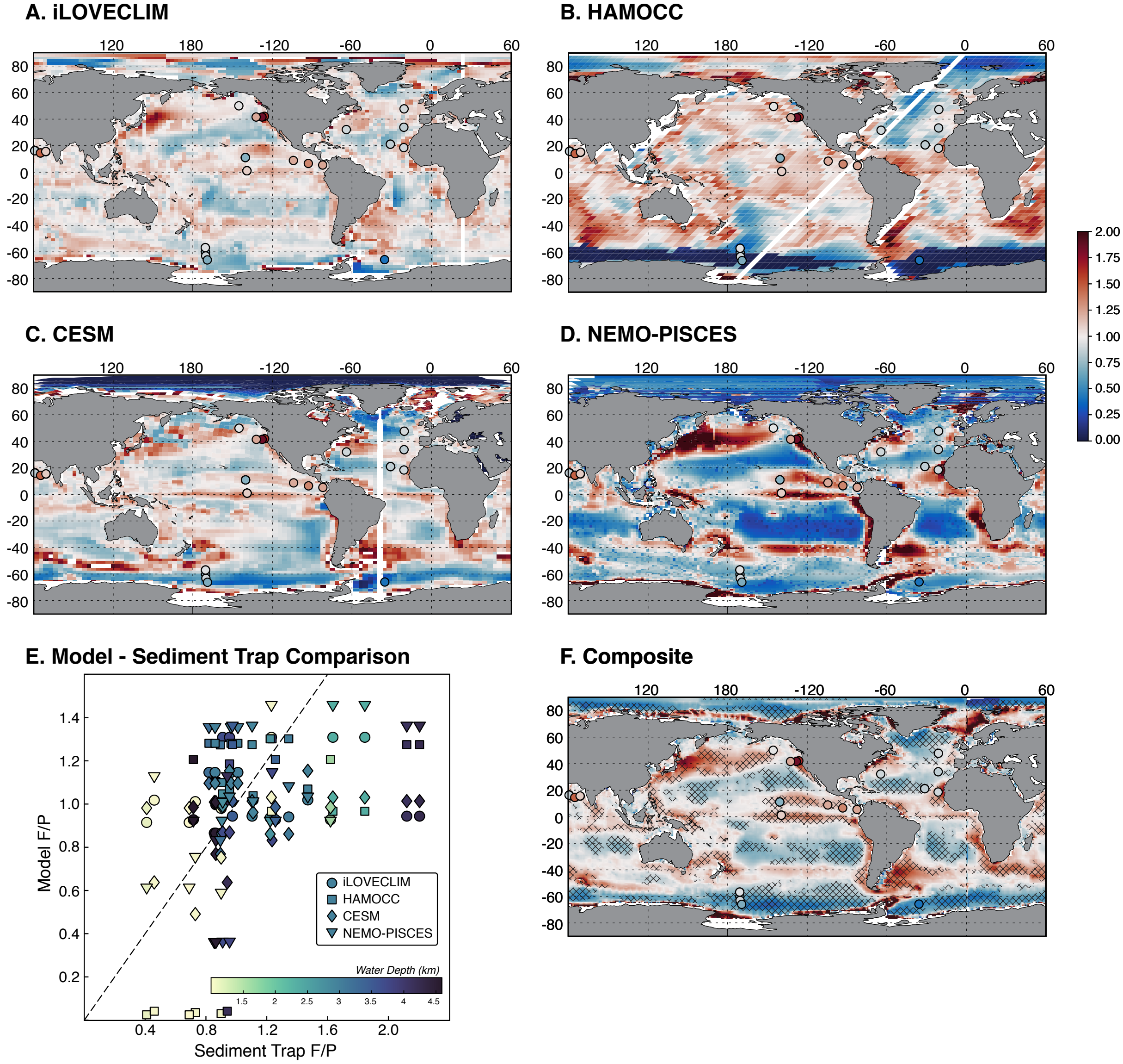

Figure 3. Modelled ^{230}Th flux to the sediment, normalized to water column production (F/P). (A) iLOVECLIM (Missiaen et al., 2019). (B) HAMOCC (Heinze et al., 2018). (C) CESM (Gu & Liu, 2017). (D) NEMO-Pisces (Dutay et al., 2009; Van Hulten et al., 2018). Overlain circles show flux to production (F/P) ratios measured at bottom-moored sediment traps (Chase et al., 2003; Lyle et al., 2014; Scholten et al., 2005; Yu et al., 2001). Colorbar is the same for all 4 maps. (E) Comparison of F/P measured in bottom-moored sediment traps to the modelled F/P at each site. Dashed black line shows 1:1. The highest correlation (R^2=0.22) occurs with NEMO-PISCES model. Both Nemo-PISCES and CESM adequately reproduce the sign (>1 or <1) for more than 61% of the sediment traps, while iLOVECLIM and HAMOCC reproduce the sign 50% or less of the sediment traps. At the same time, iLOVECLIM, HAMOCC, and CESM more realistically predict deviations from the theoretical F/P of 1 than the more extreme variability observed in NEMO-PISCES. (F) Composite of the 4 model outputs. Hatched regions highlight where at least 3 models agree on the sign (F/P of >1 or <1). A full size version of the composite map is provided in Supplementary Figure 7.

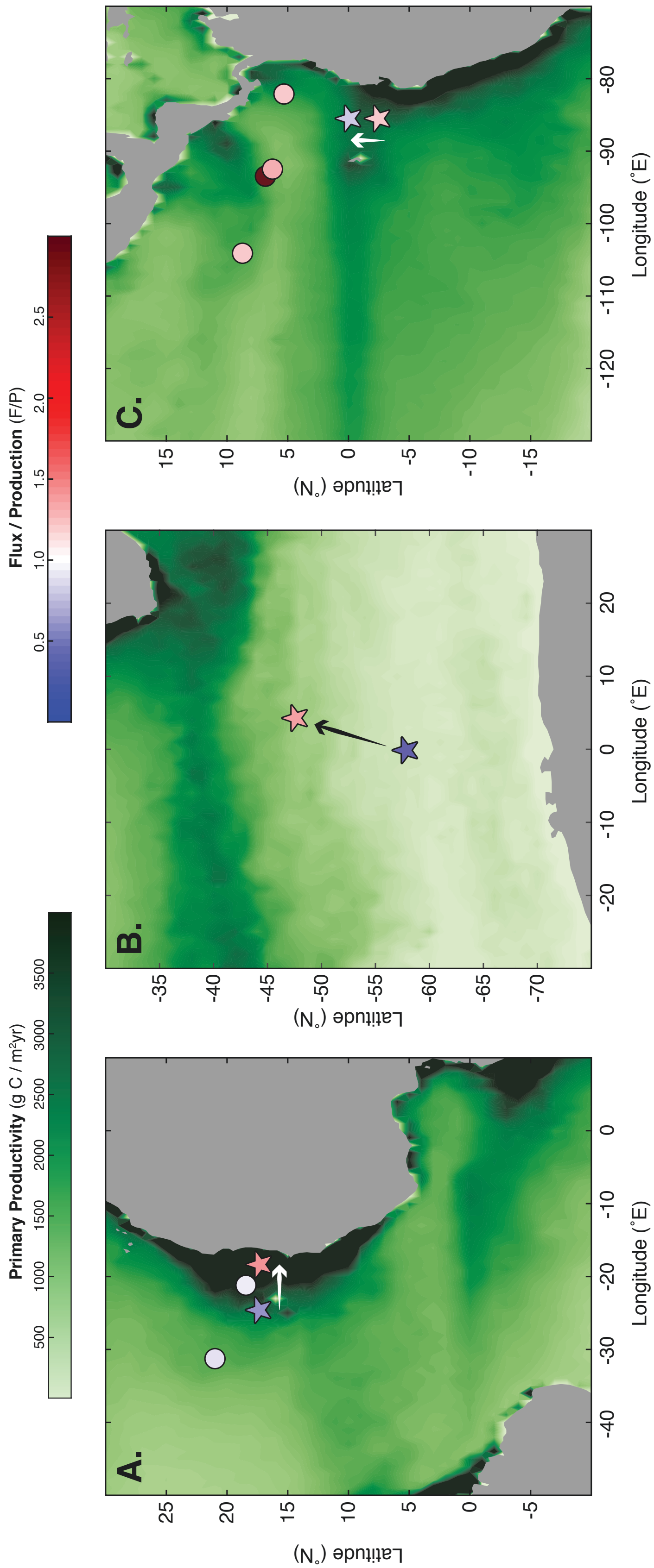

Figure 4. Lateral gradients in ^{230}Th due to boundary scavenging. (A) Northeast tropical Atlantic. (B) Atlantic sector of the Southern Ocean. (C) Eastern equatorial Pacific. Colored background (green colorbar) is a model-based estimate of net primary productivity at the base of the euphotic zone based on chlorophyll (Behrenfeld & Falkowski, 1997), as one indicator of scavenging intensity related to vertical particle flux. Colored symbols (red to blue colorbar) represent discrete estimates of the flux to production ratio (F/P), from either sediment traps (circles) or water column measurements (stars). Water column measurements are calculated based on the upper 3 km of the water column using lateral gradients in total seawater ^{230}Th concentrations and estimates of advection and diffusion rates in the area (Hayes et al., 2015a; Singh et al., 2013). Arrows show the direction of inferred lateral ^{230}Th transport.

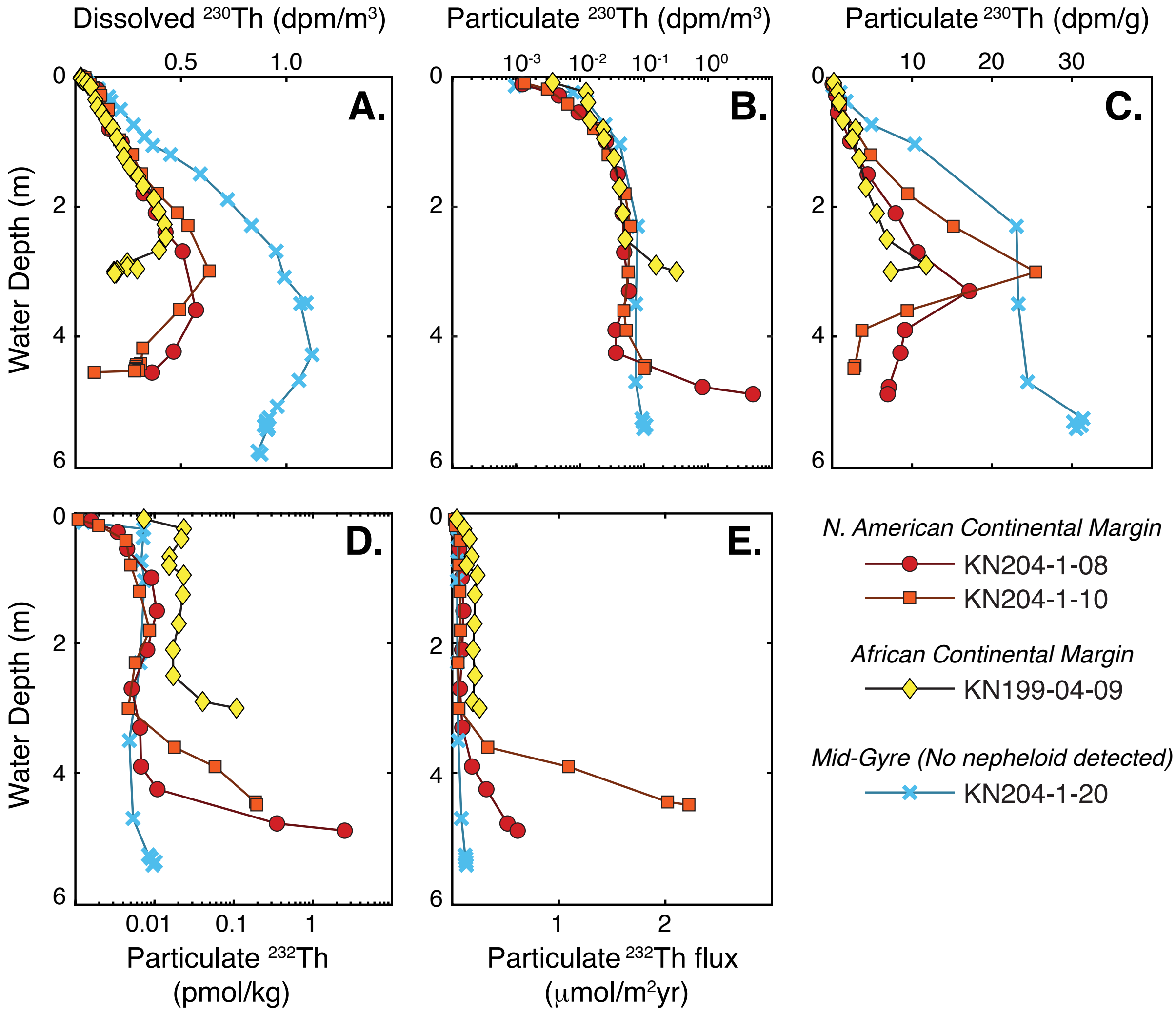

Figure 5. Influence of nepheloid layers on ^{230}Th scavenging in seawater. (A) Activities of dissolved (<0.4 μm) ^{230}Th at three stations where nepheloid layers were observed along GA03 (Hayes et al., 2015a). Stations KN204-1-08 (35.42°N, 66.52°W) and KN204-1-10 (31.83°N, 64.10°W) are near the eastern North American margin, while station KN199-04-09 (17.35°N, 18.25°W) is near the western African margin. For comparison, dissolved ^{230}Th from station KN204-1-20 (22.33°N, 35.87°W), where no strong bottom nepheloid was detected, is shown. (B) Same as (A), but for particulate ^{230}Th in the 0.8-51 μm size fraction (Hayes et al., 2015b). (C) Same as (A), but for particulate ^{230}Th activities per mass of particles. Particle concentrations in the 0.8-51 μm size-class used to calculate $^{230}Th_{pg}$ are from Lam et al. (2015). (D) Same as (A), but for particulate ^{232}Th concentrations in the 0.8-51 μm size fraction; unpublished data are available in the GEOTRACES intermediate data product (Schlitzer et al., 2018). (E) Same as (A), but for the ^{230}Th-normalized ^{232}Th flux, as provided in the appendices of (Hayes et al., 2018). Note that profiles in (B) and (D) are on a logarithmic scale to better illustrate trends within the nepheloid layer.

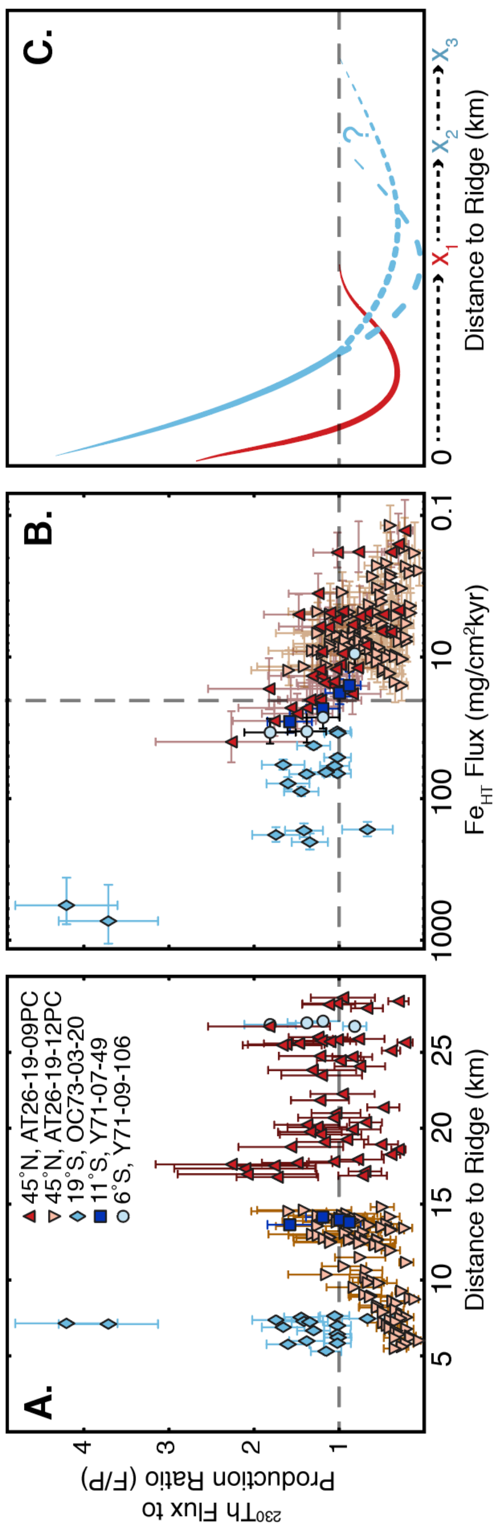

Figure 6. Compilation of F/P results from the Southern East Pacific Rise (SEPR, blue) and Juan de Fuca Ridge (JdFR, red). ^{230}Th flux to production (F/P) values are calculated by ^{3}He-normalized ^{230}Th fluxes that are then normalized to the production in the water column, and they are equivalent to flux to production (F/P) values for sediment traps, as shown in Figures 3 and 4. JdFR data are from Middleton et al. (*submitted*) and SEPR data are from Lund et al. (2019). (A) F/P vs. distance from the ridge crest, where distance is calculated using the corresponding sediment age and spreading rate for each ridge. (B) F/P vs. Fe flux (^{3}He-normalized). Dashed lines identify F/P of 1 and Fe_{HT} flux of 20 mg/cm^{2}kyr (see text). (C) Conceptual model of ^{230}Th-burial, where the F/P at the ridge axis is greater on the SEPR (blue curves) than JdFR (red curve). Near-axis fluxes are likely supplied by ^{230}Th diffusion from off-axis, causing ^{230}Th fluxes less than the water column production rate on the ridge flanks (F/P<1). The off-axis reach of ^{230}Th deficits is likely greater on the SEPR (x_2 or x_3) than on the JdFR (x_1).

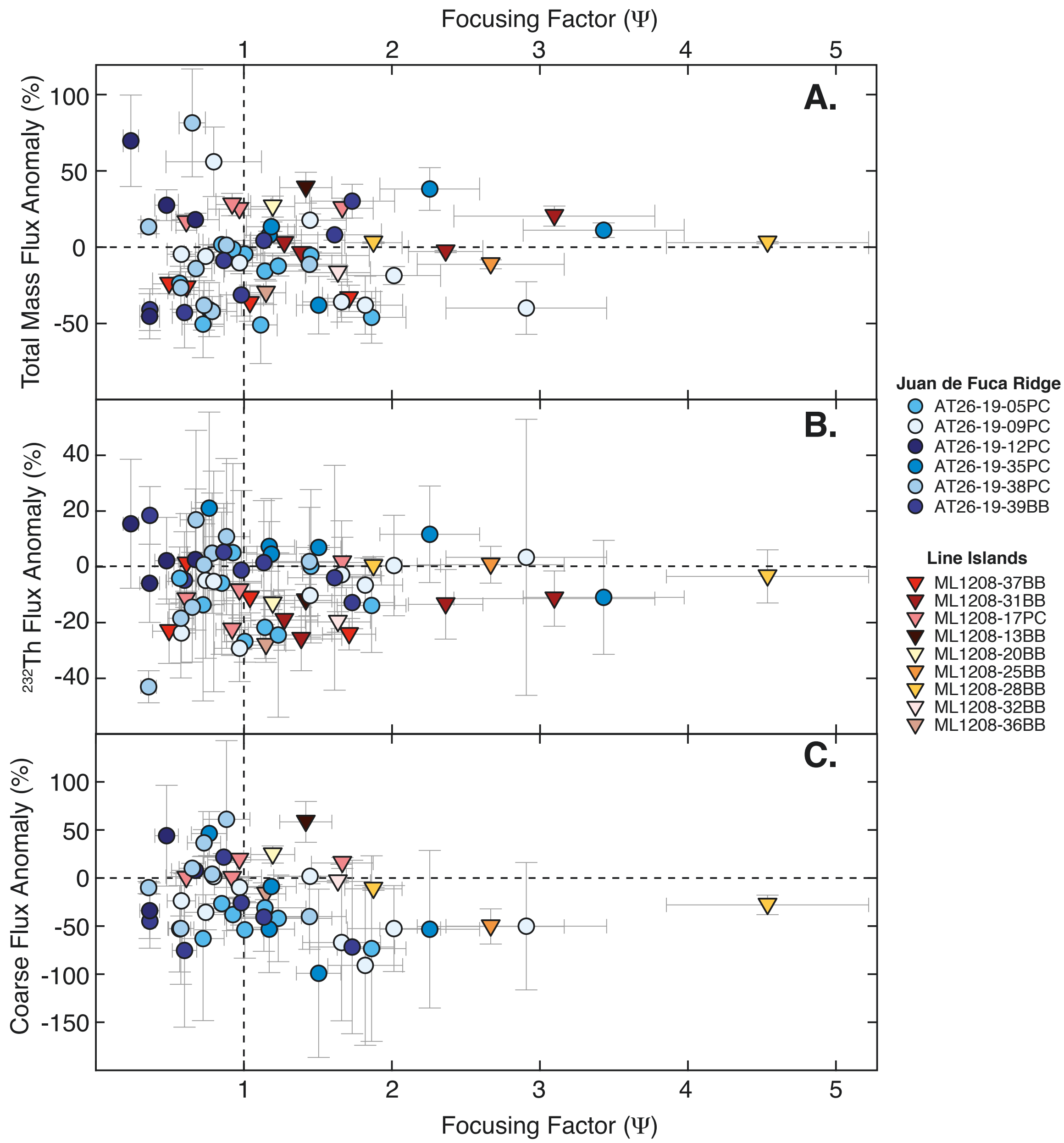

Figure 7. Flux anomalies as a function of sediment focusing factors. (A) Bulk mass flux. (B) ^{232}Th (fine) flux. (C) Coarse flux. Samples with uncertainties (1 s.e.) greater than ±100% have been excluded. Focused sites ($\Psi > 1$) would be predicted to have negative flux anomalies, plotting in the lower right quadrant. Winnowed sites ($\Psi < 1$) would have positive flux anomalies, plotting in the upper left quadrant. Instead, no systematic bias in the fluxes is apparent. The relationship between sediment focusing and bulk flux ($R^2 < 0.01$, $p = 0.81$), between sediment focusing and ^{232}Th flux ($R^2 < 0.01$, $p = 0.97$), and between sediment focusing and coarse flux ($R^2 = 0.07$, $p = 0.07$) are all insignificant. This insensitivity to sediment focusing or winnowing suggests that grain size effects cause little to no disruption to the functioning of ^{230}Th in sediment as a constant flux proxy.

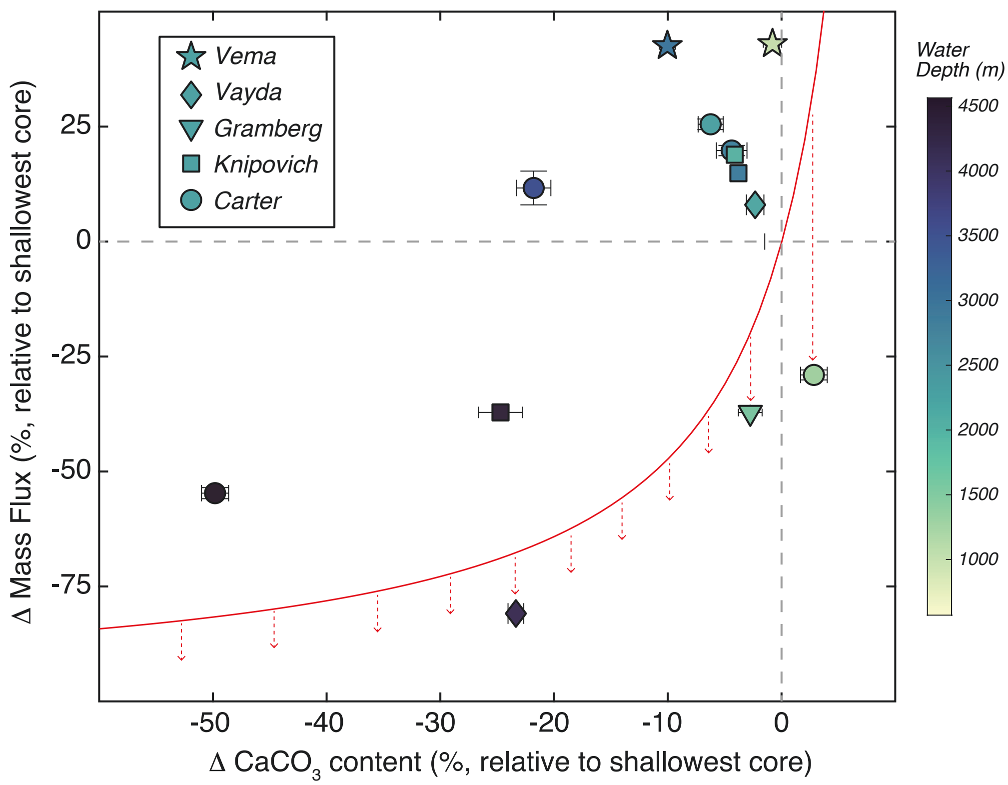

Figure 8. Changes in ^{230}Th-normalized mass fluxes in response to changes in calcium carbonate burial. Coretop mass fluxes are reconstructed from depth transects recovered from 5 seamounts in the tropical Atlantic (Rowland et al., 2017). Data are represented as deviations from the mass flux or calcium carbonate at the shallowest coretop of each seamount; that is, a $\Delta CaCO_3$ of -20% indicates that the calcium carbonate concentration is 20% lower than that of the shallowest coretop on that seamount. Red curve is the non-linear expected relationship for the changes in calcium carbonate composition and total mass flux if ^{230}Th does not dissolve in conjunction with the calcium carbonate particles. Loss of ^{230}Th during calcium carbonate dissolution (dashed red arrows) would push the data points below the red curve to mass fluxes that are too low relative to the expectation.

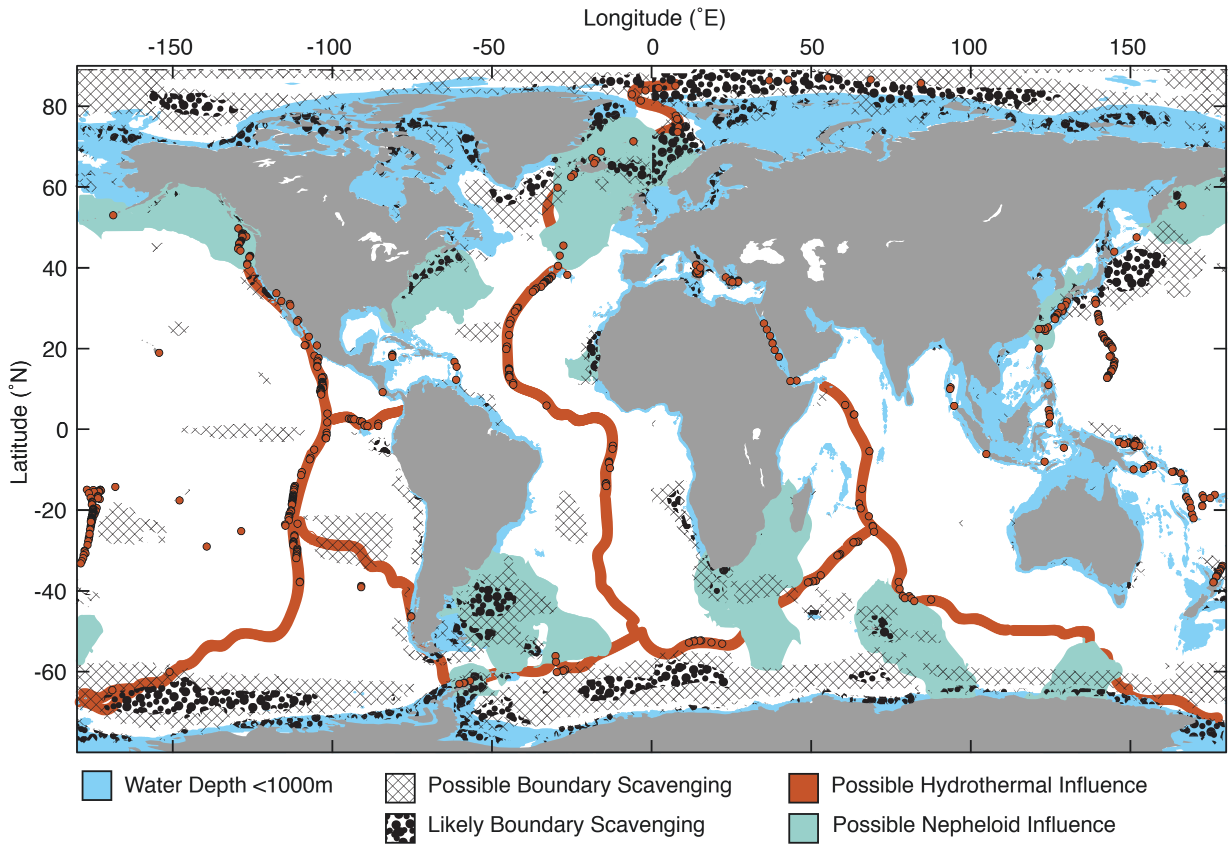

Figure 9. Potential considerations for the application of ^{230}Th normalization. The influence of boundary scavenging is defined by the composite model output of Figure 3. F/P values from 0.5-0.7 and 1.3-1.5 identify possible effects of boundary scavenging, as large uncertainties in F/P values make these values only somewhat distinct from the acceptable F/P window of 0.7-1.3. When F/P is less than 0.5 or greater than 1.5, boundary scavenging effects are considered likely. Nepheloid layers are defined by particulate matter concentrations greater than 25 µg/L in the bottom 10m of the water column (Gardner et al., 2018). Hydrothermal vents (orange dots) as compiled by (Beaulieu et al., 2013).

Criterion	**# Passing Cores**	**% Database**
1) Were raw concentrations (^{230}Th, ^{232}Th, and ^{238}U) or $^{230}Th_{xs}^{0}$ provided?	1142	97.9
2) Were errors provided for ^{230}Th, ^{232}Th, and ^{238}U provided?	778	66.7
3) Is chronology specified by either by $\delta^{18}O$ or ^{14}C?	368	31.5

Quality Level (*number of criteria passed by each record)*	**# Passing Cores**	**% Database**
3 = Optimal	261	22.4
2 = Good	605	51.8
1 = Fair	279	23.9
0 = Poor	14	1.2
Excluded	6	0.5

Table 1. Summary of quality control criteria and the subsequent quality levels of the records within the database.

Holocene (0-5 ka) Mass Fluxes (g/cm²kyr)						
	Atlantic	**Pacific**	**Indian**	**Southern**	**Arctic**	**Global**
Mean	1.92	1.38	1.54	1.16	2.39	1.56
Median	1.66	0.84	1.17	0.94	1.48	1.13
1σ	1.27	2.62	1.24	1.05	1.82	-
n	334	136	83	275	12	840
95% confidence	1.78-2.06	0.93-1.83	1.27-1.81	1.03-1.28	1.34-3.44	1.48-1.65
LGM (18.5-23.5 ka) Mass Fluxes (g/cm²kyr)						
	Atlantic	**Pacific**	**Indian**	**Southern**	**Arctic**	**Global**
Mean	3.41	1.60	1.83	1.30	0.38	2.00
Median	2.03	1.22	1.42	0.72	0.26	1.38
1σ	4.73	2.20	1.17	1.38	0.28	-
n	92	108	21	36	5	262
95% confidence	2.42-4.39	1.18-2.03	1.32-2.34	0.84-1.76	0.13-0.64	1.81-2.19
LGM/Hol Mass Flux Ratio						
	Atlantic	**Pacific**	**Indian**	**Southern**	**Arctic**	**Global**
Mean	1.84	1.39	1.21	1.16	1.60	1.45
Median	1.37	1.18	1.13	0.93	1.60	1.22
1σ	1.62	0.63	0.64	0.71	0.84	-
n	71	67	17	25	2	182
95% confidence	1.46-2.22	1.23-1.54	0.90-1.52	0.88-1.44	0.42-2.78	1.38-1.53

Table 2. Summary of Holocene, LGM, and LGM/Holocene mass flux data. Global data are computed by weighting each of the five ocean basins by volume. The 95% confidence range is calculated as the mean plus or minus two standard errors, where one standard error is equivalent to the standard deviation divided by the square root of the number of datapoints.